DOTTORATO DI RICERCA IN CHIMICA

Convenzione tra

UNIVERSITÀ DEGLI STUDI DI TRIESTE
e
UNIVERSITÀ CA' FOSCARI DI VENEZIA

CICLO XXX

TOXICOLOGICAL EFFECTS OF GRAPHENE FAMILY NANOMATERIALS AFTER CUTANEOUS EXPOSURE

Settore scientifico-disciplinare: **CHIM/06**

DOTTORANDO / A
LAURA FUSCO

COORDINATORE
PROF. MAURO STENER

SUPERVISORE DI TESI
PROF. MAURIZIO PRATO

ANNO ACCADEMICO 2016/2017

Acknowledgements

It is a pleasure to convey my sincerest gratitude to those who have inspired and supported me throughout my doctoral study by sharing their knowledge and providing me with their invaluable guidance and suggestions; in particular:

Prof. ***Maurizio Prato****, my supervisor, for providing me with the opportunity to undertake such an interesting PhD project and increase my knowledge in a novel and innovative field. It has been an honour and a privilege to have you as my mentor; your intellect and passion have truly inspired me to take the "stairway to science" two steps at a time: with motivation and enthusiasm.*

Prof. ***Aurelia Tubaro****, Dr.* ***Marco Pelin*** *and Dr.* ***Silvio Sosa****, who played a key role in encouraging, supervising, and coordinating this project. Thank you for allowing me to work at the Toxicology Laboratories at the Dept. of Life Science at the University of Trieste (Italy); it has provided me with essential experience for my professional training. I very much appreciate your comprehensive expertise and your talent as an educator.*

Prof. ***Bengt Fadeel*** *for providing me with the opportunity to complete my PhD project at his laboratories at the Dept. of Molecular Toxicology at the Karolinska Institutet (Sweden). It was a privilege to study in such an outstanding scientific environment. Also, many thanks to his research group for making me feel at home, and in particular to Dr.* ***Sourav Prasanna Mukherjee*** *for supervising my project with unforgettable kindness.*

Prof. ***Ester Vázquez****, Dr.* ***Alejandro Criado****,* ***Cristina Martín*** *and* ***Verónica León*** *for synthesizing, characterizing, and providing the nanomaterials, and for their committed*

involvement during all stages of the project. A special thanks to Dr. ***Susanna Bosi*** *for her continuous support and advice.*

Many thanks to you all,

Laura Fusco

This study was supported by the European Union H2020 Programme under grant agreement no. 696656-Graphene Flagship Core1 and by the European Union FP7 Programme under grant agreement no. 604391 Graphene Flagship EU Graphene Flagship (no.604391).

RIASSUNTO

Il grafene e i nanomateriali della famiglia del grafene (*Graphene Family Nanomaterials*, GFN), hanno attirato sia interesse accademico che industriale nel corso degli ultimi anni grazie alle loro importanti proprietà fisicochimiche che li rendono promettenti candidati per innumerevoli applicazioni in svariati settori, compreso quello delle nanotecnologie, energetico e biomedico. Tuttavia, nonostante l'enorme progresso tecnologico dei GFN, essi possono presentare rischi per la salute e, sino ad oggi, vi è un'incompleta conoscenza in merito alla loro potenziale tossicità per l'uomo. La pelle è l'organo più esteso del corpo umano e quella cutanea rappresenta una delle principali vie di esposizione ai GFN durante la loro produzione, utilizzo e smaltimento. Il contatto cutaneo con materiali correlati, quali la grafite e nanomateriali a base di carbonio, è stato associato ad un'aumentata incidenza di patologie cutanee, come la dermatite irritativa da contatto, l'ipercheratosi ed i nevi. Ciò nonostante, la tossicità dei GFN a livello cutaneo rimane largamente inesplorata. Per far luce su questo aspetto, il presente studio è stato condotto su una linea cellulare umana non tumorale ampiamente utilizzata per valutare gli effetti tossici a livello della pelle, i cheratinociti cutanei HaCaT, su cui sono stati indagati gli effetti di un *few layer graphene* (FLG) e tre campioni di grafene ossido (GO): un GO prodotto mediante il metodo di Hummer modificato (GO1), e due commerciali (GO2, prodotto da Antolin Group, e GO3, prodotto da Graphenea). A concentrazioni maggiori di 30 μg FLG/mL e di 1 μg GO/mL, sono stati osservati dei significativi danni mitocondriali e della membrana plasmatica, la cui potenza dipende dallo stato di ossidazione dei GFN: il composto meno (FLG) e più (GO3) ossidato sono risultati il meno e il più citotossico, rispettivamente. Il danno a livello della membrana plasmatica è stato confermato dalla microscopia ad epifluorescenza e dall'analisi confocale, dimostrando che i GFN risultano stabilmente ancorati alla membrana cellulare. Inoltre, le esposizioni a lungo termine (sino a 14 giorni) a basse concentrazioni di GFN (0.1 μg/mL) hanno mostrato solo lievi riduzioni dell'attività mitocondriale, risultando

significative solo dopo 10 giorni di esposizione. Gli effetti sul danno mitocondriale indotti dal composto meno (FLG) e più (GO3) citotossico sono stati ulteriormente studiati, dimostrando una depolarizzazione mitocondriale concentrazione- e tempo-dipendente. Questo effetto non è risultato essere dipendente dalla formazione dei pori mitocondriali di transizione ma è apparso dipendente da una significativa produzione concentrazione- e tempo-dipendente di specie reattive dell'ossigeno (ROS), indotta principalmente dall'attivazione di enzimi ossidativi basati sulle flavoproteine, come la NADH deidrogenasi e la xantina ossidasi. Nella seconda parte del progetto, sono stati valutati gli effetti infiammatori di FLG e GO3 a livello cutaneo. Concentrazioni sub-citotossiche di entrambi i composti (0.1 e 1.0 μg/mL) hanno indotto un rilascio significativo di mediatori pro-infiammatori (fattore stimolante le colonie di granulociti-macrofagi, interleuchina-1α, -6 e -8 ed il fattore di necrosi tumorale α) dalle cellule HaCaT, principalmente dopo un breve periodo di esposizione ai GFN (4 h), seguiti da un lungo periodo di "recovery" in terreno privo di GFN (20 o 68 h). Tuttavia, il terreno condizionato, ottenuto in seguito ad esposizione delle cellule HaCaT al FLG e al GO sotto queste condizioni, non ha indotto una differenziazione significativa dei monociti THP-1 in macrofagi o cellule dendritiche né un significativo rilascio di mediatori infiammatori da parte di queste cellule, suggerendo solo una moderata reazione infiammatoria. Questi risultati sono stati confermati dalla valutazione del potenziale sensibilizzante di FLG e GO3 sui monociti THP-1 (seguendo la linea guida n° 442E della *Organisation for Economic Co-operation and Development,* OECD), suggerendo che questi nanomateriali non siano dei sensibilizzanti cutanei. In generale, sulla base dei risultati ottenuti, nonostante questi composti siano in grado di indurre significativi danni mitocondriali e di membrana in seguito a lunghe esposizioni ad alte concentrazioni nei cheratinociti HaCaT, FLG e GO sembrano indurre solo moderati effetti tossici a livello cutaneo.

ABSTRACT

Graphene and the so-called Graphene Family Nanomaterials (GFNs) have attracted both academic and industrial interest during the last years thanking to their unique physicochemical properties, making them promising candidates for a wide range of applications in several fields, including nanotechnology, energy technology and biomedicine. However, despite the huge GFNs technologies progress, they may pose health risks, and little is known about their potential human toxicity, so far. Skin is the largest organ of human body and the cutaneous exposure represents one of the major exposure routes to GFNs, during their manufacturing, use and disposal. Even though cutaneous contact to other related materials, such as graphite and carbon nanomaterials, has been associated with increased incidence of skin diseases, such as airborne irritant contact dermatitis, hyperkeratosis and naevi, the toxicity of GFNs at the skin level remains largely unexplored. Thus, a study was carried out using a human non-tumor cell line widely used to evaluate toxic effects at cutaneous level, the HaCaT skin keratinocytes, to investigate the effects of a research grade few layer graphene (FLG) and three graphene oxides (GOs): a research grade GO (GO1) and two commercial GOs (GO2 from Antolin Group and GO3 from Graphenea). At concentrations higher than 30 μg FLG/mL and 1 μg GO/mL, these GFNs induced significant mitochondrial and plasma-membrane damages with variable potencies, depending on GFNs oxidation state: the less (FLG) and the most (GO3) oxidized compounds were the less and the most cytotoxic, respectively. The damage at the plasma membrane level was confirmed by epifluorescence microscopy and confocal analysis, demonstrating that GFNs were strongly bound to cell membranes. Moreover, long-term exposures (up to 14 days) to low GFNs concentrations (0.1 μg/mL) showed only slight reductions of mitochondrial activity, being significant only after 10 days exposure. The effects on mitochondrial damage induced by the less (FLG) and the most (GO3) cytotoxic GFN were further investigated, demonstrating a concentration- and time-dependent mitochondrial

depolarization. This effect was not dependent on mitochondrial permeability transition pores formation but appeared to be dependent on a significant concentration- and time-dependent reactive oxygen species (ROS) production, mainly induced by the activation of flavoprotein-based oxidative enzymes, such as NADH dehydrogenase and xanthine oxidase.

In the second part of the project, the inflammatory effects of FLG and GO3 at the skin level were evaluated. Sub-cytotoxic concentrations of both compounds (0.1 and 1.0 μg/mL) induced a significant release of pro-inflammatory mediators (granulocyte macrophage colony stimulating factor, interleukin-1α, -6 and -8, and tumor necrosis factor α) from HaCaT cells, mainly after a short exposure time to GFNs (4 h), followed by long recovery times in GFNs-free media (20 or 68 h). However, the conditioned media, obtained after exposure of HaCaT cells to FLG or GO3 under these conditions, did not induce a significant differentiation of THP-1 monocytes towards macrophages or dendritic cells. Similarly, they did not induce any significant release of inflammatory mediators by these cells, suggesting only a moderate inflammatory reaction. These results were confirmed by the investigation of the sensitizing potential of FLG and GO3 on THP-1 monocytes (according to the Organisation for Economic Co-operation and Development, OECD, guideline n°442E), suggesting that these nanomaterials are not skin sensitizers. On the whole, these results suggest that, even though these compounds are able to induce significant mitochondrial and plasma membrane damage after long exposure times to high concentrations, FLG and GO induce only minor toxic effects at the skin level.

1. Introduction

1.1 Graphene

Graphene is an advanced atomically-thin nanomaterial composed of carbon atoms arranged in a honeycomb network (Figure 1), deriving from its parental material graphite. Graphene pioneers, A. Geim and K. Novoselov, who first introduced the nanomaterial as monolayer and crystalline graphitic films, were awarded the 2010 Nobel Prize in Physics in recognition of their "groundbreaking experiments" (Novoselov et al., 2004) carried out at the University of Manchester. Although scientists theorized about graphene for sixty years (McClure, 1956; Slonczewski and Weiss, 1958; Wallace, 1947), it was presumed not to exist in the free state due to the unstable nature of strictly two dimensional (2D) crystals (Geim and Novoselov, 2007; Meyer et al., 2007), and it was only in 2004 that the two Nobel laureates for the first time rediscovered, isolated, identified and characterized graphene, by extracting a single-atom-thick crystallite from bulk graphite. As a consequence of their revolutionary research, worldwide interest has grown considerably around this nanomaterial and the exploration of its properties and applications.

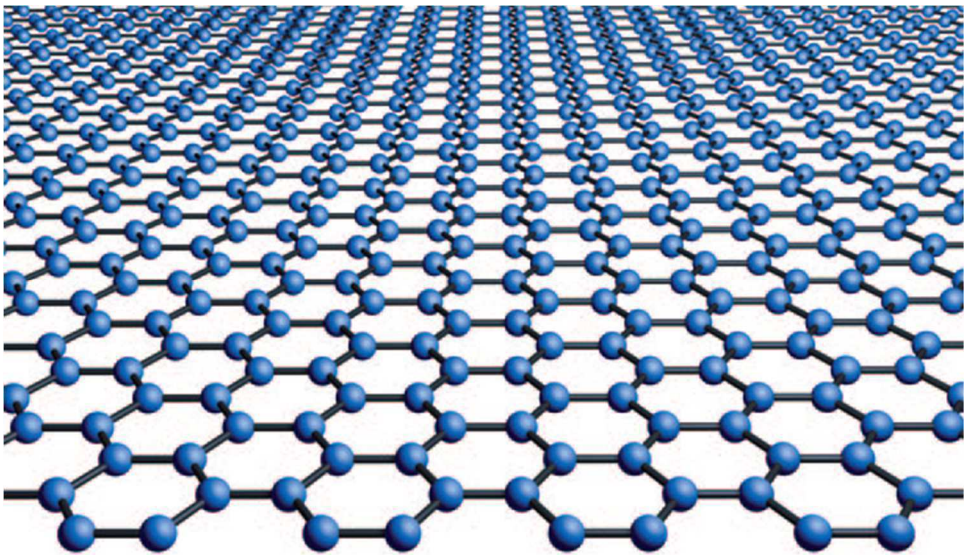

Figure 1. Honeycomb lattice structure of graphene (source: Novoselov, 2011).

Looking back at graphene's related research, the "prehistory" (Geim, 2012) of this nanomaterial started when the chemist B. C. Brodie made one of the earliest recorded attempt to study graphene in 1859, describing the highly lamellar structure of thermally reduced graphite oxide (Brodie, 1859). The structure of graphite was discovered in 1916 (Debye and Scherrer, 1916), but only in 1947 the theoretical existence of graphene was considered seriously by P. R. Wallace to explain an anomalous occurrence in the magnetic field while studying the band theory of graphite (Wallace, 1947).

In 1948, nearly ninety years after Brodie's study, G. Ruess and F. Vogt finally gave to the scientific community the earliest images of few-layer graphite by transmission electron microscopy (Figure 2) (Ruess and Vogt, 1948). These studies were continued in 1962 by H. P. Boehm who identified ultra-thin graphitic flakes (Figure 3) (Boehm et al., 1962) and, in 1986, firstly introduced the term graphene, from the combination of the word "graphite" and the suffix that refers to polycyclic aromatic hydrocarbons (Boehm, 2010; Boehm et al., 1986).

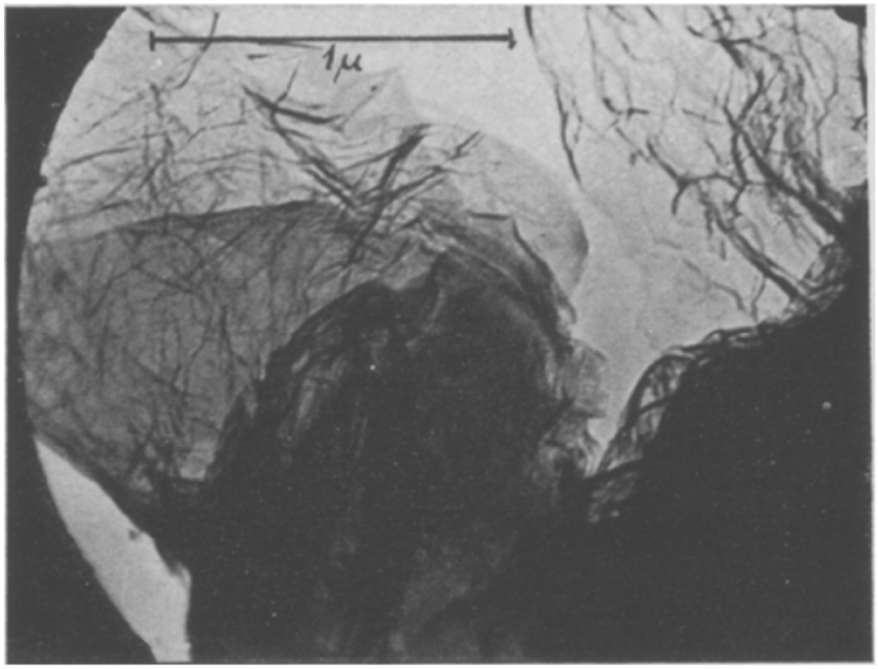

Figure 2. First TEM images of few-layer graphite (source: Ruess and Vogt, 1948).

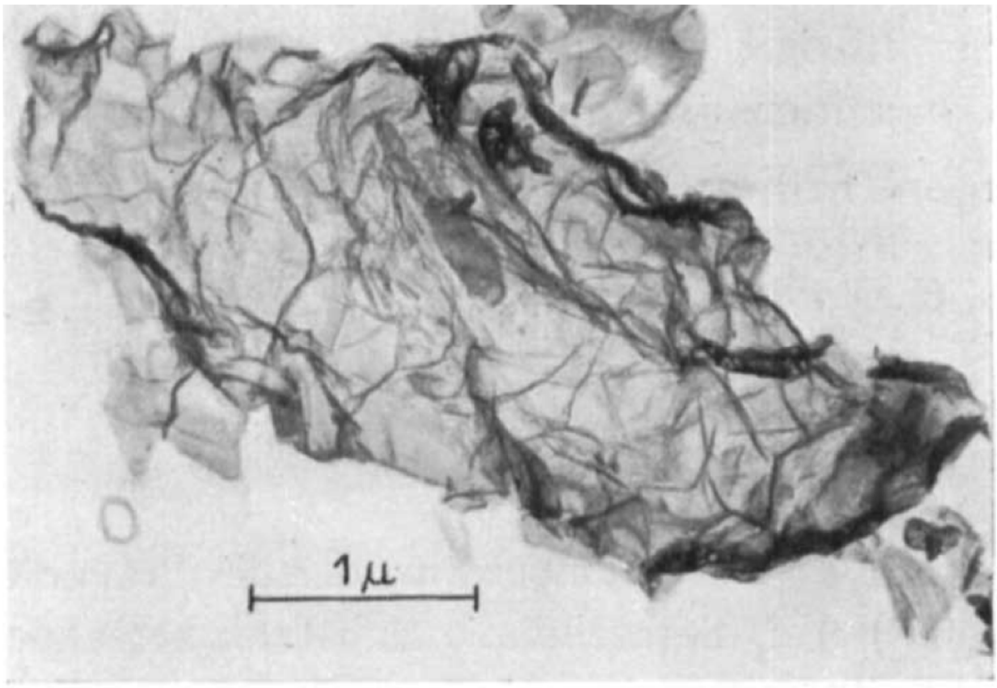

Figure 3. Ultra-thin graphitic flakes from the early 1960s (source: Boehm, 1962).

Coming to present day, thanks to A. Geim and K. Novoselov research, graphene properties have been deeply investigated and it has become a "rapidly rising star on the horizon of materials science and condensed-matter physics" (Geim and Novoselov, 2007). Graphene can be defined as the latest member of carbon allotropes. It is the basic building material of other important carbon allotropes: it can be wrapped up into 0D fullerene, rolled into 1D carbon nanotubes (CNTs) or stacked into 3D graphite (Figure 4).

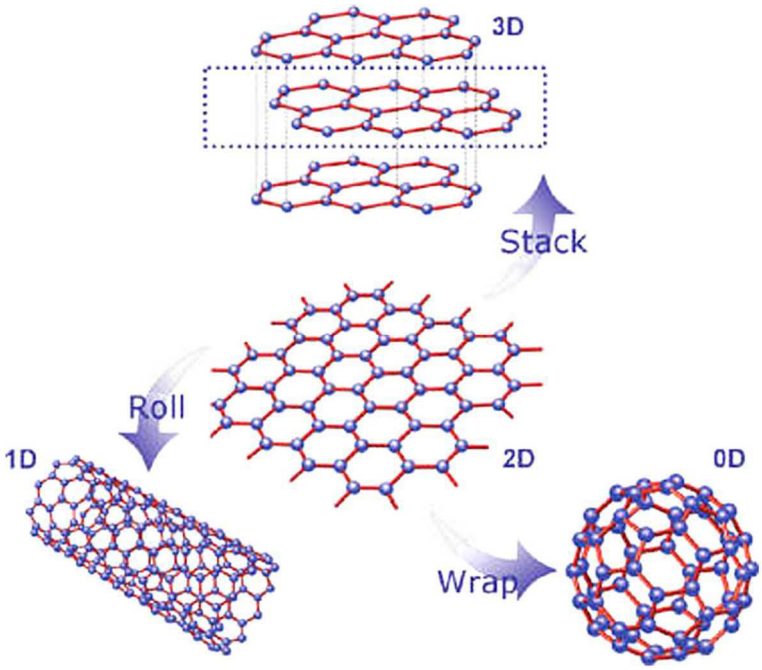

Figure 4. Graphene is a basic building material for other carbon allotropes of all other dimensionalities. It can be wrapped up into 0D fullerene, rolled into 1D nanotubes or stacked into 3D graphite (source: Abbassi, 2016).

1.1.1 Methods for graphene preparation: isolation and synthesis

In 2004, Novoselov, Geim and co-workers isolated graphene for the first time by the scotch tape method, a micromechanical exfoliation technique used to separate graphene sheets from a graphite crystal by repeated peeling using adhesive tape (Novoselov et al., 2004). This low-budget method is very simple and the quality of the resulting graphene is extremely high, with almost no defects. However, it also has disadvantages because of the difficulties in obtaining larger amounts of graphene and its variability in size and thickness.

Graphene synthesis is one of the most challenging issues for what concerns graphene introduction into real market applications. In the last few years, several methods have been proposed to produce graphene. Each of these techniques has some advantages and limitations. Generally, graphene can be synthesized by various methods which are based on two main approaches: the top-down, consisting on the exfoliation of a graphitic material, and bottom-up, involving the use of carbon-based materials to build up graphene. Some of the main synthesis techniques and their advantages or limitations are briefly described in the following section.

Top-down approaches

- *Micromechanical exfoliation* is a simple way to obtain the highest-quality graphene. This method involves the use of a scotch tape or any other mechanical approach to gradually peel more and more layers of graphene from graphite to obtain a “few layers graphene (FLG)”. It is commonly used to study fundamental properties of graphene. However, this slow method is extremely labor-intensive and doesn’t meet the requirements for commercial applications (Jayasena et al., 2013; Van Noorden, 2012).

- *Electrochemical exfoliation* is a simple technique but is not suitable for biomedical applications because it implies the use of potentially dangerous surfactants difficult to remove (Liu et al., 2013; Parvez et al., 2013)

- *Electrochemical and chemical reduction* is a commonly used strategy to reduce graphene oxide (GO), a highly-oxidized form of graphene, into large quantity of reduced graphene oxide (rGO). Since GO is not a good conductor, this method is mainly to restore the high electrical conductivity of graphene.

- *Liquid-phase exfoliation (LPE) is a* method to disperse and exfoliate graphite enabling the production of graphene in different solvents (Ciesielski and Samorì, 2014, 2016; Coleman, 2013; Hernandez et al., 2008). Typically, graphite can be exfoliated in an organic solvent with nearly the same surface energy as graphite (Lotya et al., 2010). The solution is then subjected to ultrasound treatment by sonication for several hundred hours or a voltage is applied to split graphite flakes into individual graphene sheets. Centrifugation can then be used to separate the produced flakes, characterized by different size and thickness, from unexfoliated material. LPE allows upscaling the production, to obtain a much higher amount of graphene.

- *Exfoliation of graphite oxide* is a low-budget and high-scalability method. It involves the production of graphite oxide obtained from graphite followed by reduction.

- *Arc discharge* is a simple electrical method involving high-voltage arc between graphite electrodes in a hydrogen atmosphere. The presence of hydrogen terminates the dangling carbon bonds with hydrogen and prevents the formation of closed structures.

- *Unzipping of carbon nanotubes* via chemical etching ($KMnO_4$-H_2SO_4) or plasma etching. At this scale, the unzipping has been accomplished by harsh acids and the right thermodynamic conditions (Baraton et al., 2011).

Bottom-up approaches

- *Chemical vapor deposition (CVD)* is a process based on the use of carbon-containing gaseous compounds (such as methane, ethane, or propane) as precursors that, in a reaction chamber at high temperatures, decompose on the catalytic metal surface of a substrate to create a thin film. CVD involves low costs and can produce relatively high quality graphene but a proper flow is required to remove toxic and highly volatile gaseous by-products from the reaction chamber.
- *Epitaxial growth on Silicon carbide (SiC)* is a method in which graphene is synthesized from the high temperature reduction of SiC which was firstly introduced by De Heer and co-workers (de Heer et al., 2007). Graphene is grown on SiC by several methods, including CVD on epitaxially matched metal surfaces (Sutter et al., 2008). The obtained graphene is suitable for technologic applications.
- *Carbonization* refers to the primary conversion of organic material into a carbonaceous solid, one consisting primarily of elemental carbon, regardless of the structure.

1.1.2 Graphene-family nanomaterials (GFNs): properties and applications

Graphene is an allotrope of carbon consisting of a two-dimensional sheet of sp^2-hybridized carbons arranged in a honeycomb structure. This giant aromatic macromolecule has attracted both academic and industrial interest during the last years due to its unusual and outstanding physicochemical properties, including high surface-to-volume ratio, strong mechanical strength, remarkable optical transmittance as well as extraordinary electrical and thermal conductivity. Graphene is a single atom-thick nanomaterial with a lateral dimension ranging from several nanometers to microscale. In its purest form, graphene appears as a monolayer (single-layer) with suitable properties for high-frequency electronics. To improve and expand its potential range of novel applications, new functionalization methods of graphene nanocomposites or hybrids can be applied to obtain the so-called graphene-family nanomaterials (GFNs) (Boukhvalov and Katsnelson, 2009; Chang and Wu, 2013; Gao et al., 2010; James and Tour, 2013; Kuila et al., 2012; Kumar et al., 2012; Mao et al., 2012; Park and Ruoff, 2009; Quintana et al., 2013; Yang et al., 2013a). GFNs are classified according to the international editorial team of Carbon (Bianco et al., 2013) and, recently, rationally named basing on three fundamental GFNs properties (number of layers, average lateral dimension, and atomic carbon/oxygen ratio, figure 5) (Wick et al., 2014):

- *Few-layer-graphene (FLG) / multi-layer graphene (MLG)* consisting of a small number (between 2 to 5 or 10, respectively) stacked graphene layers of extended lateral dimension, useful for composite and cover materials, as a mechanical reinforcement.
- *Graphene oxide (GO)* is an oxidized form of graphene, where C/O atomic ratio is fixed between 2 - 3. It is decorated by oxygen-containing groups, such as hydroxyl and

carboxylic groups. Thanks to its dispersibility in water, it is considered easy to process but it is not a good conductor.

- *Reduced graphene oxide (rGO)* is obtained by reductively processing of GO. It can be done by different techniques (chemical, photo-chemical, thermal, photo-thermal, microwave or microbial/bacterial methods) to reduce GO oxygen content obtaining rGO.
- *Graphene nanosheet* is characterized by a lateral dimension less than 100 nm and is freely suspended or adherent on a substrate.
- *Graphene microsheet* is characterized by a lateral dimension between 100 nm and 100 μm and is freely suspended or adherent on a substrate.
- *Graphene nanoribbon* has a longer lateral dimension exceeding the shorter lateral dimension (width) by at least an order of magnitude. The prefix "nano" can be used only if the width is less than 100 nm.
- *Graphene quantum dots (GQDs)* are an alternative and highly fluorescent form of graphene nanosheets or few-layer graphene nanosheets. Usually their lateral dimension is less than 10 nm.

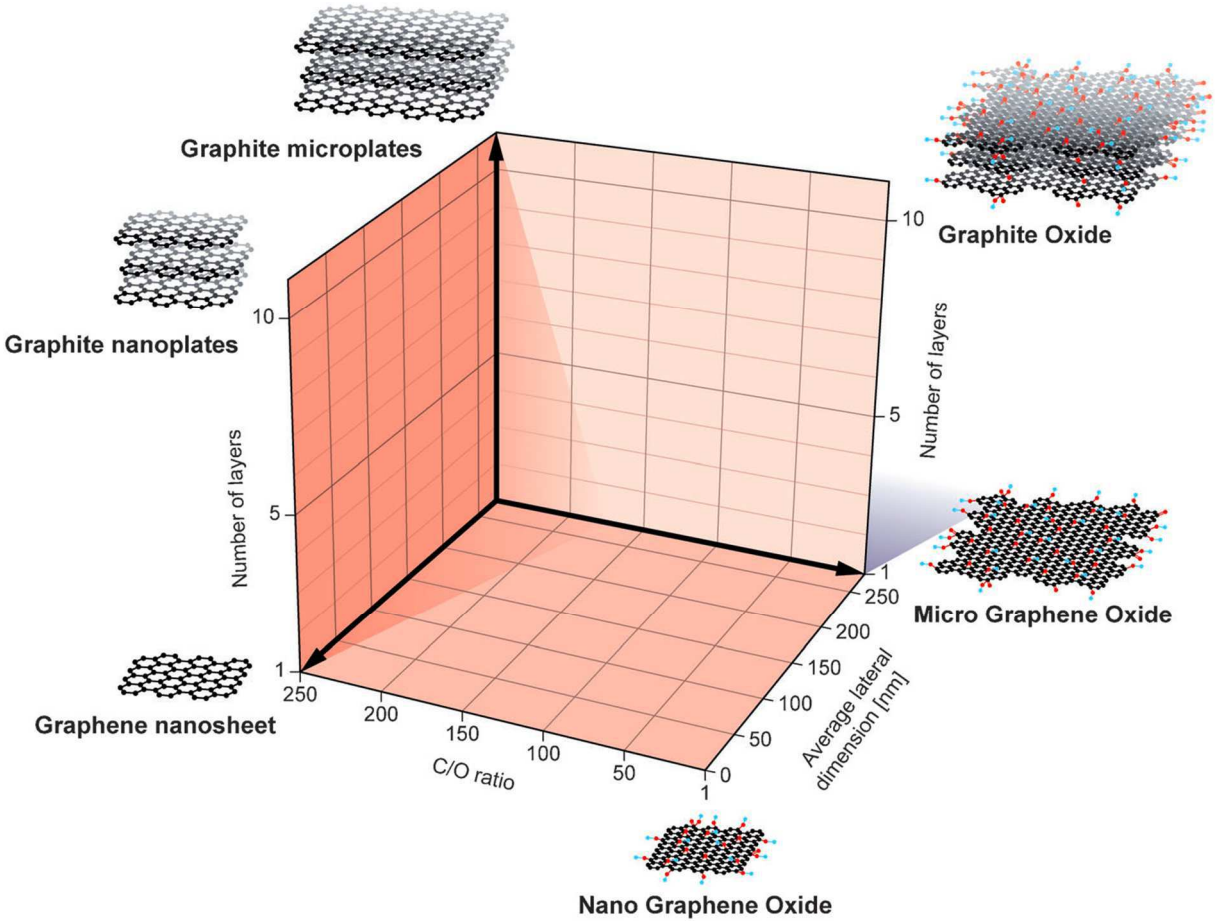

Figure 5. Categorization of GFNs based on a classification grid considering three fundamental GFNs properties: number of graphene layers, average lateral dimension, and atomic carbon/oxygen ratio (source: Wick, 2014).

It has been reported that graphene is the strongest material ever measured (Peng-Gang et al., 2011) with extraordinary mechanical properties. Indeed, it is characterized by an extremely high stiffness and breaking strength, corresponding to a Young's modulus of E = 1.0 TPa and intrinsic strength of 130 GPa. It also exhibits extremely high thermal conductivity values, measured between 4.84 and 5.30 kW m^{-1} K^{-1} (Jeong et al., 2009). In addition, high carrier mobility (200,000 cm^2 V^{-1} s^{-1}) and electron density (2x1011 cm^{-2}) are reported (Avouris, 2010;

Bao and Loh, 2012; Engel et al., 2012). It is the thinnest material in the universe, thanks to its atomic thickness, making it almost perfectly transparent to visible light.

Not surprisingly, therefore, GFNs potential applications are widely studied and applied to many fields (Boukhvalov and Katsnelson, 2009; Chang and Wu, 2013; Gao et al., 2010; James and Tour, 2013; Kuila et al., 2012; Kumar et al., 2012; Mao et al., 2012; Park and Ruoff, 2009; Quintana et al., 2013; Yang et al., 2013a), which will be shorty summarized as follows (Figure 6).

Energy applications

GFNs are promising candidates for four major energy-related areas: solar cells, supercapacitors, graphene batteries, and catalysis for fuel cells. Graphene transparent and conductive electrodes could be used to produce inexpensive, lightweight and flexible solar cells; chemical stability, high electrical conductivity, and large surface area (depending on layers) make graphene a perfect material to produce superior supercapacitor for energy storage; graphene can enhance both energy capacity and charge rate in rechargeable batteries; while multifunctional graphene mats are promising substrates for catalytic systems (Luo et al., 2012).

Nanoelectronics

GFNs allow the miniaturization of the electronics enhancing its properties. The smallest transistors have already been produced using graphene, with superior performance with respect to other circuits. Graphene semiconductors could be used for much faster computer chips then the current ones based on silicon; thanks to its transparency and flexibility graphene is an ideal candidate for transparent films, multi-touch screens and bendable or foldable mobile devices (Freitag, 2008; Roche, 2011; Westervelt, 2008).

Biomedicine

Biomedical application of GFNs could imply next-generation medical devices and therapies. Thanks to a high surface to volume ratio and capability of loading drugs or genes via chemical conjugation or physical adsorption approaches, graphene and related materials are efficient nanocarriers for drug/gene delivery and cancer therapy. Moreover, florescence quenching ability and unique electronic properties make graphene an impressive candidate for biosensing, while its derivatives, such as GO and GQDs, can be used in bioimaging, due to their intrinsic fluorescence. GFNs are also been reported to be inhibitors of bacterial growth as well as useful tools for tissue engineering, scaffolds and regenerative medicine, thanks to their excellent electrical conductivity, biocompatibility and surface area (Shen et al., 2012; Shin et al., 2016).

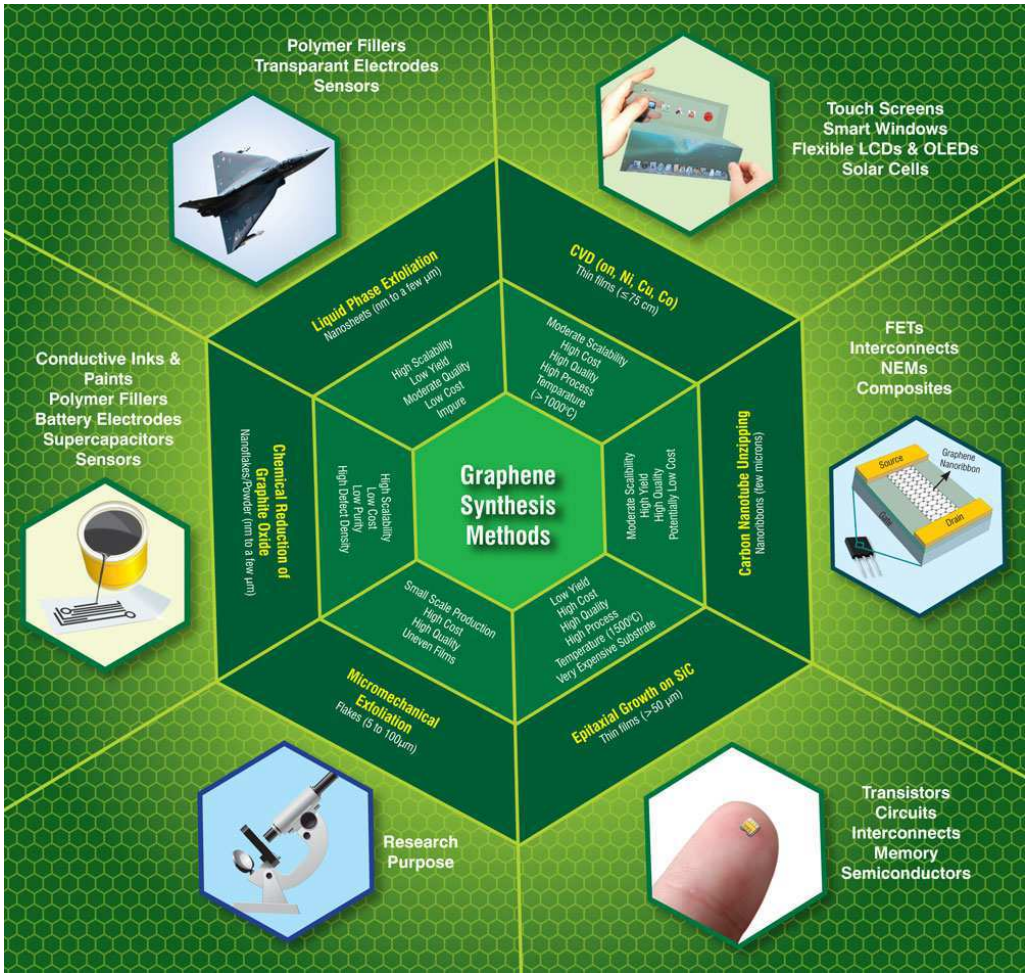

Figure 6. Commonly used methods for graphene production along with their key features, and the current and future applications. (Source: Center for Knowledge Management of Nanoscience & Technology, CKMNT).

1.2 Toxicity

1.2.1 Toxicity of graphene-family nanomaterials (GFNs)

Exposure to GFNs

Generally, GFNs could exert toxic effects after different exposure routes. Humans can be exposed to GFNs mainly by inhalation, skin contact, and oral intake, or even direct injection through biomedical interventions (Jachak et al., 2012). In some *in vivo* studies, after intravenous administration, GFNs have been reported to accumulate into the lungs for 3 months leading to inflammation, edema and granuloma formation (Zhang et al., 2011). Moreover, it has been shown that GO increased the rate of mitochondrial respiration and oxidative stress after lung instillation in mice (Duch et al., 2011) and mid-term effects were observed after pharyngeal aspiration of graphene nano-platelets in mice inducing acute lung inflammation (Schinwald et al., 2013). Graphene was also found to accumulate in the liver, kidneys and bladder following intravenous injection (Ou et al., 2016; Wang et al., 2011; Yang et al., 2011), showing thrombotic properties (Singh et al., 2011). However, after mice oral exposure, GO derivatives were rapidly excreted showing only a limited intestinal absorption (Yang et al., 2013b).

The cutaneous toxicity of GFNs remains largely unexplored (Ou et al., 2016), although skin contact is one of the major exposure routes to GFNs, especially during their production as dry powders by thermal exfoliation of graphite as well as during their use as bendable or foldable mobile devices, protective coatings, multi-touch screens, wound healing applications and skin sensors (Kim et al., 2016a; Shin et al., 2016).

GFNs toxicity

The investigation of graphene toxicity is one of the most challenging issues for the introduction of GFNs into real market applications (Bussy et al., 2015). Currently, there is insufficient data to draw conclusions about the potential hazards of GFNs and the exact mechanisms underlying their toxicity (Bianco, 2013; Seabra et al., 2014), although many *in vivo* and *in vitro* studies have investigated the biocompatibility and toxicity of GFNs (Ou et al., 2016).

In general, it has been highlighted the important correlation between the different physicochemical properties of GFNs, their composition, shape and size with their biological responses (Monteiro-Riviere and Inman, 2006; Wick et al., 2014). Moreover, in literature, contrasting results have been reported concerning the assessment of *in vitro* cytotoxicity of GFNs, therefore, generalized conclusions must be avoided because safety risks associated with GFNs depend on a plethora of factors, including cell lines, type of graphene material and their physicochemical properties. For instance, different studies have demonstrated that graphene materials cause dose-dependent cytotoxicity in a variety of cell models (Lv et al., 2012; Ou et al., 2016; Singh, 2016), but other studies reported an increase of cell viability (Ruiz et al., 2011). Nanoparticles dimension influences their possible localization inside the cells: materials with sizes smaller than 100 and 40 nm can enter the cell or nucleus, respectively (Ou et al., 2016). Thus, lateral dimension also has a key role in GFNs toxicity. However, also in this case, contrasting data have been reported, correlating the smallest size to both the most severe or the weakest toxicity (Akhavan et al., 2012; Chang et al., 2011; Ma et al., 2015). Similarly, studied devoted to the evaluation of the surface chemistries and functionalization impact on GFNs interaction with cells found contradictory results. For instance, it has been reported an association between the reduction of oxygen content and both a reduced (Das et al., 2013) or a stronger cytotoxicity (Liao et al., 2011).

The mechanisms underlying GFNs toxicity are not fully elucidated. However, it has been demonstrated that GFNs can strongly interact with biomolecules, such as nucleic acids, lipids and proteins, leading to DNA, RNA and membrane damages (Bao et al., 2011; Tu et al., 2013). On the other hand, interaction with fetal bovine serum (FBS) can mitigate the cytotoxicity of graphene by the formation of a protein corona preventing the direct contact with cell membranes (Mukherjee et al., 2017). GFNs can also indirectly impair biomolecules through the generation of reactive oxygen species (ROS), which may eventually lead to cell apoptosis or necrosis (Stone and Donaldson, 2006). Moreover, GFNs have been shown to induce mitochondrial damage in different cell lines (Hu et al., 2011; Zhang et al., 2010a).

1.2.2 Carbon-based nanomaterials effects after cutaneous exposure

Skin is the largest organ of human body and, in addition to its barrier properties, it represents one of the main surfaces through which noxious exogenous agents, including nanomaterials, can contact or even enter into the body (Monteiro-Riviere and Inman, 2006). Nevertheless, in contrast to the inhalational exposure (Kim et al., 2016b), little is known about the cutaneous toxicity of GFNs in humans, despite skin contact to graphite and other carbon nanomaterials (i.e. carbon fibers), have been associated with increased incidence of skin diseases, such as irritant contact dermatitis, hyperkeratosis and naevi (Eedy, 1996; Kasparov et al., 1989). For instance, several data indicate that skin exposure to carbon-based materials, such as carbon nanotubes (CNTs), may lead to dermal toxicity mainly due to oxidative stress and loss of cell viability (Ema et al., 2011; Shvedova et al., 2003; Zhang et al., 2007).

Concerning GFNs, Liao and co-workers investigated the biocompatibility of GO and rGO on human skin fibroblasts, suggesting that a reduction of the oxidation state could imply a stronger cytotoxicity (Liao et al., 2011); while human keratinocytes were recently used to evaluate the biocompatibility against normal skin cells of graphene oxide nanosheets as anti-cancer therapy (Mahanta and Paul, 2015). Finally, a computational molecular dynamics simulation showed the ability of few layer graphene microsheets to interact and penetrate the plasma membrane of different cell types, including keratinocytes (Li et al., 2013). In this scenario, the cutaneous toxicity of GFNs remain largely unexplored and further studies are required to shed light on their biocompatibility at the skin level.

1.3 The skin

Skin or cutis is the soft outer tissue covering vertebrates and represents the major barrier between human body and the environment, with a surface area in adults of 1.2 - 2 m^2. The anatomical structure of the skin is fundamental to perform its multiple and extraordinary functions (Figure 7). Among them, none are more important than protecting the organism against external factors, which includes physical, chemical, pathogen, immune, UV radiation and free radical defenses. Skin also has a key role in thermoregulation, sensation, insulation, and the production of vitamin D folates. Its complex structure consists of two primary layers: the avascular epidermis, composed primarily of keratinocytes, and the highly vascular dermis, made up of connective tissue, including blood vessels, sweat and sebaceous glands, hair follicles, and other structures (Monteiro-Riviere, 1991; Monteiro-Riviere, 2010).

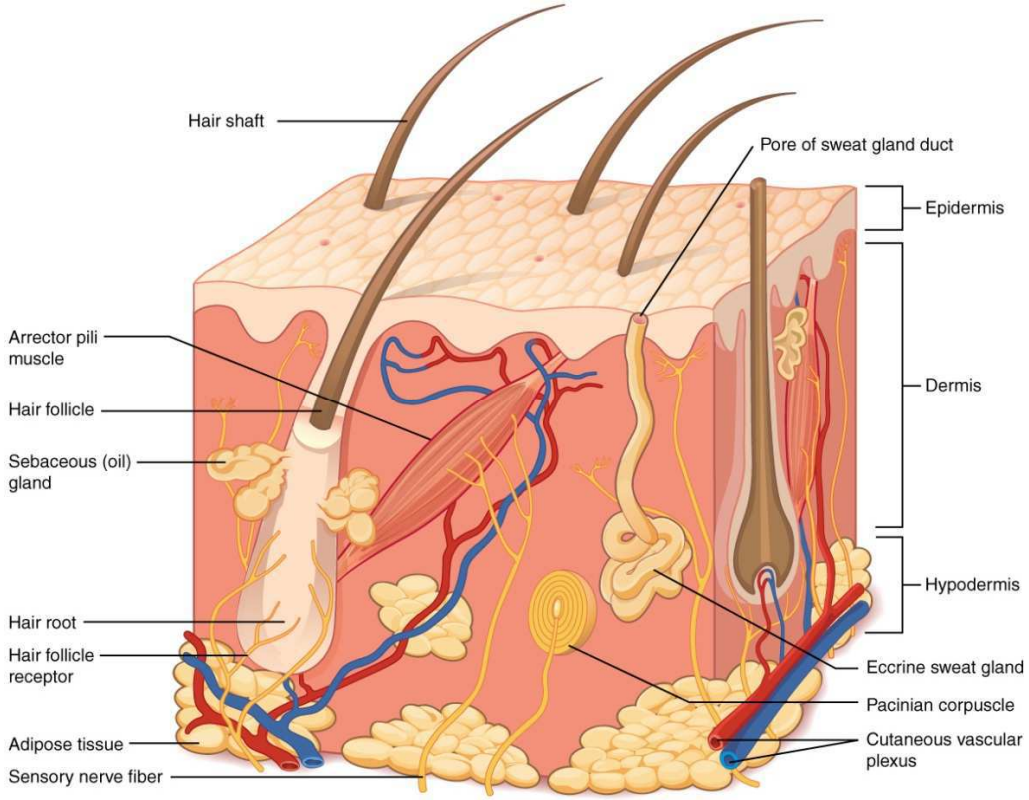

Figure 7. Scheme of generic skin composition (source: OpenStax, Anatomy & Physiology).

Epidermis

Epidermis, the outermost compartment of the skin, is a keratinized stratified squamous epithelium 100 to 150 μm thick. It consists of different cell types: keratinocytes, which are the predominant cells in skin (constituting 95% of the epidermis layer) and have both a structural and immunological role, as well as Merkel cells, functioning as mechanoreceptors, the UV-absorbing melanocytes, and the dendritic cells of the epidermis, known as Langerhans cells. Epidermis is organized into five different layers (Figure 8), named, from deep to superficial:

- *Stratum basale*, also referred to as *stratum germinativum*. It's a continuous layer of columnar or cuboidal epithelial cells that continually divide to form the keratinocytes of the *stratum spinosum*, which migrate superficially.
- *Stratum spinosum*, composed of polyhedral keratinocytes filled with keratin filaments called tonofilaments and strongly connected by desmosomes.
- *Stratum granulosum*, a thin layer of cells known as granular cells which migrate from the underlying *stratum spinosum*. These cells are rich in keratohyalin, granules which contain structural proteins involved in keratinization and barrier function.
- *Stratum lucidum*, representing a transition from the *stratum granulosum* to the *stratum corneum*. It is composed of three to five layers of flattened, dead keratinocytes filled with eleidin, an intermediate form of keratin.
- *Stratum corneum*, the most superficial layer, consists of nonliving keratinized cells (corneocytes) which are constantly being replaced by new cells from its underneath layers in the lower epidermis. The process of keratinization, also termed as cornification, occurs to differentiate the living keratinocytes into dead corneocytes. This

cytodifferentiation leads to the formation of a cornified envelope, required for the maintenance of skin homeostasis. The cells of this protective layer need no supply of blood for nourishment.

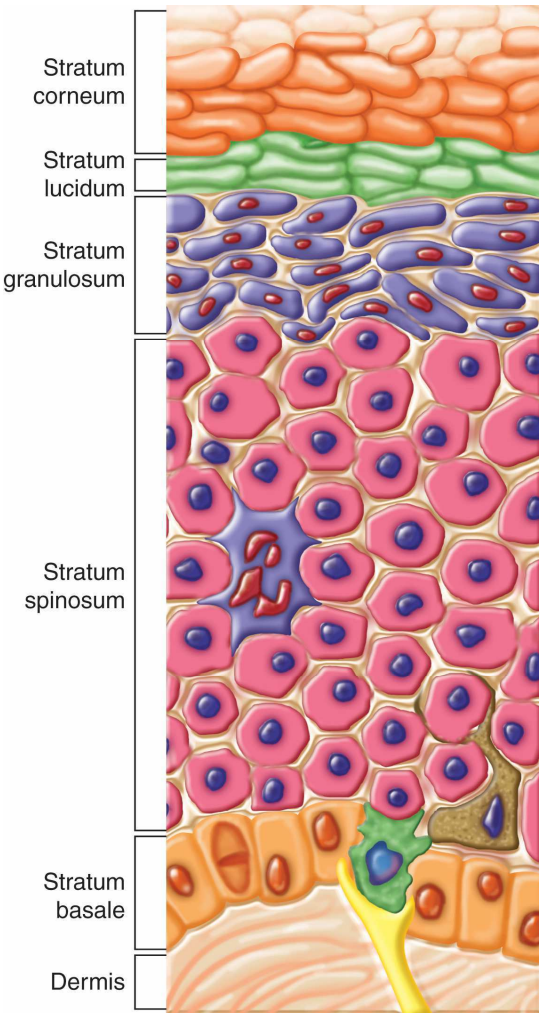

Figure 8. Layers of the epidermis (source: CC-OLI Anatomy and Physiology).

Dermis

Dermis primarily consists of extracellular matrix (ECM), made up of structural components (such as collagen, glycosaminoglycans and elastin) owning the function of supporting the epidermis, as well as stromal cells, such as fibroblasts that elaborate the ECM. Dermis also includes structural cells of the blood and lymph vessels, maintaining body temperature and providing a defense system to the body. In addition, pilosebaceous units, dermal adipose cells, sweat glands, mast cells, and infiltrating leukocytes can be found in this skin layer.

Dermis is characterized by the presence of specialized neural receptors: sensory nerve receptors of Merkel and Meissner's corpuscles (for touch), Pacinian corpuscles (for pressure), and Ruffini corpuscles (mechano-receptors). The dermis is composed by two main functional compartments, presenting a different organization and composition: the papillary dermis and reticular dermis. The former is composed by thick well-organized fiber bundles mainly consisting of type I and type III collagens, while the latter has a thin and scarcely organized collagen fiber bundles primarily composed by type III collagen (Haake et al., 2001).

1.3.1 Immune system

The immune system (from the Latin word *immunis*, which means "free" or "untouched"), composed by a network of molecules, cells, tissues and organs, is the body defense system from diseases or other harmful influences of the environment. It can be divided into two main subsystems: the innate immune system and the adaptive immune system. The former consists of cells and proteins that are always present and ready to provide an immediate, but non-specific, response. The latter, on the other hand, represents a second line of defense when pathogens or other insults successfully evade the innate immune system. The adaptive immune system consists of two types of responses: humoral immunity (or antibody-mediated response), mediated by antibodies produced by B lymphocytes differentiated in plasma cells, and cell-mediated immunity, mediated by T lymphocytes.

Cell models in skin immunity and inflammation

Keratinocytes

Skin can be considered an active immune organ, in which keratinocytes, resident epidermal cells and Langerhans cells collaborate with lymphocytes and draining regional lymph nodes, in an integrated system called "skin-associated lymphoid tissues" (SALT). Keratinocytes participate actively in immune response of skin inflammation as they can produce inflammatory mediators, including cytokines and cellular adhesion molecules, which trigger the start of inflammation allowing the recruitment and activation of a wide range of inflammatory cells and playing a key role in initiating cell-mediated immune responses in the skin. Keratinocytes constitutively express and store interleukin (IL)-1α and IL-1β until an appropriate stimulus induces the release of these cytokines (Salmon et al., 1994). Moreover, IL-6, IL-8 and

transforming growth factor (TGF)-α are potent growth factors that induce epidermal hyperproliferation.

Monocytes

Monocytes, the largest type of leukocytes (12-18 μm diameter), rise in the bone marrow from myelo-monocytic stem cells, which generate more direct precursors called monoblasts and pro-monocytes (Ziegler-Heitbrock, 2015). After maturation, newly formed monocytes enter the circulation where they circulate only for few days. In fact, the blood is a reservoir from which human peripheral blood monocytes can be recruited into tissues and possibly differentiate into potent antigen-presenting cells (APC) displaying foreign antigens complexed with the major histocompatibility complexes (MHCs) on their surface. T-cells recognize these complexes thanks to their T-cell receptors (TCRs) in a process called antigen presentation.

Recently, it has been proposed a nomenclature for monocyte subpopulations in their steady state based on specific surface markers, identifying three subsets: classical, intermediate, and non-classical monocytes (Ziegler-Heitbrock et al., 2010). Monocytes with a classical phenotype, presenting a high expression of CD14 ($CD14^{++}CD16^{-}$), are phagocytic and express genes involved in angiogenesis, coagulation and wound healing (Wong et al., 2011). The non-classical subpopulation is characterized by low expression of CD14 and a high expression of CD16 ($CD14^{+}CD16^{++}$) and is a biomarker of chronic and acute inflammatory diseases. Monocytes with an intermediate phenotype ($CD14^{++}CD16^{+}$) are found with low frequency but they expand in inflammation and have high capacity to release IL-1β, and tumor necrosis factor (TNF)-α in response to lipopolysaccharide (LPS) (Cros et al., 2010).

During inflammation, a wide range of stimuli (including damaged cells, pathogens and cytokines released by macrophages already at the site) can attract monocytes through

chemotaxis in peripheral tissues. At this site, monocytes can uptake antigen and migrate to lymphoid organs, via afferent lymphatics, produce cytokines and inflammatory mediators, and differentiate into APC. Monocytes can synthetize a wide spectrum of inflammatory mediators like TNF, IL-1 and prostaglandin E_2 (Passlick et al., 1989). It has been shown that chemokines produced by inflamed skin can rapidly accumulate in the draining lymph nodes where they directly enhance the recruitment of monocytes from the blood into lymph nodes (Palframan et al., 2001).

Macrophages

Monocytes can differentiate into inflammatory macrophages, which protect tissues from foreign substances. In fact, macrophages recognize structurally conserved molecules expressed by microbes, the so-called pathogen-associated molecular patterns (PAMPs), thanks to a set of Toll-like receptors (TLRs) and scavenger receptors, removing microorganisms, foreign substances, and cell debris via phagocytosis. Their amoeboid movements, helps these professional phagocytes to engulf microbes and migrate in the circulatory fluid. Macrophages have a key role in innate immunity and their help is also critical in the initiation of adaptive immunity as APC recruiting other immune cells like lymphocytes. They can be divided into two main groups: M1 “killer” macrophages, which encourage inflammation, and M2 “repair” macrophages, which, on the contrary, decrease inflammation and encourage tissue repair (Mills, 2012, Murray et al., 2014). The former group, activated by LPS and interferon (IFN)-γ, secretes high levels of IL-12 and low levels of IL-10. The latter participate in wound healing and tissue repair producing high levels of IL-10, TGF-β and low levels of IL-12. Macrophages express specific proteins like CD14, CD40, CD11b and CD64.

Dendritic cells

Steinman and Cohn firstly introduced dendritic cells (DCs) as stellate cells isolated from mouse spleen (Steinman and Cohn, 1973). DCs are derived from hematopoietic bone marrow progenitor cells. Initially, they act as immature dendritic cells, which can recognize pattern recognition receptors (PRRs) through TLRs. DCs serve as messengers between the innate and the adaptive immune systems. In fact, they are APC cells that switch into mature DCs once they meet a presentable antigen, transport it to lymph nodes and present it to T cells.

Langerhans cells represent a specialized population of dendritic cells in human skin, which migrate to the epidermis in response to a gradient of macrophage colony-stimulating factor (M-CSF) and IL-34 produced by epidermal keratinocytes. Langerhans cells are recognized as the major APC of the skin. Indeed, dermal DCs are class II major histocompatibility complex (MHC)-bearing cells which present antigen to T cells and enable their shifting towards T helper 1 (Th1) or Th17 phenotypes under the influence of cytokines, such as IL-12 and TNF (Pasparakis et al., 2014).

1.3.2 Skin inflammation

Inflammation is a complex response of immune system to harmful stimuli which has a key role in many physio/pathological states (Kalden, 1987). Different cell populations are involved in all phases of inflammatory process, including monocytes/macrophages dendritic cells, neutrophils and lymphocytes.

Inflammatory mediators are soluble, diffusible molecules that can act locally or at a distance from the site of tissue damage and infection, and have a key role in inflammation (Medzhitov, 2008). Inflammatory mediators induce vasodilation and increased permeability to allow the migration of leukocytes outside the blood vessels (extravasation or, less commonly called, diapedesis) into the site of injury along a chemotactic gradient. The release of inflammatory mediators is responsible for the five cardinal signs of inflammation which consist in: *rubor* (redness), *calor* (heat), *dolor* (pain), *tumor* (swelling) and *functio laesa* (immobility) (Robbins, 2013).

Based on their biochemical properties, inflammatory mediators can be divided into different groups: vasoactive amines and peptides, fragments of complement components, lipid mediators, proteolytic enzymes and cytokines (Medzhitov, 2008). The latter can be further classified into different groups according to functions, origin and chemical structures: interleukins (ILs), tumor necrosis factors (TNFs), interferons (IFNs), colony-stimulating factors (CSFs), growth factors (GFs) and chemokines (Feliciani et al., 1996).

Skin inflammation occurs when skin is exposed to harmful hazards such as UV radiation, an irritant, or to allergens. The result of these initial “triggering” stimuli is the amplification of a large inflammatory response aimed at the protection of the skin, which may actually cause damages to the skin varying in severity from mild skin rash to severe dermatitis or even cancer development. “Dermatitis” is a general term for any skin inflammation which literally describes

the organ of the skin and indicates the presence of inflammation. The most common types of dermatitis are atopic dermatitis (AD) and contact dermatitis (CD). The former, is a chronic or relapsing inflammatory disease that manifests as immunological abnormalities in which the endogenous component is of great relevance (Briganti and Picardo, 2003).

The latter, instead, can be broadly categorized into allergic contact dermatitis, a cell-mediated hypersensitivity condition that requires an initial sensitizing exposure to the allergen, and irritant contact dermatitis, due to the activation of the skin's innate response system, where no such previous exposure is necessary. Numerous components of the immune system are found within skin, including keratinocytes, resident mast cells, and the dendritic cells of the epidermis, known as Langerhans cells (Bangert et al., 2011; Salmon et al., 1994).

At the cutaneous level, noxious agents, including nanomaterials, could induce a dermatitis involving not only the immune cells but also the epidermal keratinocytes, which could release a series of inflammatory mediators, growth factors, chemotactic factors and cells adhesion molecules (Luo et al., 2015). Therefore, keratinocytes can function as "signal transducers", converting environmental exogenous stimuli into the production and release of inflammatory mediators (Monteiro-Riviere et al., 2014). In particular, keratinocytes play a key role in the initiation and modulation of cutaneous inflammatory reactions, being the major source of cytokines in the epidermis, including: IL-1, -3, -6, -8, granulocyte-macrophage colony stimulating factor (GM)-CSF, granulocyte colony stimulating factor (G)-CSF, macrophage colony stimulating factor (M)-CSF, TNF-α, platelet-derived growth factor (PDGF), TGF-α and -β. Apart from keratinocytes, other skin resident cells can secrete cytokines, including Langerhans cells, melanocytes, and even Merkel cells (Ansel et al., 1990; Hänel et al., 2013). Several agents can mediate the production of cytokines that normally are not actively released by keratinocytes and even cytokines themselves can exert a positive auto-feedback stimulating

their own expression (Ansel et al., 1990). The main cytokines secreted by keratinocytes are briefly described in the following section.

- *Interleukin 1 alpha (IL-1α)* release by keratinocytes is an essential primary event of inflammation (Kupper and Groves, 1995) and stimulates further secretion of inflammatory mediators, including IL-8 (Coquette et al., 2003). It modulates NF-kB pathway and key factors in the regulation of epidermal homeostasis and inflammation (Welss et al., 2004). IL-1α is chemotactic for keratinocytes, induces the expression of keratin 6, decreases bacteria adherence to keratinocytes, and exerts a protective effect against TNF-related apoptosis-inducing ligand (TRAIL)-induced apoptosis. IL-1α also induces accumulation and maturation of dendritic cells in the lymph nodes draining the site of irritation.

- *Interleukin 6 (IL-6)* is released by different cells, including fibroblast, Langherans cells, melanoma cells, monocytes, endothelial cells and keratinocytes. The latter, when unstimulated, usually produce low levels of IL-6 which increase in presence of stimulants, such as IL-1 or injury. IL-6 may increase proliferation of keratinocytes. Several biological effects of IL-1 and IL-6 overlap and synergize in augmenting antigen presentation (Feliciani et al., 1996).

- *Interleukin 8 (IL-8)* plays a key role in the initiation phase of skin inflammation, together with IL-1α. Cellular sources of IL-8 include monocytes, fibroblasts, melanocytes, endothelial cells, keratinocytes, and Langerhans cells. IL-8 is a chemokine that promotes dendritic cells migration and it is also a potent neutrophil chemoattractant (Barker et al., 1991).

.

- *Interleukin 10 (IL-10)* is an anti-inflammatory cytokine and may inhibit the production of other cytokines as well as T-cell proliferation. It is produced by several cells, including macrophages, B cells and keratinocytes (Feliciani et al., 1996). IL-10 may prevent severe damage to the skin as a co-factor in the recovery phase of skin inflammation, by suppressing irritant responses and limiting immunopathologic damage at the skin level (Welss et al., 2004).

- *Tumor necrosis factor alpha (TNF-α)* is a pleiotropic pro-inflammatory cytokine that mediates biological responses such as proliferation and apoptosis. It has a key role in the development of inflammation by inducing the expression of cell adhesion molecules. TNF-α is stored in the epidermal mast cells, monocytes, macrophages, lymphocytes and produced by keratinocytes after stimulation (Welss et al., 2004). TNF-α, being an endogenous pyrogen, can induce fever and cachexia.

- *Interferons* can be divided into group I interferons, which include IFNα, IFNβ and IFNω (interacting with the IFNα receptors, IFNAR), and group II interferons, where IFNγ is the only member (binding to INFγ receptors, IFNGR). IFNs have a many different biological functions, including regulation of cell proliferation and differentiation (Feliciani et al., 1996).

Keratinocytes irritation or sensitization

Irritants and sensitizers (haptens) can initiate similar responses in epidermis. For instance, some sensitizers also show irritant properties. The difference is that a sensitizer owns the ability to induce a specific immune response involving "immunological memory", while an irritant initiates a nonimmunologic, local and reversible inflammatory reaction. The "activation" of keratinocytes, following irritant or sensitizer exposure, leads to inflammatory mediators

expression and release. Those act as signals for recruitment of Langerhans cells and T cells. The resulting pathophysiological signs are erythema, edema, and epidermal scaling and thickening, as summarized in figure 9. In addition, keratinocytes can modulate the inflammatory reaction by the expression of several immune and nonimmune related cell surface receptors, cell adhesion molecules, and ECM factors.

Skin sensitization, resulting in allergic CD, occurs following the exposure to a skin sensitizer which has the ability to induce a cutaneous immune response resulting in immunological priming (sensitization). The four biological phases leading to skin sensitization are described in the Adverse Outcome Pathway (AOP) published by the Organization for Economic Co-operation and Development (OECD) (OECD, 2017):

- *First phase:* usually, a stable association of the sensitizer with protein, forming an hapten-protein conjugate that is recognized and internalized by Langerhans cells, is required.
- *Second phase:* keratinocytes release of pro-inflammatory cytokines and activate cyto-protective pathways.
- *Third phase:* activation and maturation of monocytes, and their migration into the regional lymph nodes induced by cytokines.
- *Forth phase:* in lymph nodes, dendritic cells acquire the properties of mature dendritic cells presenting antigen effectively to naïve T lymphocytes which leads to their differentiation into allergen specific memory T cells. The resulting selective clonal expansion of allergen-responsive T lymphocytes leads to the skin sensitization. During subsequently encounters to the same sensitizer, the acquired “immunological memory”

will result in an accelerated and more aggressive secondary immune response (Casati et al., 2005).

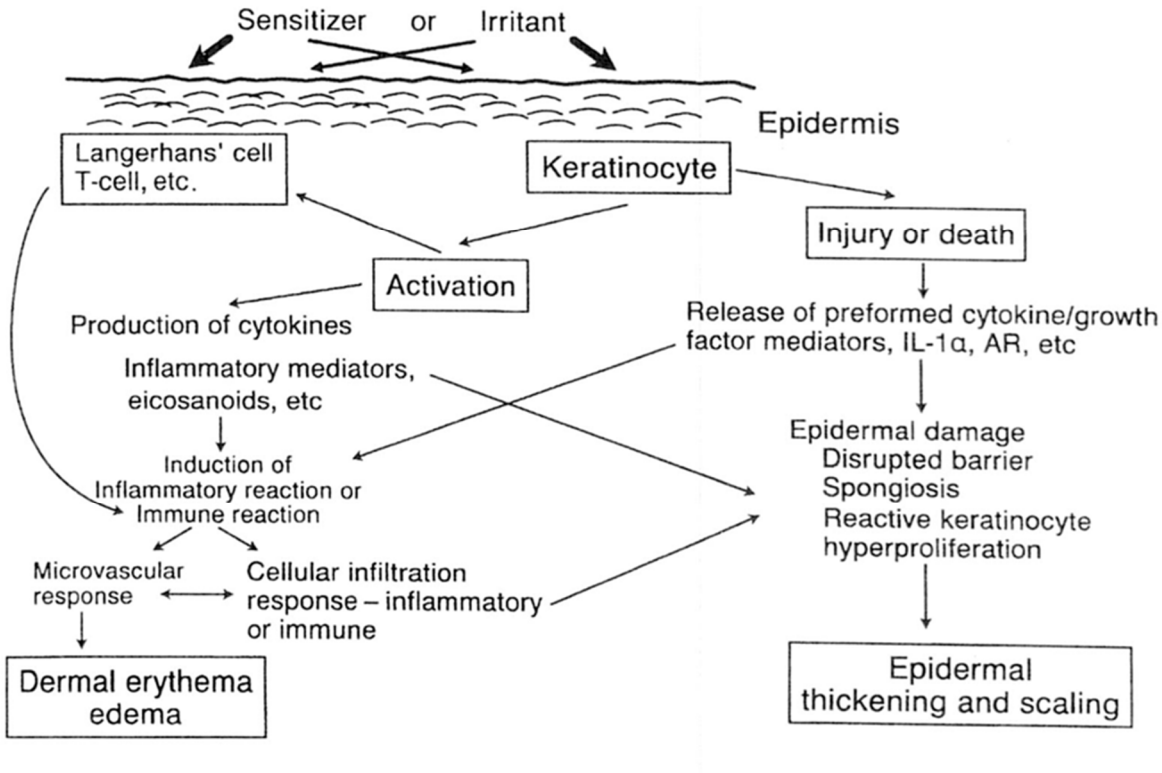

Figure 9. Sequence of cellular and biochemical events following irritant or sensitizing stimuli at the epidermis (Source: Coquette et al., 2000).

2. Aim of the study

Graphene and its related materials, included in the so-called Graphene Family Nanomaterials (GFNs), as the highly-oxidized form of chemically modified graphene (graphene oxide, GO), have extraordinary physicochemical properties, making them promising tools for several applications in the field of nanotechnology and biomedicine. However, safety concerns need to be addressed before mass production of GFNs starts. Indeed, despite the huge interest in GFNs technological progress, their potentially adverse effects on human health are still scarcely elucidated. Humans can be exposed to GFNs by different routes, especially by inhalation, skin, and oral exposures, or even direct injection through biomedical interventions. Among them, skin is one of the most feasible exposure routes to these nanomaterials, especially during their production as dry powders by thermal exfoliation of graphite as well as during their use as bendable or foldable mobile devices, protective coatings and multi-touch screens. Nevertheless, skin toxicity of GFNs remains largely unexplored, despite cutaneous contact to graphite and other carbon nanomaterials have been associated with increased incidence of skin diseases, such as irritant contact dermatitis, hyperkeratosis and naevi (Eedy, 1996; Kasparov et al., 1989). Hence, considering the potential hazards induced by these carbon nanomaterials, the aim of this study was to investigate GFNs effects after cutaneous exposure and to elucidate their putative mechanism(s) of toxicity at the skin level. Thus, an *in vitro* toxicity study had been carried out on spontaneously immortalized human keratinocytes (HaCaT cells), a non-tumor cell line widely used to evaluate toxic effects at the skin level, as a first-round screening of dermotoxicity.

To this aim, a comparative study of four GFNs had been initially carried out. In particular, four different GFNs, differing by size and oxidation state, were considered: a few layer graphene, prepared by ball-milling treatment (FLG), and three samples of graphene oxide (GOs, a research-grade GO1, and two commercial GOs, GO2 and GO3).

As a second step of the project, the putative mechanism underlying their toxicity at the skin level had been elucidated, with a particular focus on the mechanism of mitochondrial damage. To this aim, GFNs were evaluated for their ability to increase reactive oxygen species (ROS) production and induce mitochondrial membrane depolarization, investigating the role of specific ROS-generating enzymes.

Finally, in the last step of the study, the inflammatory effects of GFNs at the cutaneous level had been evaluated *in vitro*. To this aim the effect of GFNs-conditioned HaCaT skin keratinocytes media on monocytes was evaluated to investigate the role of keratinocytes in modulating the inflammatory response at the skin level after GFNs exposure. The inflammatory reaction was evaluated by means of monocytes differentiation and cytokines release. As a final goal, the obtained results were confirmed by the investigation of the sensitizing potential of GFNs on THP-1 monocytes following one of the specific Organisation for Economic Co-operation and Development (OECD) guidelines.

3. Materials and methods

3.1 Chemicals

FLG and GO1 were prepared starting from graphite (from Bay Carbon, Inc. SP-1 graphite powder batch N°04100, lot N°011705, www.baycarbon.com). FLG was prepared by ball-milling treatment of graphite through interaction with melamine (Sigma-Aldrich; Milan, Italy), used as received without further purification, in solvent free conditions (Leon et al., 2011). GO1 was prepared by a modified Hummers' method (Marcano et al., 2010). GO2 and GO3 were obtained from Antolin group (Burgos, Spain, www.grupoantolin.com) and Graphenea group (San Sebastián, Spain, www.graphenea.com), respectively.

All reagents of analytical grade for *in vitro* experiments were purchased from Sigma-Aldrich (Milan, Italy), if not otherwise specified.

Synthesis of FLG and GO:

FLG

The few layer graphene (FLG) used in this study was synthetized by the group of Prof. Ester Vázquez at the Department of Organic Chemistry, Facultad de Ciencias y Tecnologías Químicas-IRICA of the University of Castilla-La Mancha (Ciudad Real, Spain). It was obtained by a technique based on mechanochemical activation by ball-milling treatment, according to published procedures (León et al., 2016; León et al., 2011; León et al., 2014) to exfoliate graphite through interactions with melamine (2,4,6-triamine-1,3,5-triazine). In a typical experiment, 7.5 mg of graphite and 0.16 mmol of melamine were ball-milled in a Retch PM100 Planetary Mill (Haan, Germany) at 100 rpm for 30 minutes in air atmosphere. The resulting solid mixtures were dispersed in 20 mL of Milli-Q-water to produce stable black suspensions. The as-prepared dispersions were filtered and washed in hot water to remove melamine.

Graphene water dispersions were obtained at a final concentration of 0.09 mg/mL in Milli-Q-water.

GO1

The GO1 used in this study was synthetized by the group of Prof. Maurizio Prato at the Department of Chemical and Pharmaceutical Sciences of the University of Trieste (Trieste, Italy). It was prepared using the improved Hummer's method (Marcano et al., 2010). A mixture of concentrated H_2SO_4/H_3PO_4 (180:20 mL), was added into a mixture of powdered graphite (1.5 g) and $KMnO_4$ (1.8 g). Then, the resulting mixture was heated to 50 °C and stirred for 12 h. The reaction was then cooled to room temperature (RT) and poured in ice water (200 mL) with the addition of 30% H_2O_2 (0.5 mL). The mixture was filtered and washed with water. The resulting wet solid was re-dissolved in water (200 mL) and dialyzed until neutral pH and colorless aqueous solution was observed. The dialyzed suspension was centrifuged (4000 rpm, 1 h) to separate the graphite material. The supernatant was filtered and washed with ethyl ether, obtaining 2.6 g of brown solid material.

Endotoxin removal:

To obtain FLG-endotoxin free samples, the nanomaterial was lyophilized as reported elsewhere (León et al., 2016), and the FLG powder was subsequently treated in the thermogravimetric analysis (TGA; Q50 instrument) using the following program: ramp 10ºC/min to 129ºC, isothermal for 20 min and ramp 2ºC/min to 25ºC.

Concerning GO3, the endotoxin removal was performed by heat treatment of samples at 200°C for 1 h in a protective Argon atmosphere.

3.2 Cells culture

3.2.1 HaCaT cells (immortalized human skin keratinocytes)

HaCaT cells were purchased from Cell Line Service (DKFZ; Eppelheim, Germany) and cultured in Dulbecco's Modified Eagle's medium (DMEM) high glucose, supplemented with 10% fetal bovine serum (FBS), $1.0x10^{-2}$ M L-Glutamine, $1.0x10^{-4}$ g/mL penicillin and $1.0x10^{-4}$ g/mL streptomycin at 37°C in a humidified 95% air/5% CO_2 atmosphere. Cell passage was performed 2 days post-confluence, once a week. All the experiments were performed between passage 44 and 70.

3.2.2 THP-1 cells (human undifferentiated monocytes)

THP-1 cells were purchased from ATCC (Manassas, USA) and cultured in RPMI-1640 supplemented with 10% fetal bovine serum (FBS), $1.0x10^{-2}$ M L-glutamine, $1.0x10^{-4}$ g/mL penicillin and $1.0x10^{-4}$ g/mL streptomycin at 37°C under a humidified 95% air/5% CO_2 atmosphere. Cell passage was performed twice a week. All the experiments were performed between passage 7 and 20. As positive controls were added: 10^{-7} M phorbol-12-myristate-13-acetate (PMA) for 72 h (Auwerk, 1991; Gutowska et al., 2010) to differentiate THP-1 monocytes into macrophages; a mix of 100 ng/mL interleukin (IL)-4 and granulocyte-macrophage colony-stimulating factor (GM-CSF) for 120 h (Berges et al., 2005) to differentiate THP-1 monocytes into immature dendritic cells (iDCs); and a mix of 200 ng per mL IL-4, 100 ng/mL GM-CSF, 10 ng/mL tumor necrosis factor-α (TNF-α) and 200 ng/mL ionomycin in serum-free medium for 48 h (Berges et al., 2005) to differentiate THP-1 monocytes into mature dendritic cells (mDCs).

3.3 Spectroscopic tests

3.3.1 WST-8 reduction assay

Cells were seeded overnight at a density of 5×10^3 cells/well in 96-wells plates and exposed to FLG or GOs (0.005 - 100 μg/mL) for different exposure times (24 up to 72 h). Then, cells were washed three times with phosphate buffered saline (PBS; 200 μL/well) and incubated for 4 h with fresh culture medium (100 μL/well) containing 10 μL of 2-(2-methoxy-4-nitrophenyl)-3-(4-nitrophenyl)-5-(2,4-disulfophenyl)-2H-tetrazolium (WST-8) reagent to measure mitochondrial activity. Absorbance was subsequently read at 450 nm by an Automated Microplate Reader EL 311 s (Bio-Tek Instruments, Winooski, VT, USA). Data are reported as % of mitochondrial activity in cells exposed to FLG or GOs with respect to untreated control cells and are the mean ± SE of 3 independent experiments performed in triplicate.

3.3.2 Sulforhodamine B assay

Cells were seeded overnight at a density of 5×10^3 cells/well in 96-wells plates and exposed to FLG or GOs (0.005 - 100 μg/mL) for different exposure times (24 up to 72 h). Then, cells were washed three times with PBS (200 μL/well), fixed with 50% (v/v) trichloroacetic acid for 1 h at 4 °C and stained for 30 min with 0.4% sulforhodamine B (SRB) solution in 1% (v/v) acetic acid. After washings with 1% (v/v) acetic acid, the protein-bound dye (an index of cell mass extrapolated to measure cell proliferation) was dissolved in 10 mM TRIZMA base solution and the absorbance was read by an Automated Microplate Reader EL 311 s (Bio-Tek Instruments, Winooski, VT, USA) at 570 nm. Data are reported as % of cell proliferation after FLG or GOs

exposure with respect to untreated control cells and are the mean ± SE of 3 independent experiments performed in triplicate.

3.3.3 NBT assay

Cells were seeded overnight at a density of 5×10^3 cells/well in 96-wells plates and exposed to FLG or GO (0.4 - 100 μg/mL) for 24 h. Then, cells were washed three times with PBS (200 μL/well) before adding fresh medium (100 μL/well) containing Nitro Blue Tetrazolium (NBT; final concentration of 0.5 mg/mL) to measure reactive oxygen species (ROS). After 4 h, the diformazan crystals were solubilized by 140 μL of DMSO and 120 μL of 2 M KOH. 2,2-azobis(2-amidinopropane) dihydrochloride (AAPH) 1 mM was included as a positive control. The absorbance was read by an Automated Microplate Reader EL 311s (Bio-Tek Instruments, Winooski, VT, USA) at 630 nm. Data are expressed as % of ROS production with respect to untreated controls and are the mean ± SE of at least 3 independent experiments performed in triplicate.

3.4 Fluorimetric tests

3.4.1 Propidium iodide uptake

Cells were seeded overnight at a density of 5×10^3 cells/well in 96-wells plates and exposed to FLG or GOs (0.005 - 100 μg/mL) for different exposure times (24 up to 72 h). Then, cells were washed three times with PBS (200 μL/well) and exposed to $3.0\text{x}10^{-6}$ M propidium iodide (PI) in PBS for 30 min at 37 °C. As a positive control, 4 μl of 0.1% (v/v) Triton-X in PBS were added. Fluorescence intensity was read by a Fluorocount Microplate Fluorometer (Packard, Germany) with excitation wavelength of 485 nm and emission wavelength of 590 nm. Each sample was subsequently permeabilized by 0.1% Triton-X for 30 min to measure total fluorescence (index of total cell content). Data are reported as % of PI with respect to positive control cells, after normalization on cell content, and are the means ± SE of 3 independent experiments performed in triplicate.

3.4.2 DCFDA probe

Cells were seeded overnight at a density of 1×10^4 cells/well in 96-wells plates and subsequently incubated with medium (200 μL/well) containing 2',7'-dichlorofluorescin diacetate (DCFDA; final concentration 100 μM) for 30 min at 37 °C in the dark. Cells were then washed twice with PBS with Ca^{2+} and Mg^{2+} (200 μL/well) and exposed to FLG or GO (0.4 - 100 μg/mL) in complete medium without phenol red for increasing exposure times (3-72 h). (AAPH) 1 mM was included as a positive control. Fluorescence was read after increasing intervals of time by a Fluorocount Microplate Fluorometer (Packard, Germany) with excitation wavelength of 485 nm and emission wavelength of 570 nm to measure ROS production. Data are expressed as %

of ROS production with respect to untreated controls and are the mean ± SE of at least 3 independent experiments performed in triplicate.

3.4.3 JC-1 probe

Cells were seeded overnight at a density of 5×10^3 cells/well in 96-wells plates and exposed to FLG or GOs for increasing exposure times (24 up to 72 h). Then, cells were washed three times with PBS (200 µL/well) and incubated for 20 minutes at 37°C with 100 µL/well working solution of 0.5 µM JC-1 (JC-1 Mitochondrial Staining Kit; Sigma-Aldrich; Milan, Italy). As positive control, 0.1 µg/mL valynomicin was used. Cells were then washed twice with ice-cold culture medium and fluorescence was immediately measured by a Fluorocount Microplate Fluorometer (Packard, Germany). Red fluorescence given by JC-1 aggregates (intact mitochondria) was detected with an excitation wavelength of 530 nm and an emission wavelength of 590 nm whilst the green fluorescence given by JC-1 monomers (disrupted mitochondria) with a 485 nm and 570 nm filter combination. Data are the mean ± SE of 3 independent experiments performed in triplicate and presented as % of JC-1 fluorescence shift with respect to untreated control cells calculated on the ratio between red (530/590 nm) and green (485/570 nm) fluorescence.

3.5 Chemiluminescence tests

3.5.1 Luminol assay

Cells were seeded overnight at a density of 1×10^4 cells/well in 96-wells plates and exposed to FLG or GO (0.4 - 100 μg/mL) for 24 h before adding luminol (1 μM, final concentration) to each well. AAPH 1 mM was included as a positive control. Chemiluminescence was recorded 15 minutes after luminol addition by a multi-well Luminometer (Wallac 1450 Microbeta counter, PerkinElmer, Milan, Italy) to measure ROS poduction. Data are expressed as % of ROS production with respect to untreated controls and are the mean ± SE of at least 3 independent experiments performed in triplicate.

3.6 Epifluorescence microscopy analysis

Cells were seeded overnight at a density of 5×10^4 cells/well in 24-wells plates. After staining of plasma-membrane with 1 μM 1,1′-Dioctadecyl-3,3,3′,3′-tetramethylindocarbocyanine perchlorate (DiL), cells were exposed to FLG or GOs (10 μg/mL) for 72 h. Subsequently, cells were washed three times with PBS (1 mL/well), fixed in 4% paraformaldehyde (PFA) for 30 min at RT, and washed twice with PBS (1 mL/well). Samples were mounted in mowiol on coverslips of 1 mm thickness. Cell membrane morphology was observed by an epifluorescent microscope (Eclipse E800, Nikon) at 60x magnification.

3.7 Confocal microscopy analysis

Cells were seeded overnight at a density of 5×10^4 cells/well in 24-wells plates. After staining of plasma-membrane with 1 μM DiL, cells were exposed to FLG or GOs (10 μg/mL) for 72 h.

Cells were then washed three times with PBS (1 mL/well), fixed in 4% PFA for 30 min at RT and washed twice with PBS (1 mL/well). Samples were mounted in mowiol on coverslips of 1 mm thickness. Images were taken by a confocal microscope (Eclipse C1si, on an inverted microscope TE2000U, Nikon) at 60x magnification. FLG and GOs were visualized by the reflection mode property during the confocal acquisitions. Reconstructions of the images were performed offline using the image-processing package Fiji.

3.8 Transmission electron microscopy (TEM)

For TEM analyses, cell culture media (Dulbecco's Modified Eagle Medium, DMEM) dispersions of FLG or GOs were diluted as necessary and dip-cast on a Lacey copper grid (3.00 mm, 200 mesh, coated with carbon film), and dried under vacuum. Samples were analyzed by High-Resolution Transmission Electron Microscopy (HRTEM) JEOL 2100. Lateral dimension distribution was carried out using Fiji-win32.

3.9 TNF-α expression test (TET) assay

After endotoxin removal from GO by heat treatment at 200°C for 1 h in a protective Argon atmosphere, TNF (tumor necrosis factor)-α expression test (TET) was carried out to detect the LPS contamination of GO. In this assay, the difference between the TNF-α expression induced by GO with or without the endotoxin inhibitor polymyxin B (Poly-B) sulfate corresponds to the endotoxin present in the sample.

3.9.1 Isolation of primary monocytes and differentiation to human monocyte-derived macrophages (HMDM)

Peripheral blood mononuclear cells (PBMC) were isolated from buffy coats from healthy human blood donors (Karolinska University Hospital; Stockholm, Sweden) by density gradient centrifugation using Lymphoprep™ (Axis-Shield; Oslo, Norway). Subsequently, monocytes were purified from peripheral blood mononuclear cells (PBMCs) by positive selection based on CD14 expression using CD14 MicroBeads (Miltenyi Biotec; Bergisch Gladbach, Germany). To obtain human monocyte-derived macrophages (HMDM), CD14+ monocytes were seeded in 96-well plates and cultured in RPMI-1640 cell medium supplemented with 2 mM L-glutamine, 100 IU/mL penicillin, 100 µg/mL streptomycin, and 10% heat inactivated FBS, supplemented with 50 ng/mL recombinant macrophage colony-stimulating factor (M-CSF) (Novakemi, Handen, Sweden) for three days.

3.9.2 Alamar Blue assay

HMDM were exposed to GO (12.5 - 75 µg/mL) or to 5% DMSO (positive control) for 24 h and cell viability was evaluated by the Alamar Blue (AB) assay. Briefly, after cells exposure to GO,

the culture medium was removed and cells were incubated for 2 h with fresh RPMI-1640 medium (100 µl) containing 10 % AlamarBlue® reagent (v/v). Fluorescence was subsequently measured at the respective excitation and emission wavelength of 531 nm and 595 nm, using a Tecan Infinite F200 plate reader. Data are reported as % of cell viability of cells exposed to GO with respect to untreated control cells and are the mean ± SE of 3 independent experiments performed in triplicate.

3.9.3 Endotoxin detection

HMDM were incubated with GO (25 - 50 µg/ml) in presence or absence of Poly-B (10 µM) for 24 h. LPS (0.1 µg/mL) was included as a positive control. Subsequently, the culture media were collected and the secretion of TNF-α was quantified by a commercial ELISA kit according to the manufacturer's instruction (MABTECH; Nacka Strand, Sweden). To quantify the endotoxin present in the GO sample, a standard curve was generated based on LPS (0.0001 - 0.1 µg/mL)-induced TNF-α expression by HMDM.

3.10 Inflammatory mediators release

3.10.1 Cytokines release from HaCaT cells

The effect of sub-cytotoxic concentrations of FLG and GO on inflammatory mediators release by HaCaT cells was evaluated using the Procarta Plex Mix & Match kit (eBioscience). The sub-cytotoxic concentrations of FLG and GO (0.01, 0.1 and 1.0 μg/mL) and cells exposure conditions were chosen on the basis of preliminary cytotoxic assays (WST-8) carried out on HaCaT cells. HaCaT cells were seeded overnight at a density of 1×10^4 cells/well in 48-wells plates and exposed to FLG or GO (0.01, 0.1 and 1.0 μg/mL) for 4, 24 and 72 h (continuous exposure). Alternatively, cells were exposed to FLG or GO (0.01, 0.1 and 1.0 μg/mL) for 4 h, washed three times with PBS (200 μL/well) and incubated for additional 20 or 68 h in fresh media without FLG or GO (recovery exposure). Control cells were cultured in FLG- and GO-free medium. Thereafter, the supernatant was collected to quantify the release of following panel of inflammatory mediators: IL-1α, IL-6, IL-8, IL-10, interferon (IFN)-α, macrophage inflammatory protein (MIP)-1β, TNF-α, and GM-CSF. The analysis was performed by the IRCCS Burlo Garofalo of Trieste (Italy), using the Procarta Plex immunoassay based on Luminex® technology.

3.10.2 Cytokines release from THP-1 cells

THP-1 cells were seeded at a density of $2x10^5$ cells/well in 24-well plates and exposed overnight to HaCaT cells-conditioned media collected after recovery conditions (4 h exposure to 0.1 or 1.0 μg/mL FLG or GO, followed by 20 or 68 h culture in fresh medium) or control HaCaT cells-conditioned media, followed by 24 h culture in fresh media. Subsequently, the supernatants were collected and kept at -80° C. The following inflammatory mediators, released

by THP-1 cells in culture media, were quantified by Luminex® system using Bio Plex Pro™ human cytokine standard 27-plex, Group I kit (BioRad; Solna, Sweden) according to the manufacturer's instructions: interleukin-1 receptor antagonist (IL-1Ra), IL-1β, IL-2, IL-4, IL-5, IL-6, IL-7, IL-8, IL-9, IL-10, IL-12, IL-13, IL-15, IL-17, Eotaxin, basic fibroblast growth factor (FGF basic), G-CSF, GM-CSF, IFN-γ, interferon gamma-induced protein (IP-10), monocyte chemoattractant protein (MCP)-1, platelet-derived growth factor (PDGF)-BB, Regulated on Activation Normal T Cell Expressed and Secreted (RANTES), TNF-α, vascular endothelial growth factor (VEGF), MIP-1α and -1β .

3.11 Flow cytofluorimetry analysis

THP-1 cell differentiation was evaluated by the expression of specific differentiation markers (CD14, CD54, CD86, CD11b and HLA-DR). Cells were labeled with specific fluorescent mouse monoclonal antibodies (mAbs) conjugated with: Alexa Fluor 700 specific for CD14; PE-CyTM 5 specific for CD54; fluorescein isothiocyanate (FITC) specific for CD86; and with phycoerythrin (PE) specific for HLA-DR and CD11b, according to the manufacturer's instructions (BD Pharmingen™, San Diego, CA, USA).

THP-1 cells ($2x10^5$ cells/well) were seeded in 6-well plates and exposed to HaCaT-conditioned media after recovery conditions (4 h exposure to 0.1 or 1.0 µg/mL FLG or GO followed by 20 or 68 h culture in fresh medium) or control HaCaT-conditioned media for 48 and 120 h. Subsequently, cells were collected using a cell scraper, washed with PBS and fixed with 1 mL of 4% paraformaldehyde for 30 minutes at 4 °C. Cells were then washed with 1 mL of PBS and the pellet was suspended in 50 µl of FACS buffer (0.5% bovine serum albumin, BSA, and 0.01% sodium azide in PBS) in presence of 4% Fc receptor blocking reagent (Miltenyi Biotec, Auburn, CA, USA) in which 3 µL of each antibody targeting the considered markers were added. Cells were incubated with antibodies at 4 °C for 30 minutes and subsequently washed with 300 µL of FACS buffer. The pellet was then suspended in 300 µL of FACS buffer. Fluorescence was measured with a BD LSRFortessa™ Cell Analyzer (BD Biosciences). Ten thousand cells were counted and analyzed by the BD FACSDiva Software (BD Biosciences). To ensure that the fluorescent signal detected was due to the mAbs of interest, for each fluorochrome a process of compensation was applied to remove the signal falling within the detector of another fluorochrome by using Compbeads® (BD Biosciences).

3.12 Human Cell Line Activation Test (h-CLAT)

To verify the potential sensitizing properties of FLG and GO, the human Cell Line Activation Test (h-CLAT) was carried out following the specific Organization for Economic Co-operation and Development (OECD) guidelines 442E (OECD 442E). The h-CLAT assay is able to predict the sensitizing properties during the third phase of the sensitization process (monocytes activation). In particular, the expression of cells surface markers CD86 and CD54 associated with the activation of THP-1 cells (Yoshida et al., 2003) was evaluated after cells exposure to FLG or GO for 24 h. The assay was divided in three steps:

Reactivity check

Two weeks after thawing, the reactivity check of THP-1 cells was performed using the known allergen 2,4-dinitrochlorobenzene (DNCB; 4 μg/mL), as positive control, and the non-allergen lactic acid (LA) 1500 μg/mL as negative control. Only the cells which passed the reactivity check, showing a positive response for both CD86 and CD54 cell surface markers induced by DNCB, and a negative response for both CD86 and CD54 cell surface markers induced by LA, were used in the following steps.

Dose finding assay

The dose finding assay identifies the concentration of the test substance resulting in 75% of cell viability (CV75), as compared to the solvent/vehicle control, used to determine the concentrations range for the CD86/CD54 expression measurement. The dose finding assay is carried out using a fixed concentration range of the test substance (7.81 - 1000 μg/mL) to evaluate PI uptake cytofluorimetrically. However, due to the low cytotoxicity of GFNs

observed in the dose finding assay, it was not possible to calculate the CV75 for these materials. Therefore, 12 μg/mL was selected as starting concentration to determine 8 concentrations of FLG and GO (3.4 - 12 μg/mL) using a 1:1.2 dilution factor. The starting concentration was chosen on the basis of the OECD guidelines, suggesting that, if the CV75 cannot be determined, the highest stably dispersed concentration of test chemical should be used as starting concentration to determine the range of concentrations to test.

Cell staining and analysis

THP-1 cells were seeded at a density of $0.2x10^6$ cells/mL, and cultured for 48 h. The day of the test, cells were seeded at a density of $1x10^6$ cells/well in 24-wells plates and exposed to 8 concentrations of FLG or GO (3.4 - 12 μg/mL) for 24 h. The final concentration of DMSO, used as a solvent, in culture media was less than 0.2%. Subsequently, cells were washed twice with 1 mL of staining buffer (0.1% BSA in PBS) and suspended in 600 μL of staining buffer for 30 min at 4 °C, containing 5 μL of anti-human CD86 and CD54 antibodies (Sigma Aldrich) conjugated with FITC. Subsequently, cells were washed three times with 300 μL of staining buffer, collected in cytofluorimetric tubes, and expression of cell surface antigens was analyzed by flow cytometry. Dead cells were revealed by staining with PI (0.625 μg/mL). DNCB (4 μg/mL) and LC (1000 μg/mL) were added as a positive and negative control, respectively.
Flow cytometry was performed with a FACScalibur (Becton Dickinson; Milan, Italy), equipped with an air-cooled 15-mW Argon-ion laser, operating at 488 nm. FITC Green fluorescence (FL1) was collected using a 530 ± 30 bandpass filter, red fluorescence emitted from PI (FL3) was collected by using a 650 ± 13 bandpass filter. The data were collected using linear amplification for FSC and SSC, and logarithmic amplification for FL1 and FL3. Ten thousand cells were counted and analyzed per sample. The data were then analyzed by using CellQuest

software (Becton Dickinson). Markers were used to identify positive cells. Based on the geometric mean of fluorescence intensity (MFI), the relative fluorescence intensity (RFI) of CD86 and CD54 for positive control cells and chemical-treated cells were calculated according to the guideline instructions. The test chemical can be considered a sensitizer when two independent experiments satisfy the acceptance criteria reported in the guideline (CD54 RFI ≥ 200% and CD86 RFI ≥ 150%, cell viability ≥ 50%, assessed by PI uptake).

-

3.13 Statistical analysis

Cytotoxicity data (mitochondrial and plasma membrane damage, cell proliferation and ROS production) are presented as mean ± SE from at least three independent experiments performed in triplicate. Statistical analysis was performed by a two-way ANOVA followed by Bonferroni's post test (PrismGraphPad, Inc.; San Diego, CA, USA) and statistical significance was considered for $p < 0.05$. Non-linear regression of concentration-effect data was performed using GraphPad Prism version 4.00 for computing the concentration giving the 50% of the effect (EC_{50}). Statistical differences among EC_{50} values were evaluated by Student t-test (significant differences, $p < 0.05$). Data obtained by long-term analysis were analyzed by a one-way ANOVA analysis followed by Bonferroni's post-test (PrismGraphPad, Inc.; San Diego, CA, USA) and significant differences were considered at $p < 0.05$.

Cell differentiation and inflammatory mediator data were analyzed by one-way ANOVA and Bonferroni post-test (PrismGraphPad, Inc.; San Diego, CA, USA) and differences were considered significant at $p < 0.05$. Hierarchical cluster analysis was performed by the group of Prof. Bengt Fadeel at the Institute of Environmental Medicine (IMM) of the Karolinska Institutet (Stockholm, Sweden), similarly as performed using R-program (version 3.3.2) in earlier study (Bhattarcharya, 2017).

4. Results and discussion

4.1 FLG and GOs characterization

A few layer graphene (FLG), prepared by ball-milling treatment, according to published procedures (León et al., 2016; León et al., 2011; León et al., 2014), and three samples of graphene oxide (GOs), a research-grade GO1, prepared by the improved Hummer's method, and two commercial GOs (GO2 and GO3), were characterized by Prof. Ester Vázquez group at the Department of Organic Chemistry, Facultad de Ciencias y Tecnologías Químicas-IRICA of the University of Castilla-La Mancha (Ciudad Real, Spain).

In particular, the four GFNs were thoroughly characterized by High-Resolution Transmission Electron Microscopy (HRTEM) to determine the influence of the lateral dimension on their cytotoxicity. The lateral dimension distribution analysis of the corresponding GFNs in culture medium (Figure 10) showed that FLG and GO1 possess the smallest lateral sizes, with average lateral dimensions of 552 and 622 nm, respectively. The size of GO2 and GO3 was higher than that of the previous materials, corresponding roughly to double lateral dimensions compared to FLG.

Further characterization was carried out by the University of Castilla-La Mancha to determine also the influence of the four GFNs chemical composition on their toxicity. The chemical composition, carbon/oxygen (C/O) ratio and type of oxygen-containing functional groups were determined by elemental analysis (Table 1, appendix), TGA (Figure 1, panel A, appendix), and XPS spectroscopy (Figure 2, appendix). As expected, FLG did not show a significant amount of oxygen content, whereas GO1, GO2 and GO3 exhibited a large and similar content of oxygen groups. Moreover, the quality of graphene layers was monitored by Raman spectroscopy (Ferrari and Basko, 2013) corroborating the low number of defects generated by the ball milling treatment in comparison with the strong oxidation conditions used to prepare GO derivatives (Figure 1, panel B, appendix).

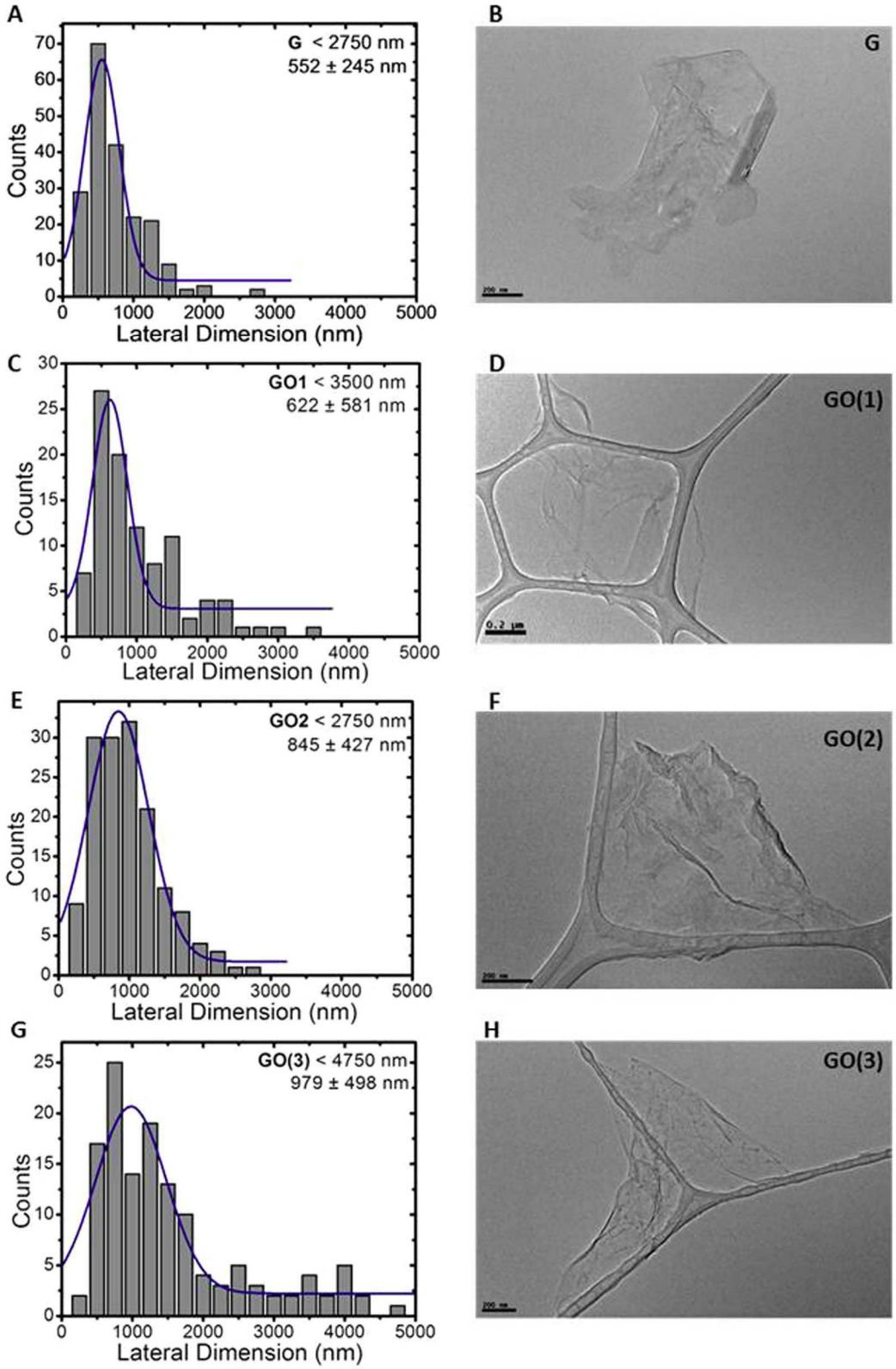

Figure 10. Lateral dimension distribution from TEM images (A, C, E, G) and representative TEM images (B, D, F, H) of GFNs in culture medium. Scale bar 200 nm.

4.2 Comparative cytotoxicity of graphene (FLG) and graphene oxides (GOs) toward skin HaCaT keratinocytes

The cytotoxicity of FLG and GOs toward HaCaT cells was evaluated by different *in vitro* assays able to measure cell viability by means of mitochondrial activity (WST-8 assay), cell proliferation (SRB assay) and plasma membrane integrity (PI uptake). Considering that it is very difficult to predict a potential human exposure since no industrial-scale adoption of graphene has taken place, so far (Bussy et al., 2015), cells were treated with a range of concentrations of FLG or GOs (0.005 - 100 μg/mL), expressed as mass per volume, that was chosen on the basis of literature, according to their physicochemical properties. However, the biokinetics *in vitro* of these nanomaterials could affect the real exposure concentrations of the cells due to a possible adsorption of these nanomaterials to the vials or microplates plastic. Moreover, it must be considered that the interaction with fetal bovine serum can mitigate the cytotoxicity by the formation of a protein corona preventing the direct contact of GFNs with cell membranes (Mukherjee et al., 2017).

4.2.1 Effects of FLG and GOs on HaCaT cells mitochondrial activity

The physicochemical proprieties of GFNs, their shape, size, surface functionalization, layers number as well as starting material used for their production could influence their biological and toxicological properties (Monteiro-Riviere and Inman, 2006; Wick et al., 2014). Thus, the cytotoxic effects of FLG and GOs were investigated toward human HaCaT skin keratinocytes, a widely used *in vitro* model for first round screening of dermotoxic substances (Gibbs, 2009). Initially, FLG and GOs (0.005 - 100 μg/mL) were evaluated for their effect on cell viability by means of mitochondrial activity after different exposure times (24 up to 72 h). To fulfill this

aim, the WST-8 assay was preferred to the most common methylthiazolyldiphenyl-tetrazolium bromide (MTT) assay, since the latter fails to predict the toxicity of GFNs because of the spontaneous reduction of MTT reagent by GFNs, resulting in an overestimation of cell viability due to a false positive signal (Liao et al., 2011). The cytotoxic effect of 24, 48 and 72 h HaCaT cells exposure to FLG or GOs is represented in Figure 11. The less oxidized GFN (FLG; 0.005 - 100 μg/mL) did not show any significant cytotoxic effect after 24 h exposure (Figure 11, panel A), whereas after 48 and 72 h exposure it significantly reduced mitochondrial activity: 48 h exposure reduced mitochondrial activity at the concentration of 30 μg/mL (16% reduction) and above (Figure 11, panels B and C). The most oxidized GFN (GO3) exerted a significant cytotoxic effect already after 24 h exposure (Figure 11, panel A), inducing a significant reduction of mitochondrial activity at the concentration equal or higher than 3 μg/mL (25% reduction). After 48 and 72 h exposure, GO3 significantly reduced mitochondrial activity at the concentration of 3 μg/mL (38 and 41% reduction, respectively) and above (Figure 11, panels B and C). Due to the relatively low cytotoxic effects observed after 24 and 48 h, it was not possible to calculate the concentrations of FLG and GO3 reducing mitochondrial activity by 50% (EC_{50}), which were computed only prolonging the exposure time to 72 h: EC_{50} were equal to 62.8 μg/mL (95% confidence intervals, CI = 53.8 - 73.3 μg/mL) and 5.4 μg/mL (95% CI = 2.2 - 12.9 μg/mL) for FLG and GO3, respectively. The significant difference between the two EC_{50} values ($p < 0.001$) demonstrates that FLG is significantly less potent than GO3 in reducing mitochondrial activity, being twelve times less active, suggesting a role of the oxidation state of the GFNs in their cytotoxic potential.

Panels D - F of figure 11 show the effect of similarly oxidized GFNs differing by lateral dimensions (GO1, GO2 and GO3) after 24 (panel D), 48 (panel E) and 72 h of exposure (panel F). Each GO was significantly effective already after 24 h exposure, inducing a significant

reduction of the mitochondrial activity starting at concentrations of 3 μg/mL (21% and 25% reduction for GO1 and GO3, respectively) and 10 μg/mL (29% reduction for GO2). The relatively low cytotoxic effects allowed the computation of the EC_{50} values of these GFNs only after 72 h exposure, which were equal to 12.9 μg/mL (95% CI = 7.1 - 23.4 μg/mL), 18.6 μg/mL (95% CI = 12.2 - 28.2 μ g/mL) and 5.4 μg/mL (95% CI = 2.2 - 12.9 μg/mL) for GO1, GO2 and GO3, respectively. A significant difference ($p < 0.05$) was recorded only between GO2 and GO3 EC_{50}, suggesting that the cytotoxic potential of these GFNs is only partially influenced by the lateral dimension of the material. In addition, this significance could rise from the presence of large flakes (> 2 μm) mainly for GO3.

These results are in agreement with previous studies on human umbilical vein endothelial cells (HUVEC), showing an association between the reduction of oxygen content and a reduced oxidative stress-dependent cytotoxicity of GOs (Das et al., 2013). On the other hand, Liao and coworkers (2011) suggested that a reduction of the oxidation state of GO could imply a stronger cytotoxicity on fibroblasts (Liao et al., 2011). However, as discussed by Das et al. (Das et al., 2013), these diverging data could be related to dissimilar nanomaterials properties, such as size, shape or different synthetic procedures. Indeed, the graphene used by Liao and co-workers was produced by acidic dehydration of GO, a material presenting a high number of defects and oxygen containing groups. This aspect, together with its irreversible aggregation observed in culture medium, resulting in a significantly larger material (about 4 μm) (Liao et al., 2011), impaired a direct comparison with our data. Corroborating this suggestion, GO3, the most effective compound, shows the largest average dimension, due to the presence of flakes larger than 2 μm, scarcely present in the other materials. This observation suggests that also the size could be a critical feature, even though further studies are needed to clarify this aspect. On the

contrary, it seems that the use of carbon fibers as starting material, such as in the case of GO2, does not significantly influence the cytotoxicity of the material.

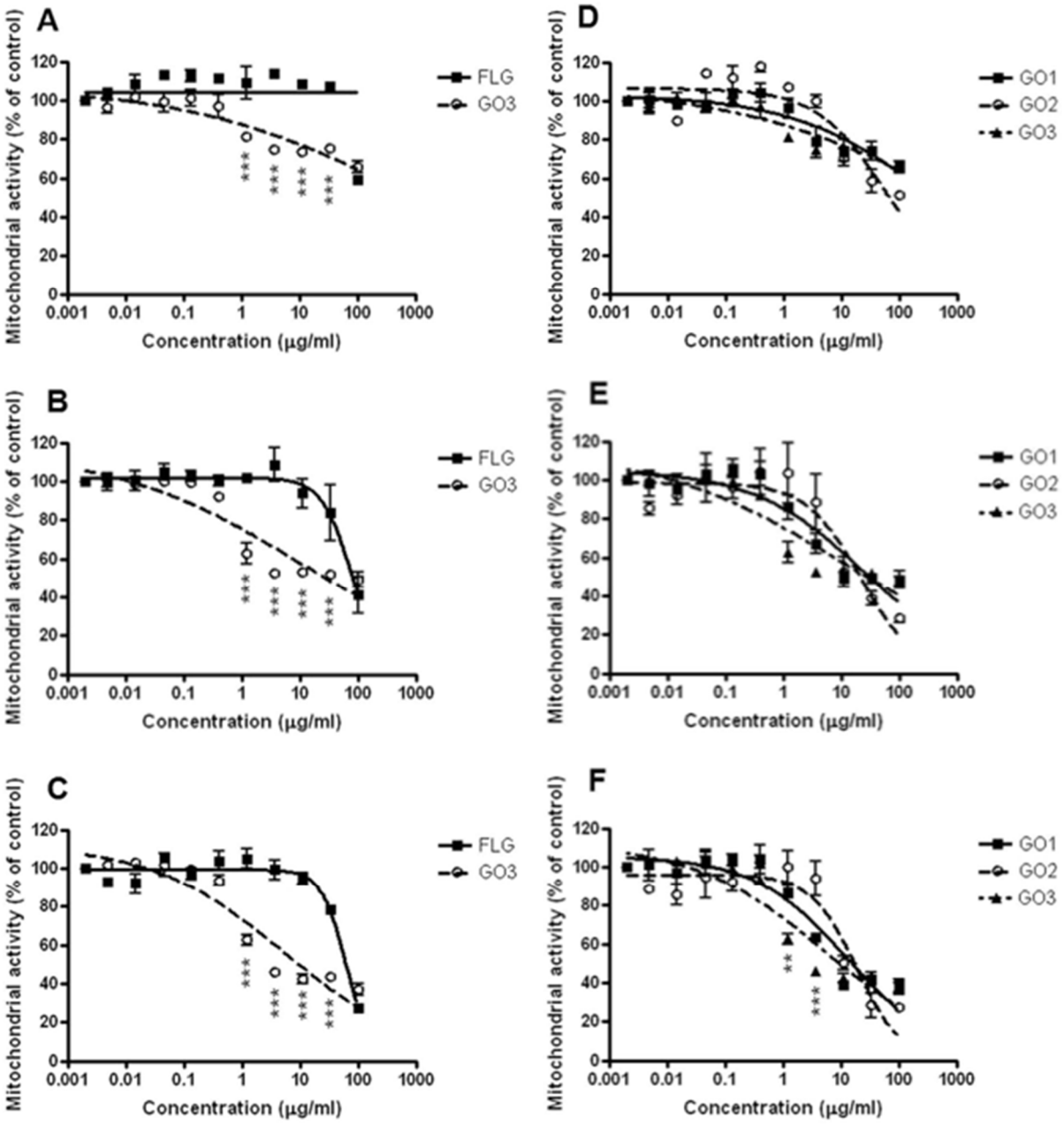

Figure 11. Effect of FLG and GOs (0.005 to 100 µg/mL) on mitochondrial activity of HaCaT cells evaluated by the WST-8 assay. Comparison between the less (FLG) and most (GO3) oxidized GFNs after 24 h (A), 48 h (B) and 72 h (C) exposure. Comparison between similarly

oxidized GFNs differing by average lateral dimension (GO1, GO2, GO3) after 24 h (D), 48 h (E) and 72 h (F) exposure. Data are the mean ± SE of 3 independent experiments performed in triplicate. Statistical differences: **p < 0.01; ***p < 0.001 (Two-way ANOVA and Bonferroni's post test).

4.2.2 Effects of FLG and GOs on HaCaT cells proliferation

Intriguingly, the significant mitochondrial activity reduction in HaCaT cells exposed to FLG or GOs does not seem to imply a reduced cell proliferation, as demonstrated by the SRB assay. In fact, HaCaT cells exposure to FLG or GOs for 24 and 48 h did not induce any significant effects on cell proliferation. Even increasing the exposure time up to 72 h, only the highest concentration (100 μg/mL) induced a slight reduction of cell proliferation, equal to 24, 15, 12 and 22% for FLG, GO1, GO2 and GO3, respectively (Figure 12). These results are in line with previous studies showing very weak cytotoxic and anti-proliferative effects of some GFNs, such as graphene films (Ryoo et al., 2010) and GO (Jaworski et al., 2015) in murine NIH-3T3 fibroblasts or U87 and U118 glyoma cells, respectively.

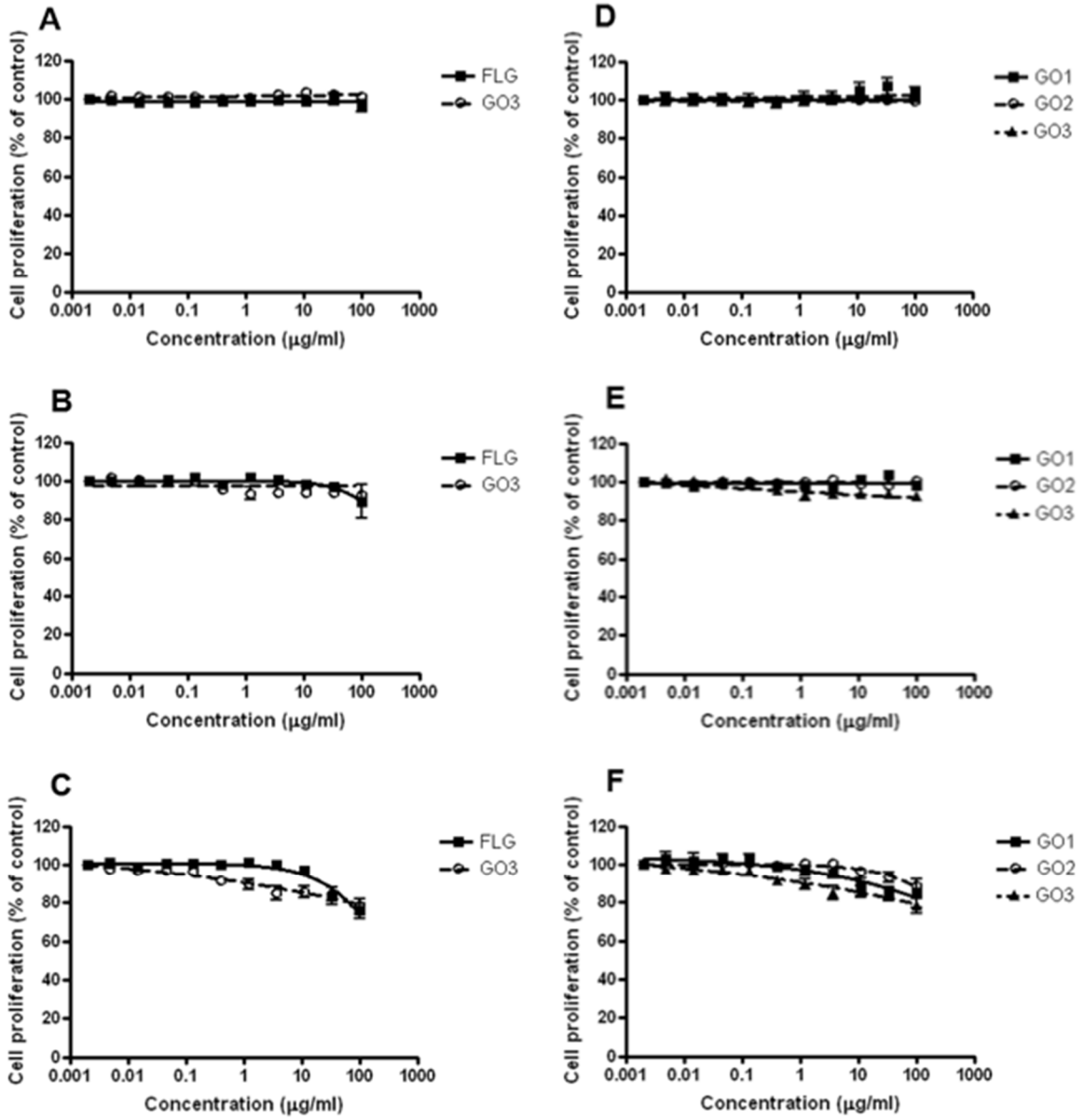

Figure 12. Effect of FLG and GOs (0.005 to 100 μg/mL) on HaCaT cells proliferation evaluated by SRB incorporation assay. Comparison between the less (FLG) and most (GO3) oxidized GFNs after 24 h (A), 48 h (B) and 72 h (C) exposure. Comparison between similarly oxidized GFNs differing by average lateral dimension (GO1, GO2, GO3) after 24 h (D), 48 h (E) and 72 h (F) exposure. Data are the mean ± SE of 3 independent experiments performed in triplicate.

4.2.3 Effects of FLG and GOs on HaCaT cells plasma membrane integrity

The effects of FLG and GOs (0.005 to 100 μg/mL) on HaCaT cells plasma membrane were initially evaluated by means of propidium iodide (PI) uptake after different exposure times up to 72 h. A comparison between the effect of the less (FLG) and that of the most oxidized (GO3) GFNs after 24 (panel A), 48 (panel B) and 72 h cells exposure (panel C) is shown in Figure 13 (panels A - C). The obtained results show that, despite the absence of anti-proliferative effects, GFNs induced a significant cytotoxic effect in HaCaT cells, consisting in a significant plasma membrane damage. Cells exposure to FLG or GO3 for 24 h induced only a negligible plasma membrane damage, while a significant concentration-dependent effect was observed after 48 and 72 h exposure. In particular, 48 h exposure to FLG induced a slight, but significant, PI uptake by the cells starting from the concentration of 30 μg/mL (8% increase of PI uptake) while GO3 exerted a significant effect already at the concentration of 1 μg/mL (25% increase of PI uptake). The relatively low effect recorded after 48 h exposure did not allow the computation of EC_{50} values, whereas prolonging the exposure time to 72 h, EC_{50} values were 45.5 μg/mL (95% CI = 38.2 - 54.2 μg/mL) and 2.9 μg/mL (95% CI = 2.1 - 4.2 μg/mL) for FLG and GO3, respectively. The significant difference between the two EC_{50} values ($p < 0.001$) confirms that FLG is significantly less potent than GO3 to induce PI uptake, as already observed for mitochondrial activity reduction, which corroborates the hypothesis that GFNs cytotoxic potential is dependent on the oxidation state of the material.

A comparison between similarly oxidized compounds differing by later dimensions (GO1, GO2 and GO3) is shown in panels D - F of Figure 13. Also in this case, the evaluation of the EC_{50} values were calculated only after 72 h cells exposure and were 23.5 μg/mL (95% CI = 15.8 - 34.9 μg/mL), 8.7 μg/mL (95% CI = 5.9 - 12.9 μg/mL) and 2.9 μg/mL (95% CI = 2.1 - 4.2 μg/mL) for GO1, GO2 and GO3, respectively. Even though significant differences were found

comparing the EC_{50} values of GO1 vs GO2 ($p < 0.01$), GO1 vs GO3 ($p < 0.001$) and GO2 vs GO3 ($p < 0.001$), the small difference among these values suggests only a slight role of GFNs dimension, confirming the hypothesis of the WST-8 assay on the effect on mitochondrial activity.

As expected, the EC_{50} values related to the increased PI uptake are comparable to those estimated for the mitochondrial activity reduction (WST-8 assay). This finding suggests that, at least after 72 h exposure, FLG and GOs induce a plasma membrane damage that impairs mitochondrial activity, without a consequent influence on cell proliferation. This is the first study demonstrating a significant plasma membrane damage, even though previous studies reported negligible effects of graphene and GOs on other cell models (Chang et al., 2011; Li et al., 2011; Sasidharan et al., 2012; Wang et al., 2013; Zhang et al., 2010b). However, these findings were obtained using methods (i.e., cells release of lactate dehydrogenase) different from that used in this study, which could be less sensitive than PI uptake measurement.

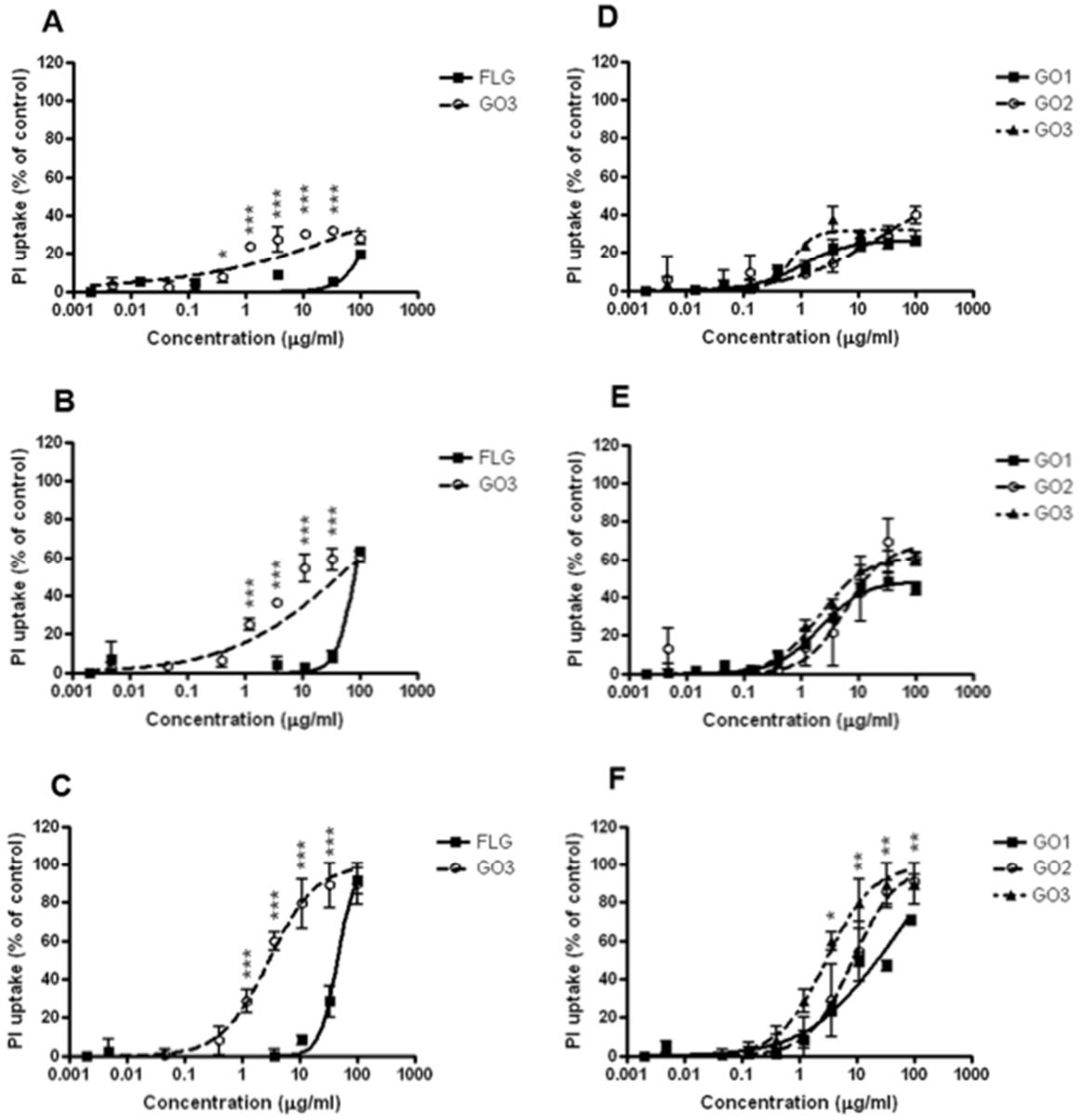

Figure 13. Effect of FLG and GOs (0.005 to 100 µg/mL) on plasma membrane integrity of HaCaT cells evaluated by PI uptake assay. Comparison between the less (FLG) and most (GO3) oxidized GFNs after 24 h (A), 48 h (B) and 72 h (C) exposure. Comparison between similarly oxidized GFNs differing by average lateral dimension (GO1, GO2, GO3) after 24 h (D), 48 h (E) and 72 h (F) exposure. Data are the mean ± SE of 3 independent experiments performed in triplicate. Statistical differences: *$p < 0.05$; **$p < 0.01$; ***$p < 0.001$ (Two-way ANOVA and Bonferroni's post test).

To deeper investigate the plasma membrane damage induced by FLG and GOs, HaCaT cells morphology was analyzed by epifluorescence microscopy after labeling plasma membranes with DiL fluorescence probe. As shown in Figure 14, 72 h exposure of HaCaT keratinocytes to FLG, GO1, GO2 or GO3 (10 μg/mL) impaired the cell membrane integrity and morphology. In particular, treated cells lost their typical flattened and cuboidal structure, becoming swollen and presenting nuclear perturbations, characterized by an irregular shape.

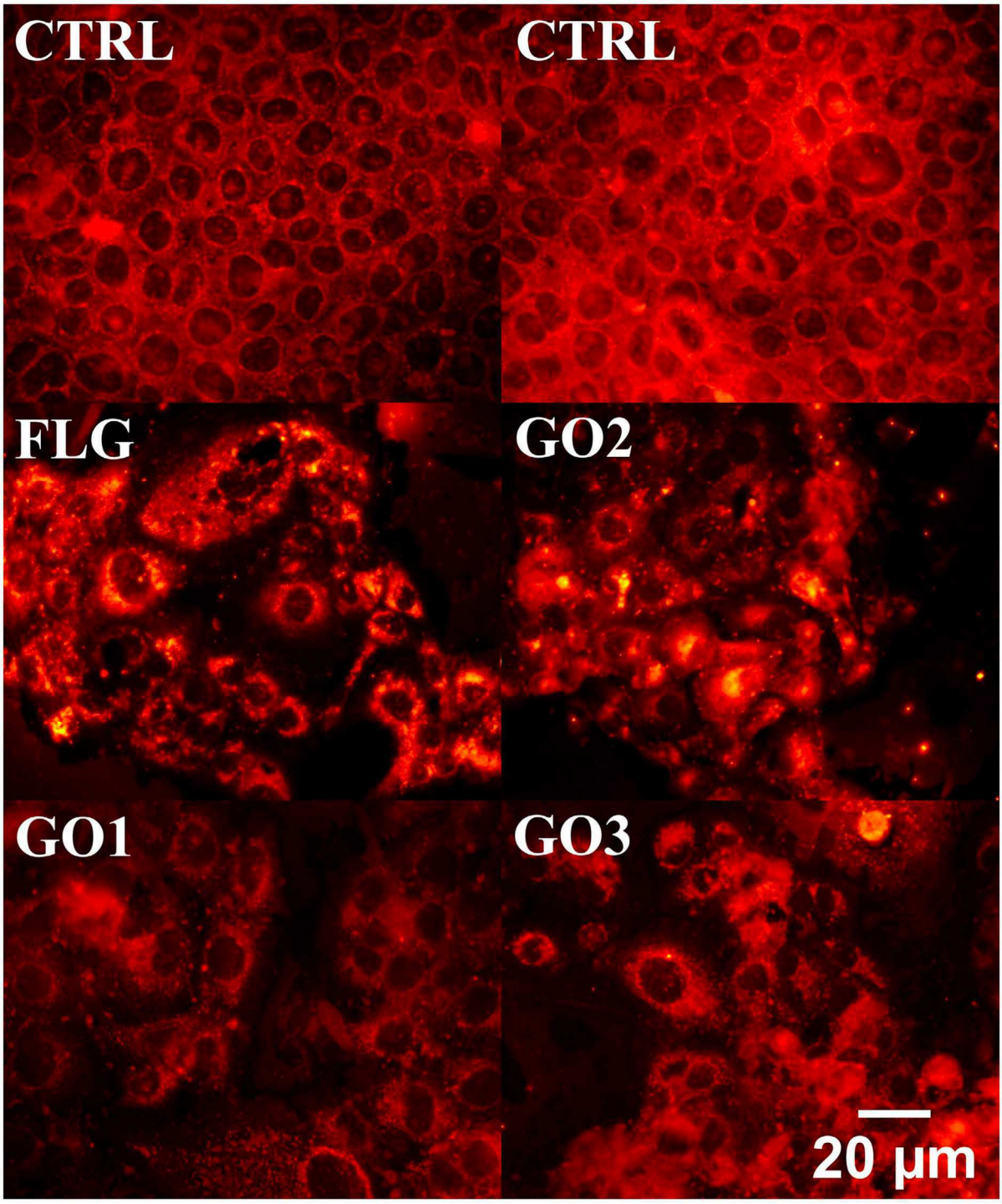

Figure 14. Epifluorescence micrographs of HaCaT keratinocytes exposed to 10 µg/mL of FLG, GO1, GO2 or GO3 for 72 h. Plasma membrane of HaCaT cells is stained with the fluorescence probe DiL. Original magnification: 60x. Scale bar: 20 µm.

4.2.4 Interaction of FLG and GOs with cell membrane of HaCaT cells

The interaction between GFNs and the plasma membrane of HaCaT cells was investigated by confocal microscopy after 72 h exposure to FLG or GOs (10 μg/mL). Cell plasma membranes were labeled with DiL fluorescence probe, while GFNs were visualized in yellow exploiting their reflection property during the confocal acquisition. As shown in Figure 15, FLG, GO1, GO2 and GO3 were able to interact with cells: by merging the red fluorescence given by the plasma membranes and the reflected yellow light by GFNs, FLG and GOs appeared diffusely associated with the cells membrane. Moreover, considering that the fixation procedure for the confocal analysis requires repeated washings, FLG and GOs appear also to be strongly attached to the cells membrane.

This finding is supported by a computational molecular dynamics simulation as well as electron microscopy imaging carried out by Li and coworkers, showing the ability of few-layer graphene microsheets to interact and penetrate the plasma membrane of different cell types (Li et al., 2013). Similarly, transmission electron microscopy analysis showed that GO and graphene nanoplatelets penetrate through the membrane into the cytosol of human hepatocellular carcinoma HepG2 cells (Lammel et al., 2013).

In agreement with these observations, the confocal images acquired on HaCaT keratinocyes, representing a slice along the z stack internal to the cells, demonstrate that FLG and GOs can be localized also inside the cells, suggesting a possible penetration inside skin keratinocytes. The obtained results need to be corroborated by other techniques.

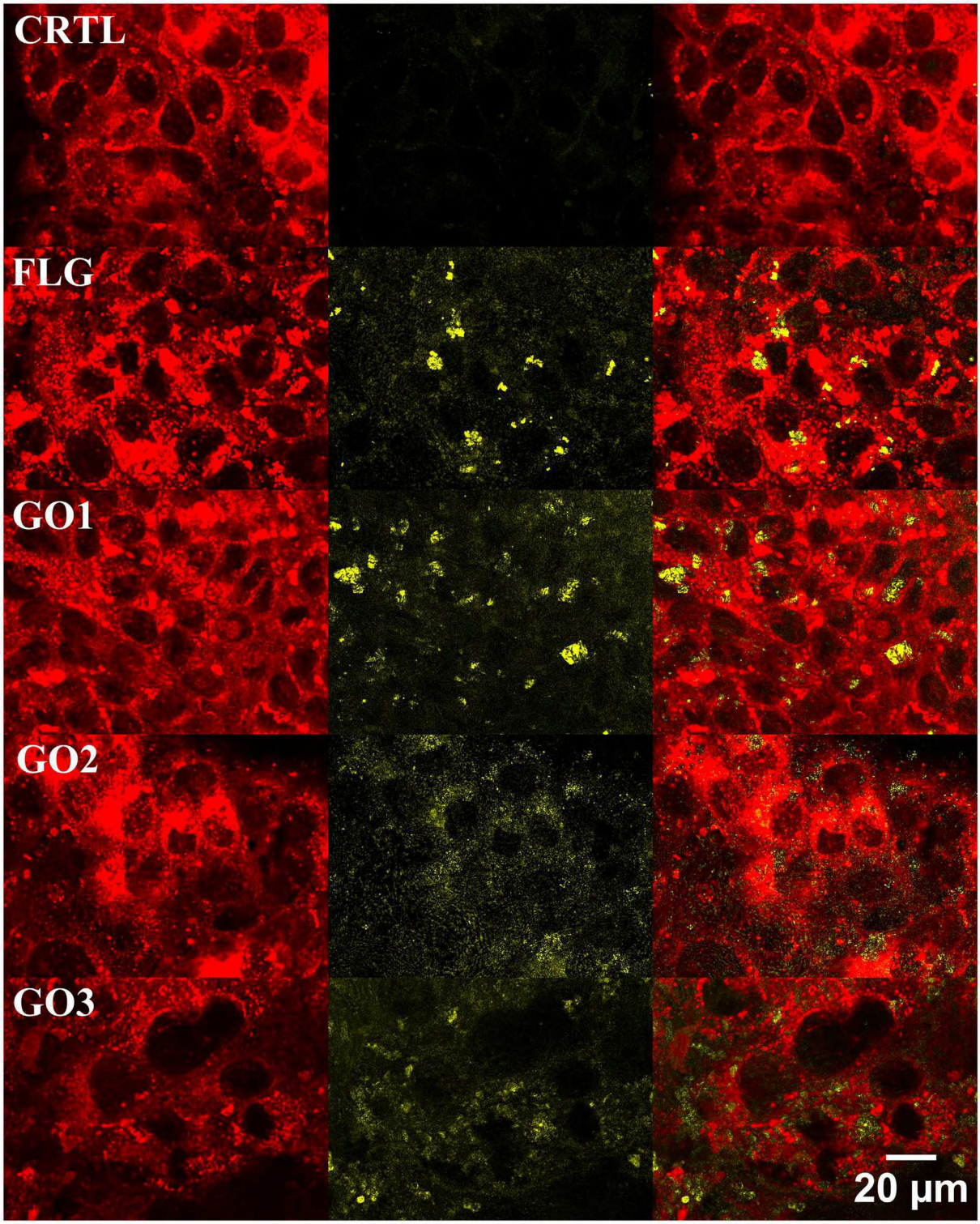

Figure 15. Reconstructed confocal micrographs of HaCaT keratinocytes exposed to FLG, GO1, GO2 or GO3 (10 µg/mL) for 72 h. Plasma membrane of HaCaT cells is labeled with the fluorescence probe DiL (red, left panel); GFNs are visualized by reflection mode acquisition (yellow, middle panel); confocal reconstruction of red DiL labeled HaCaT cells merged with

yellow reflecting GFNs (merged Figures, right panel). Original magnification: 60x. Scale bar: 20 μm.

4.2.5 Long-term cytotoxicity of FLG and GOs on HaCaT cells

Since exposure of HaCaT cells to FLG and GOs induced significant cytotoxic effects only after long exposure times (72 hours) to high GFNs concentrations, the effects of long-term HaCaT cells exposures to low GFNs concentrations were evaluated by means of mitochondrial activity (WST-8 assay). Cells were exposed to the highest concentration of FLG and GOs devoid of significant effects (0.1 μg/mL) up to 14 days. As shown in Figure 16, FLG and GOs induced only a low reduction of mitochondrial activity. Only after 10 days exposure a slight, but significant, effect was recorded (mitochondrial activity reductions: 6%, 16%, 12% and 12% for FLG, GO1, GO2 and GO3, respectively). These data suggest that long-term exposure to low GFNs concentration exerts only slight cytotoxic effects.

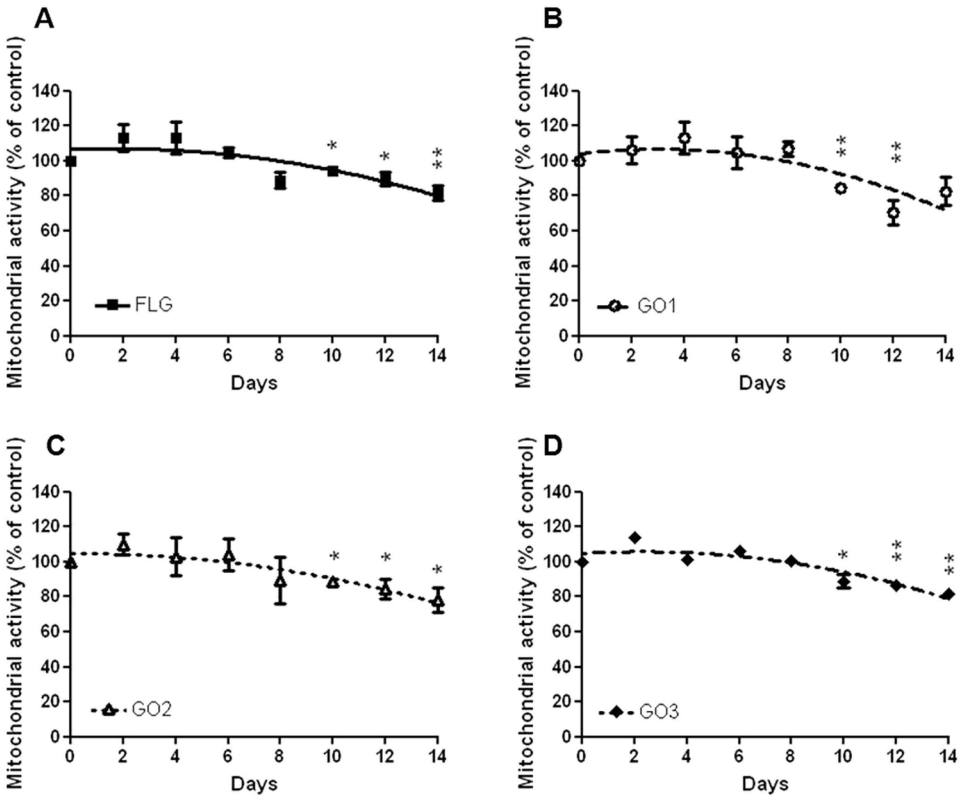

Figure 16. Effect of long-term exposure to FLG and GOs on mitochondrial activity of HaCaT cells evaluated by the WST-8 assay. Cells were exposed to 0.1 μg/mL FLG (A), GO1 (B), GO2

(C) or GO3 (D) up to 14 days. Data are the mean ± SE of 3 independent experiments performed in triplicate. Statistical differences: *p < 0.05; **p < 0.01 (One-way ANOVA and Bonferroni's post test).

4.3 Mechanism of cytotoxicity of few layer graphene (FLG) and graphene oxide (GO)

The less (FLG) and the most (GO3, hereinafter referred to as GO) cytotoxic GFNs were selected to investigate the putative mechanism(s) involved in their effects toward skin keratinocytes.

4.3.1 Effects of FLG and GO on mitochondrial depolarization in HaCaT cells

To further characterize the observed mitochondrial damage induced by GFNs on HaCaT keratinocytes, FLG and GO were deeper investigated for their effect on mitochondrial membrane depolarization (JC-1 fluorescence shift; Figure 17), after 24 (panel A), 48 (panel B) and 72 hours of exposure (panel C). Both FLG and GO (1, 10 and 100 μg/mL) induced a concentration- and time-dependent mitochondrial membrane depolarization, significant already after 24 h exposure (29 and 31% at 100 μg/mL for FLG and GO, respectively). Increasing the exposure time up to 72 h, the highest concentration (100 μg/mL) of FLG or GO increased mitochondrial depolarization by 47% or 56%, respectively, an effect comparable to that induced by the positive control valinomycin (45% at 0.1 μg/mL). The obtained results suggest that FLG and GO can induce a significant mitochondrial membrane depolarization, as a possible cause of the sustained mitochondrial damage. Those observations are in line with previous studies demonstrating the ability of other GFNs to induce mitochondrial depolarization, such as pristine graphene (Li et al., 2012), carboxyl graphene (Lammel et al., 2013), and few layer graphene obtained by the arc discharge method (Sasidharan et al., 2016).

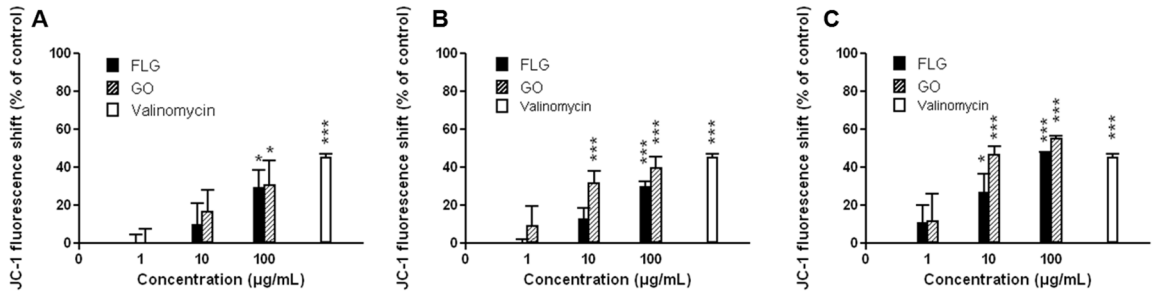

Figure 17. Mitochondrial membrane depolarization induced by FLG and GO (1, 10 and 100 µg/mL) after 24 h (panel A), 48 h (panel B) and 72 h (panel C) exposure. Data are the mean ± SE of 3 independent experiments performed in triplicate and presented as % of JC-1 fluorescence shift with respect to the untreated control cells, calculated on the ratio between red (530/590 nm) and green (485/570 nm) fluorescence. Data are the mean ± SE of 3 independent experiments performed in triplicate. Statistical differences: *, $p < 0.05$; ***$p < 0.001$ (Two-way ANOVA and Bonferroni's post test).

4.3.1.1 FLG and GO effects at mitochondrial level: role of mitochondrial permeability transition pores (MPTPs)

The mechanism of mitochondrial membrane depolarization induced by FLG and GO in HaCaT cells was evaluated in presence of cyclosporine A (CsA), a well-known inhibitor of mitochondrial permeability transition pores (MPTPs) formation (Norman et al., 2010) after 72 h exposure. HaCaT cells were pre-exposed to CsA (2.0 x 10^{-7} M) for 1 h, followed by 72 h exposure to FLG or GO (1, 10 and 100 μg/mL). The obtained results show that CsA was unable to prevent FLG- and GO-induced mitochondrial membrane depolarization, suggesting that MPTPs are not involved in the mitochondrial depolarization induced by these materials (Figure 18).

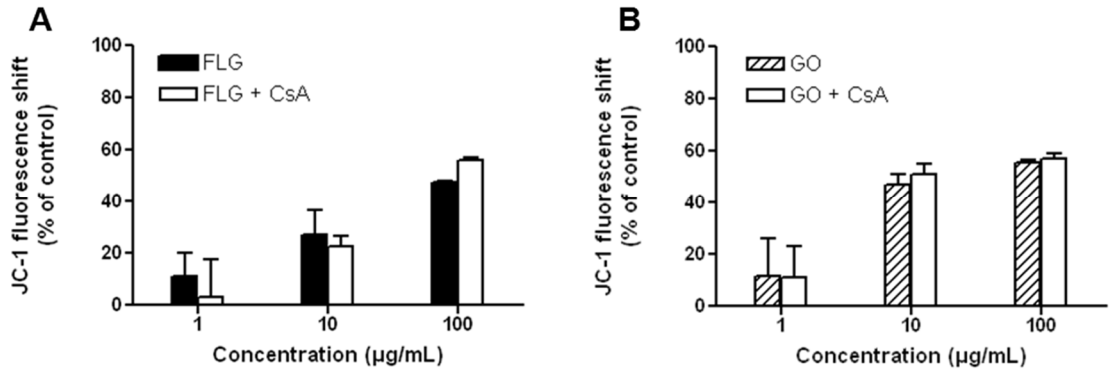

Figure 18. Role of MPTP opening in the mitochondrial depolarization induced by FLG (A) or GO (B). HaCaT cells were pre-exposed for 1 h to 2.0 x 10^{-7} M CsA and then to GFNs (1, 10 and 100 μg/mL) for 72 h. The effects of FLG and GO in presence of CsA are compared to those of FLG and GO alone. Results are the mean ± SE of 3 independent experiments performed in triplicate and are presented as % of JC-1 fluorescence shift with respect to the untreated control cells calculated on the ratio between red (530/590 nm) and green (485/570 nm) fluorescence.

4.3.2 FLG and GO effects on oxidative stress: concentration- and time-dependent reactive oxygen species production (ROS) in HaCaT cells

Considering that reactive oxygen species (ROS) overproduction can be one of the main causes of mitochondrial damage (Ott et al., 2007), their role was evaluated as possible mechanism of mitochondrial membrane depolarization induced by FLG and GO in HaCaT cells. HaCaT keratinocytes were exposed to FLG or GO for 24 h and ROS production was measured by spectrophotometric (NBT), chemiluminescent (luminol) and fluorometric (DCFDA) detection assays, which specifically detect superoxide anion, hydrogen peroxide and peroxynitrite/hydroxyl radicals, respectively. AAPH (1mM) was included as a positive control. As shown in Figure 19, a significant concentration-dependent increase of ROS production, detected by all the three methods, was observed for both FLG and GO (0.4 - 100 μg/mL). The highest concentration (100 μg/mL) of FLG increased ROS production by 25%, 9% and 39%, as assessed by the DCF-DA, NBT and luminol assay, respectively. GO (100 μg/mL) increased ROS production by 39% (DCFDA assay), 36% (NBT assay) and 21% (luminol assay). The positive control AAPH increased ROS production by 150%, 32% and 90%, as assessed by the DCF-DA, NBT and luminol assay, respectively.

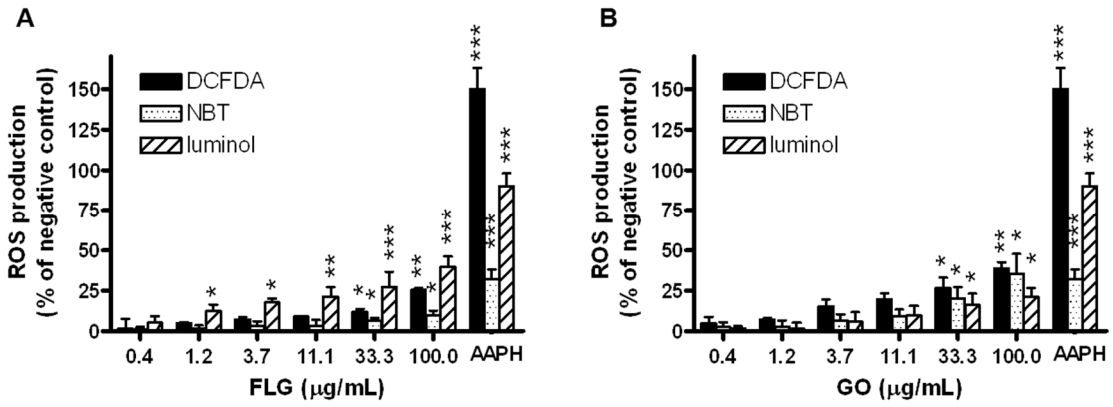

Figure 19. Reactive oxygen species (ROS) production induced by FLG (A) and GO (B). Cells were exposed to FLG and GO (0.4 - 100 μg/mL) for 24 h and ROS production was evaluated by the NBT reduction assay, DCFDA fluorescence assay and luminol assay. Data are expressed as % of ROS production with respect to untreated controls and are the mean ± SE of at least 3 independent experiments performed in triplicate. Statistical differences: *$p < 0.05$; **$p < 0.01$; ***$p < 0.001$ (Two-way ANOVA and Bonferroni's post test).

To further investigate the role of GFNs-increased ROS production in mitochondrial dysfunction, the kinetic of their production was evaluated in HaCaT cells exposed to FLG or GO (0.4 - 100 μg/mL) for 3 up to 72 h by a time-dependency DCFDA assay, the most suitable method to perform a time-course ROS measurement. AAPH (1mM) was included as a positive control. As shown in Figure 20, at all the concentrations tested, FLG and GO induced a time-dependent ROS production. In particular, FLG induced a significant ROS production starting from 24 h exposure, at 0.4 μg/mL and above ($p<0.05$), whereas GO determined a significant ROS production already after 12 h exposure, at 100 μg/mL ($p<0.05$). After 72 h exposure, the highest concentration (100 μg/mL) of FLG or GO significantly increased ROS production (85% or 124%, respectively; $p<0.001$), GO being significantly more potent ($p<0.01$) than FLG. On the whole, comparing the effects of FLG to those of GO, ROS production induced by GO was

significantly higher than that induced by FLG, starting from the concentration of 33 μg/mL ($p<0.001$) after 48 h exposure ($p<0.05$).

Consistent with our observation, previous findings suggested that the higher oxygen content on GO surface in comparison to that of FLG can enhance ROS production (Zou et al., 2016). Altogether, these observations are in agreement with previous results, demonstrating that the oxidation state of GFNs is a critical feature for their cytotoxic potency (Das et al., 2013). Furthermore, in line with our findings, previous studies showed an increased ROS production in cells exposed to other GFNs, such as FLG (obtained with different methodologies) in PC12 (Zhang et al., 2010b) and HUVEC cells after 24 h exposure (Sasidharan et al., 2016), and GO (obtained by Hummers' method) after 24 h exposure in A549 cells (Chang et al., 2011), MCF7 cells (Gurunathan et al., 2013), HeLa cells (Zhang et al., 2012), MDA-MB-231 cells (Wu et al., 2015) and BEAS-2B cells (Mittal et al., 2016). Moreover, a previous study has shown that commercial pristine graphene can induce ROS overproduction and depletion of the mitochondrial membrane potential in murine RAW 264.7 macrophages after 24 h exposure, triggering apoptosis by activation of the mitochondrial pathway (Li et al., 2012). Similarly, GO appears to increase the activity of mitochondrial electron transport complexes inducing alterations at the mitochondrial level in MHS cells (Duch et al., 2011). Moreover, Mittal and co-workers (Mittal et al., 2016) suggested that oxidative stress may indirectly derive also by a decreased activity of antioxidant enzymes, such as superoxide dismutase and glutathione peroxidase, as reported for GO (Mittal et al., 2016; Ou et al., 2016). However, the molecular mechanism of ROS generation induced by GFNs is still unexplored, so far. Hence, the putative mechanism(s) underlying ROS production induced by GFNs was investigated.

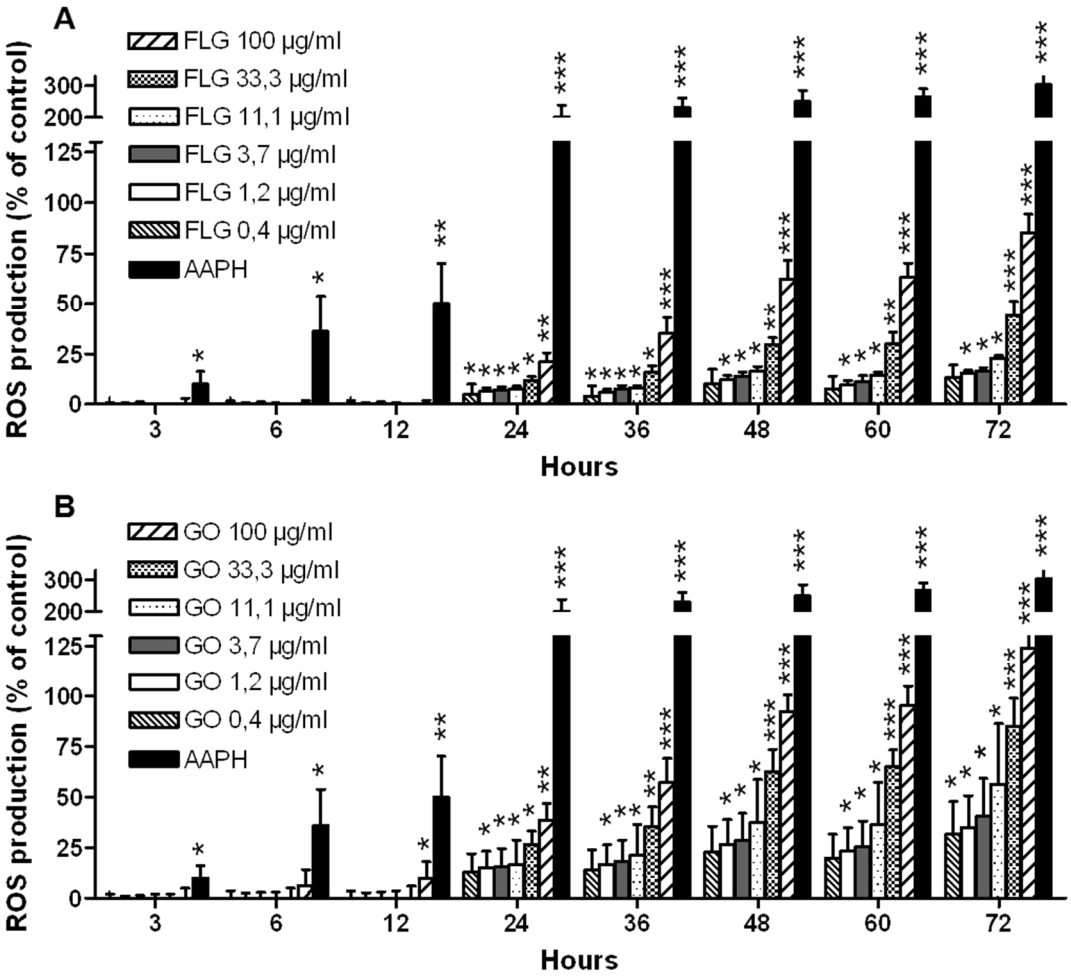

Figure 20. Kinetic of ROS production induced by different concentration (0.4 - 100 µg/mL) of FLG (A) and GO (B) evaluated by the DCFDA assay up to 72 h exposure. Results are expressed as % of ROS production with respect to untreated controls and are the mean ± SE of at least 3 independent experiments performed in triplicate. Statistical differences: *p < 0.05; **p < 0.01; ***p < 0.001 (Two-way ANOVA and Bonferroni's post test).

4.3.3 Mechanism of FLG- and GO-induced ROS production in HaCaT cells

To investigate the putative mechanism(s) underlying the increased ROS production induced by FLG and GO in HaCaT cells, the effects of these materials were evaluated by the DCFDA assay in presence of six inhibitors of the major ROS-producing enzymes. In particular, HaCaT cells were pre-exposed for 1 h to diphenyliodonium chloride (DPI; $5.0x10^{-6}$ M), an inhibitor of flavoprotein enzymes, apocynin ($1.0x10^{-5}$ M), a selective inhibitor of NADPH oxidase (NOX), L-N^G-monomethyl arginine citrate (L-NMMA; $1.0x10^{-4}$ M), a selective inhibitor of nitric oxide synthase (NOS), rotenone ($5.0x10^{-6}$ M), a selective inhibitor of mitochondrial complex I (NADH dehydrogenase), indomethacin ($1.0x10^{-4}$ M), inhibitor of cyclooxygenase (COXs), and allopurinol ($1.0x10^{-4}$ M), inhibitor of xanthine oxidase (XO). Subsequently, cells were exposed for additional 72 h to FLG or GO (1 - 100 μg/mL) in presence of the specific inhibitors. As shown in Figure 21 (panels A-B), starting from the concentration of 10 μg/mL, ROS overproduction induced by FLG (panel A) and GO (panel B) was significantly reverted or even abolished by the inhibitor of flavoprotein-based enzymes, DPI, by the inhibitor of the NADH dehydrogenase, rotenone, and by the inhibitor of xanthine oxidase, allopurinol. At the highest concentration tested (100 μg/mL), FLG-induced ROS production was significantly reduced by 30% ($p<0.001$), 51% ($p<0.001$) and 52% ($p<0.001$) by DPI, rotenone and allopurinol, respectively, as compared to control cells exposed to 100 μg/mL FLG, without any inhibitor. ROS production induced by GO (100 μg/mL) was reduced by 130% ($p<0.001$), 173% ($p<0.001$) and 187% ($p<0.001$) by DPI, rotenone and allopurinol, respectively.

On the contrary, the other inhibitors did not prevent FLG- or GO-induced ROS production. The ability of rotenone and allopurinol to inhibit GFNs-induced ROS production suggests a role for mitochondrial electron transport chain complex I (NADH dehydrogenase) and xanthine oxidase

in the oxidative stress induced by these materials. These findings, in agreement with a previous study demonstrating that GO increases the activity of mitochondrial electron transport complexes in MHS cells (Duch et al., 2011), are further supported by the inhibitory efficacy of DPI, able to inactivate flavoprotein-based enzymes, such as NADH dehydrogenase and xanthine oxidase (Chakraborty and Massey, 2002; O'Donnell et al., 1994).

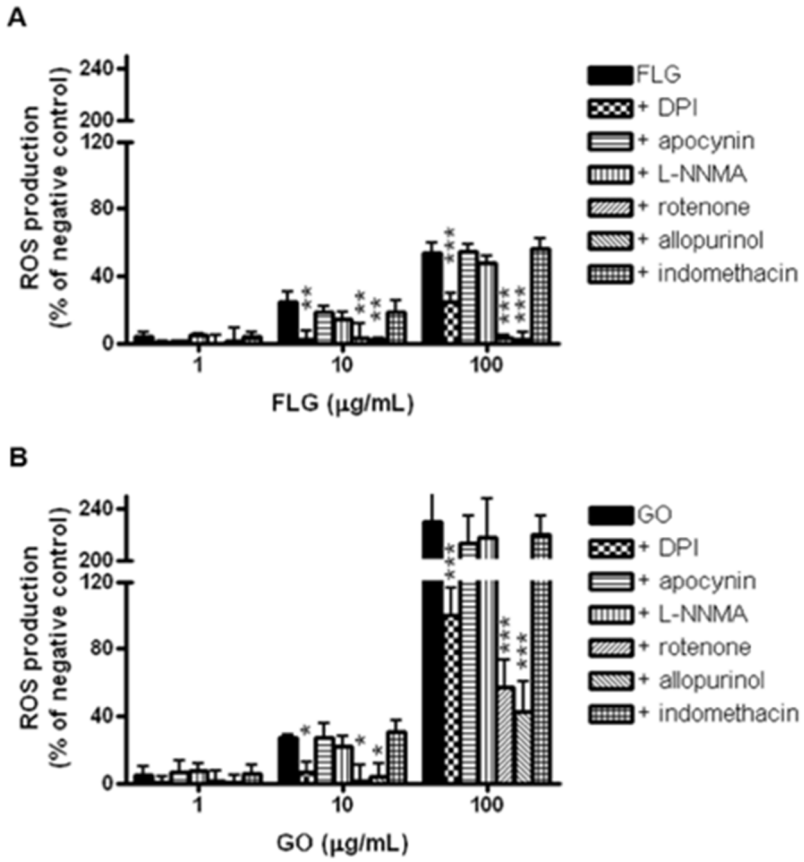

Figure 21. Effect of inhibitors of the major ROS-producing enzymes on ROS production by HaCaT cells exposed to FLG (panel A) or GO (panel B). Cells were exposed for 1 h to $5.0x10^{-6}$ M DPI, $1.0x10^{-5}$ M apocynin, $1.0x10^{-4}$ M L-NMMA, $5.0x10^{-6}$ M rotenone, $1.0x10^{-4}$ M indomethacin or $1.0x10^{-4}$ M allopurinol followed by exposure to FLG or GO for 72 h. ROS production was measured by DCFDA assay. Data are expressed as % with respect to untreated controls and are the mean ± SE of 4 independent experiments performed in triplicate. Statistical differences: *, $p < 0.05$; **$p < 0.01$; ***$p < 0.001$ (Two-way ANOVA and Bonferroni's post test).

4.3.4 Mechanism of FLG- and GO-induced mitochondrial damage in HaCaT cells

To investigate the relationship between oxidative stress and mitochondrial damage induced by FLG- and GO in HaCaT cells, the mitochondrial membrane depolarization induced by FLG and GO (JC-1 assay) was assessed in presence of the ROS-producing enzymes inhibitors used in the previous set of experiments. Cells were pre-exposed for 1 h to the inhibitors and subsequently to FLG or GO (1 - 100 μg/mL) for 72 h in presence of the same inhibitors. As observed by the DCFDA assay, mitochondrial depolarization induced by FLG (Figure 22, panel A) or GO (Figure 22, panel B) was significantly reduced by DPI, rotenone and allopurinol, starting from the GFNs concentration of 10 μg/mL. At the highest concentration tested (100 μg/mL), FLG-induced mitochondrial depolarization was significantly reduced by 32%, 45% and 54% by DPI, rotenone and allopurinol, respectively, as compared to control cells exposed to 100 μg/mL FLG, without any inhibitor. Mitochondrial depolarization induced by GO (100 μg/mL) was significantly reduced by 40%**,** 48% and 57% by DPI, rotenone and allopurinol, respectively. On the contrary, the other inhibitors did not reduce FLG- and GO-induced mitochondrial depolarization.

This finding suggests that the mitochondrial damage induced by FLG or GO could be dependent on a significant concentration- and time-dependent ROS production, mediated mainly by the activation of flavoprotein-based oxidative enzymes, such as NADH dehydrogenase and xanthine oxidase.

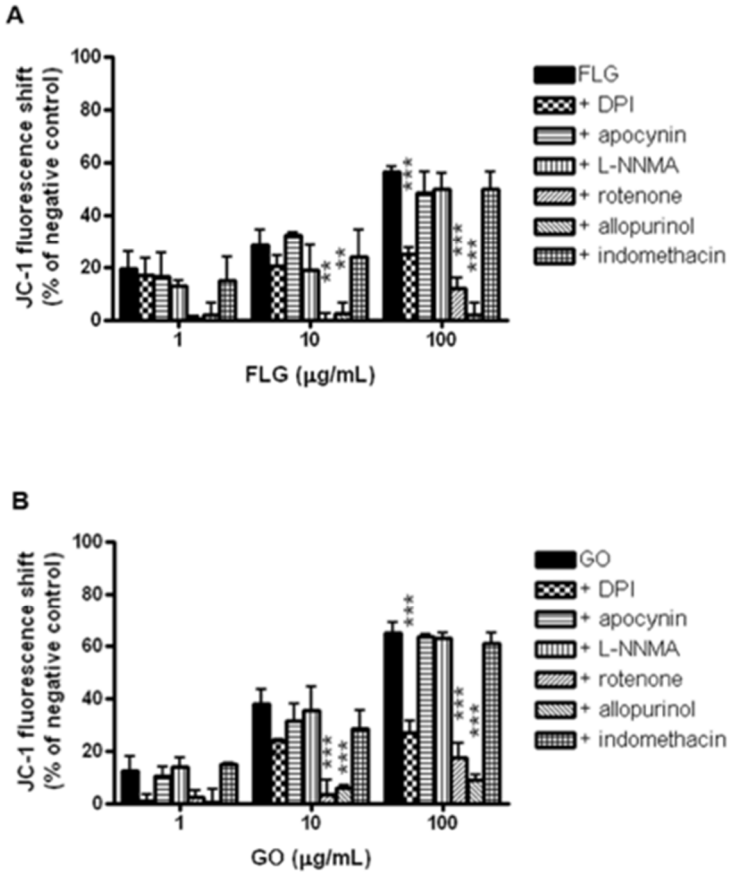

Figure 22. Effect of inhibitors of the major ROS-producing enzymes on mitochondrial membrane depolarization in HaCaT cells exposed to FLG (panel A) or GO (panel B). Cells were exposed for 1 h to $5.0x10^{-6}$ M DPI, $1.0x10^{-5}$ M apocynin, $1.0x10^{-4}$ M L-NMMA, $5.0x10^{-6}$ M rotenone, $1.0x10^{-4}$ M indomethacin or $1.0x10^{-4}$ M allopurinol followed by exposure to FLG or GO for 72 h. Mitochondrial membrane depolarization was evaluated by JC-1 fluorescence shift. Data are expressed as % with respect to untreated controls and are the mean ± SE of 4 independent experiments performed in triplicate. Statistical differences: *, $p < 0.05$; **$p < 0.01$; ***$p < 0.001$ (Two-way ANOVA and Bonferroni's post test).

4.4 Inflammatory effects of graphene (FLG) and graphene oxide (GO) at the skin level

In the second part of the project, the inflammatory and sensitizing potential of FLG and GO at the skin level were evaluated.

4.4.1 Detection and removal of endotoxin contamination in GO

Nanomaterials can be commonly contaminated with endotoxin (Dobrovolskaia et al., 2009), a lipopolysaccharide (LPS) of the outer membrane of Gram-negative bacteria cells (Rietschel et al., 1994). Endotoxin is a biologically active molecule with significant toxic and inflammatory effects. In fact, it can induce a variety of cells to release cytokines and chemokines *via* pattern recognition receptors (PRRs), a primitive part of immune system which allows cells, such as macrophages, to detect the conserved bacterial structures called pathogen-associated molecular patterns, PAMPs (Bishop, 2005). Therefore, to evaluate the potential inflammatory and sensitizing effects of FLG and GO at the skin level, the use of endotoxin-free nanomaterials is required to avoid any interference by LPS (Mukherjee et al., 2017). To this aim, FLG endotoxin removal was performed by Prof. Ester Vázquez group of the University of Castilla-La Mancha, while, endotoxin-free GO was prepared at Karolinska Institutet in Stockholm, in collaboration with Prof. Bengt Fadeel. In particular, endotoxin was removed from GO by heat treatment of samples at 200°C for 1 h in a protective Argon atmosphere, and endotoxin contamination was evaluated by the TNF-α expression test (TET), a novel assay recently developed by Mukherjee and co-workers (Mukherjee et al., 2016). A similar approach was used by the University of Castilla-La Mancha to evaluate FLG endotoxin contamination.

To carry out the TET assay, peripheral blood mononuclear cells (PBMC) were isolated from buffy coats obtained from healthy human blood donors (Karolinska University Hospital; Stockholm, Sweden) by density gradient centrifugation using Lymphoprep™ (Axis-Shield; Oslo, Norway). Monocytes were purified from PBMCs by positive selection based on CD14 expression using CD14 MicroBeads (Miltenyi Biotec, Bergisch Gladbach, Germany). To obtain human monocyte-derived macrophages (HMDM), CD14+ monocytes were seeded in 96 well plate and cultured with 50 ng/mL recombinant macrophage colony-stimulating factor (M-CSF) (Novakemi; Handen, Sweden) for three days.

The obtained HMDM were exposed to GO (12.5 - 75 μg/mL) or to 5% DMSO (positive control) for 24 h and the effect on cell viability was evaluated by the Alamar Blue (AB) assay. As shown in Figure 23, HMDM exposure to GO for 24 h did not induce significant effects on cells viability up to 75 μg/mL, while, as expected, the positive control (5% DMSO) significantly reduced cells viability.

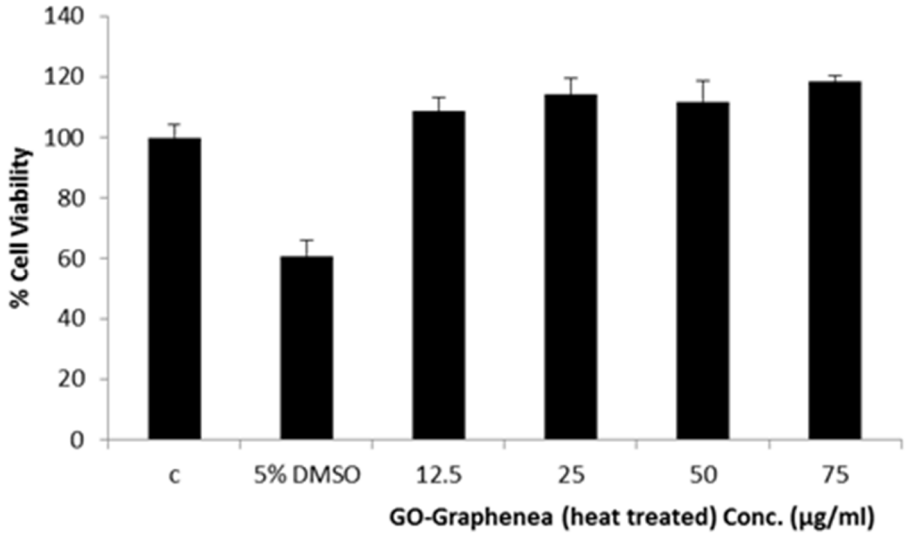

Figure 23. Primary human monocyte-derived macrophages (HMDM) viability after exposure to GO (12.5 - 75 µg/mL) or 5% DMSO for 24 h, evaluated by Alamar Blue assay. Data are the mean ± SE of 3 independent experiments performed in triplicate.

Basing on this result, sub-cytotoxic concentrations of GO (25 and 50 µg/mL) were chosen for the TET assay, based on the detection of TNF-α in the presence or absence of the specific endotoxin inhibitor polymyxin B sulfate (Poly-B, 10 µM). LPS (0.1 µg/mL) was used as a positive control in the assay. To quantify the endotoxin in GO sample, a standard curve was generated based on LPS (0.0001 - 0.1 µg/mL)-induced TNF-α expression by HMDM. As shown in Figure 24, no significant differences were observed between the TNF-α expression induced by GO alone or that induced in presence of Poly-B sulfate, providing evidence that the removal of endotoxin from GO samples was successful.

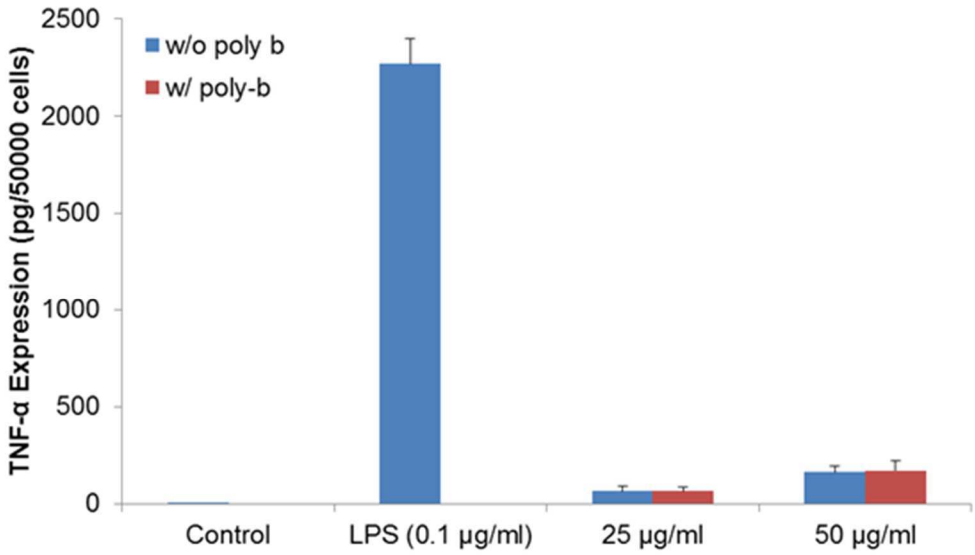

Figure 24. TNF-α Expression Test (TET) for endotoxin detection. The TET was performed to detect endotoxin in GO by HMDM exposure to this material for 24 h. Data are the mean ± SE of 3 independent experiments performed in triplicate.

4.4.2 Effects of FLG and GO on HaCaT cells viability after continuous exposure and recovery exposure

To define the most suitable conditions of HaCaT cells exposure to the GFNs for the quantitation of inflammatory mediators release, cells viability was evaluated after different exposure conditions to sub-cytotoxic concentrations of FLG or GO (0.01, 0.1 and 1.0 μg/mL), chosen on the basis of preliminary WST-8 cytotoxic assay. HaCaT cells were exposed to FLG or GO (0.01, 0.1 and 1.0 μg/mL), for 4, 24 and 72 h (continuous exposures) or, alternatively, to the same concentrations of FLG or GO for 4 h, followed by three times washing with PBS and incubation for 20 or 68 h in fresh media (recovery exposures "4h+20h" and "4h+68h", respectively). Those wide range of conditions represent both long-medium (72 and 24 h continuous exposure) and short (4 h continuous exposure and recovery exposures "4h+20h" or "4h+68h") exposures. The latter were chosen as an average time of occupational exposure, representing at least half of an 8-hour shift of work schedule.

As shown in Figure 25, neither continuous nor recovery exposures induced a significant reduction of HaCaT cell viability, at any time of exposure.

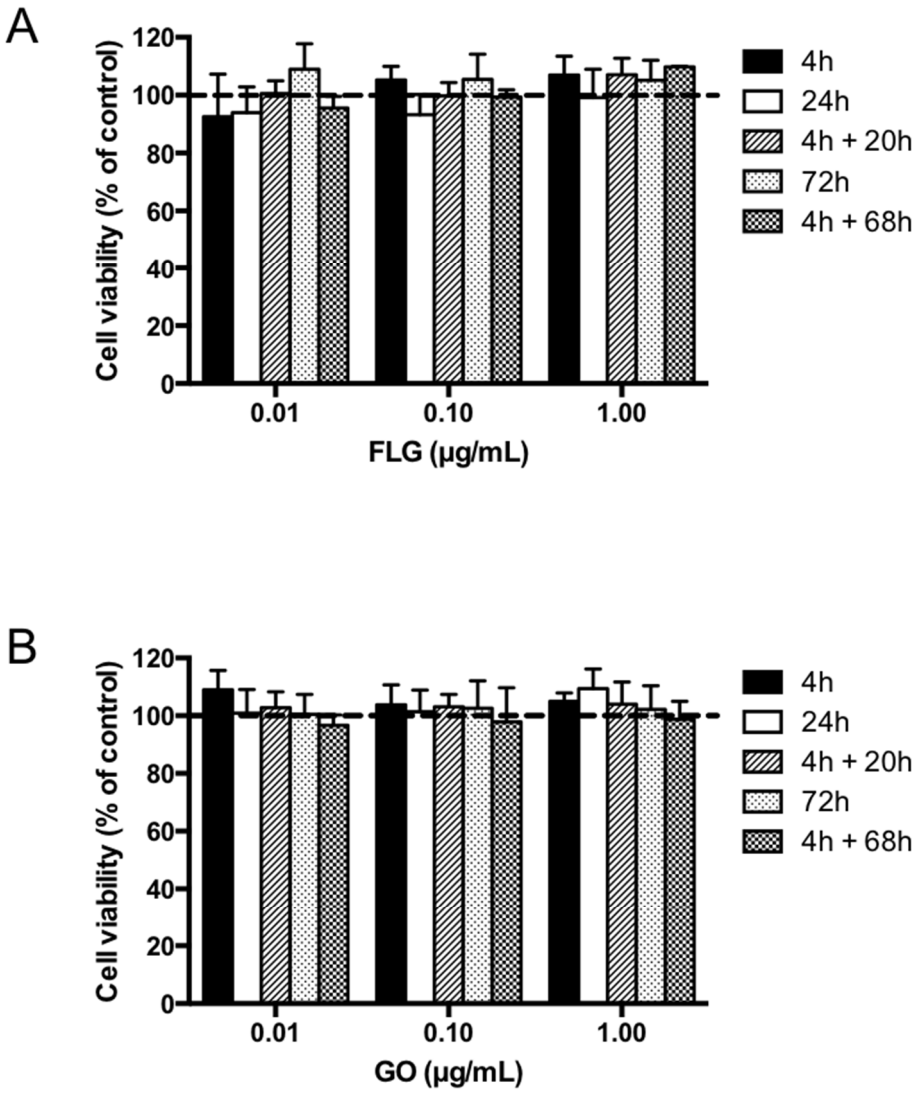

Figure 25. Effect of FLG (panel A) and GO (panel B) on HaCaT cells viability after continuous (4, 24 and 72 h) and recovery ("4h+20h" and "4h+68h") exposures, evaluated by the WST-8 assay. Data are the mean ± SE of 3 independent experiments performed in triplicate.

4.4.3 Inflammatory mediators release by HaCaT cells exposed to FLG or GO

To evaluate the inflammatory effects of FLG and GO on HaCaT skin keratinocytes, a panel of inflammatory mediators (IL-1α, IL-6, IL-8, IL-10, TNF-α, IFN-α, GM-CSF, and MIP-1β) released by the cells was quantified by Luminex® technology after continuous (4, 24 and 72 h) or recovery ("4h+20h" and "4h+68h") exposures to sub-cytotoxic concentrations of FLG or GO (0.01, 0.1 and 1.0 μg/mL). Control media were collected from HaCaT keratinocytes cultured in FLG- and GO-free medium.

IL-1α, IL-6, IL-8 and IL-10 release

Figure 26 shows changes in IL-1α (panel A and B), IL-6 (pannel C and D), IL-8 (panel E and F) and IL-10 (panels G and H) release by HaCaT cells after continuous or recovery exposures to FLG or GO as compared to controls.

A significant release of IL-1α induced by FLG (panel A) or GO (panel B) was observed after "4h+20h" recovery exposure to FLG (0.01, 0.1 and 1.0 μg/mL) as well as after "4h+68h" recovery exposure to FLG or GO (0.1 and 1.0 μg/mL). The release of IL-1α induced by "4h+20h" recovery exposure to 0.01, 0.1 and 1.0 μg/mL FLG was equal to 44.1±17.1 pg/mL ($p < 0.05$), 50.4±18.2 pg/mL ($p < 0.01$) and 56.6±16 pg/mL ($p < 0.01$), which correspond to 24, 28 and 31-fold increase compared to untreated control cells, respectively. The release of IL-1α induced by "4h+68h" recovery exposure to 0.1 and 1.0 μg/mL FLG was equal to 44.7±14.6 pg/mL ($p < 0.05$) and 50.6±12.5 pg/mL ($p < 0.01$), corresponding to 25 and 28-fold increase compared to untreated control cells, respectively. Regarding GO, "4h+68h" recovery exposure to 0.1 and 1.0 μg/mL of the material induced an IL-1α release equal to 26.4±10.6 pg/mL ($p <$

0.01) and 28.2±11.0 pg/mL ($p < 0.01$), corresponding to 15 and 16-fold increase compared to untreated control, respectively.

FLG and GO increased also the release of IL-6. A significant increase of IL-6 release was observed after "4h+20h" recovery exposure to FLG (0.01, 0.1 and 1.0 μg/mL, panel C) or GO (0.1 and 1.0 μg/mL, panel D) as well as after "4h+68h" recovery exposure to FLG (0.01, 0.1 and 1.0 μg/mL). The release of IL-6 induced by "4h+20h" recovery exposure to 0.01, 0.1 and 1.0 μg/mL FLG was equal to 60.8±5.4 pg/mL ($p < 0.001$), 63.7±3.0 pg/mL ($p < 0.001$) and 79.5±8.7 pg/mL ($p < 0.001$), corresponding to 15, 16 and 19-fold increase compared to untreated control, respectively. Also "4h+68h" recovery exposure to 0.01, 0.1 and 1.0 μg/mL FLG induced a significant release of IL-6 of 46.0±1.6 pg/mL ($p < 0.001$), 57.8±3.4 pg/mL ($p < 0.001$) and 61.3±0.7 pg/mL ($p < 0.001$), corresponding to 11, 14 and 15-fold increase compared to untreated control, respectively. Regarding GO, a significant release of IL-6 was induced by "4h+20h" recovery exposure to 0.1 and 1.0 μg/mL of the GFN, equal to 7.7±0.7 pg/mL ($p < 0.001$) and 8.6±1.2 pg/mL ($p < 0.001$), respectively, which correspond to about 2-fold increase compared to untreated controls. Similarly, continuous cells exposure to FLG or GO (0.01, 0.1 and 1.0 μg/mL) for 4, 24 or 72 h induced a significant release of IL-6. In particular, 4 h of continuous exposure to 0.01, 0.1 and 1.0 μg/mL FLG induced the release of 22.7±1.9 pg/mL ($p < 0.01$), 24.0±2.8 pg/mL ($p < 0.01$) and 29.6±6.8 pg/mL ($p < 0.001$) of IL-6, corresponding to 6, 6 and 7-fold increase compared to untreated control, respectively. After 24 h of continuous exposure, 0.01, 0.1 and 1.0 μg/mL FLG induced a significant release of IL-6 equal to 25.5±5.2 pg/mL ($p < 0.001$), 23.8±0.9 pg/mL ($p < 0.001$) and 35.5±4.6 pg/mL ($p < 0.001$), corresponding to 6, 6 and 9-fold increase compared to untreated control, respectively. Similarly, 72 h of continuous exposure to 0.01, 0.1 and 1.0 μg/mL FLG induced a significant release of IL-6 equal to 24.3±3.5 pg/mL ($p < 0.01$), 27.4±0.8 pg/mL ($p < 0.01$) and 34.3±3.2 pg/mL ($p < 0.001$),

corresponding to 6, 7 and 8-fold increase compared to untreated control, respectively. Regarding GO, it increased IL-6 release by HaCaT cells after 24 h and 72 h of continuous exposure to the material. In particular, 24 h exposure to 1.0 μg/mL GO induced the release of 7.1±0.6 pg IL-6/mL ($p < 0.01$), corresponding to 2-fold increase compared to untreated control. After 72 h of continuous exposure, 0.1 and 1.0 μg/mL GO induced a significant release of IL-6 equal to 7.2±0.6 pg/mL ($p < 0.01$) and 7.4±1.2 pg/ml ($p < 0.01$), corresponding to 2-fold increase compared to untreated control, respectively.

Regarding IL-8, it was significantly released by HaCaT cells exposed to FLG (panel E) or GO (panel F) under the following recovery conditions: "4h+20h" for FLG (1.0 μg/mL) or GO (0.1 and 1.0 μg/mL) and "4h+68h" for FLG (0.1 and 1.0 μg/mL) or GO (0.01, 0.1 and 1.0 μg/mL). In particular, after "4h+20h" recovery exposure to 1.0 μg/mL FLG, HaCaT cells released 4010±463 pg IL-8/mL ($p < 0.001$), corresponding to 2-fold increase compared to untreated control. After "4h+68h" recovery exposure, 0.1 and 1.0 μg/mL FLG induced a significant IL-8 release equal to 2587±299 pg/mL ($p < 0.01$) and 3573±210 pg/mL ($p < 0.001$), respectively, corresponding to about 2-fold increase compared to untreated control. IL-8 release induced by 0.1 and 1.0 μg/mL GO after "4h+20h" recovery exposure was equal to 3715±776 pg/mL ($p < 0.05$) and 4043±784 pg/mL ($p < 0.01$), respectively, corresponding to about 2-fold increase compared to untreated control. After "4h+68h" recovery exposure to 0.01, 0.1 and 1.0 μg/mL GO, a significant IL-8 release from HaCaT cells, equal to 4389±990 pg/mL ($p < 0.01$), 4944±438 pg/mL ($p < 0.001$) and 5327±55 pg/mL ($p < 0.001$), respectively, was recorded. These values correspond to about 3-fold increase compared to untreated control. Moreover, the highest concentration of GO (1.0 μg/mL) induced a significant increase of IL-8 also after 72 h of continuous exposure, equal to 3565±377 pg/mL ($p < 0.05$) and corresponding to 2-fold increase compared to untreated control.

A slight but significant release of IL-10 was observed only after 72 h of continuous cells exposure to 1.0 μg/mL FLG (panel G), equal to 2.9±0.5 pg/mL ($p < 0.001$). This cytokine was not detected in any of the other samples.

IFN-α, TNF-α, GM-CSF and MIP-1β release

Figure 27 shows changes in IFN-α (panel A and B), TNF-α (panel C and D), GM-CSF (panel E and F) and MIP-1β (panels G and H) release from HaCaT cells after continuous or recovery exposures to FLG or GO.

Considering IFN-α, "4h+20h" and "4h+68h" recovery exposures to the highest concentration of FLG (1.0 μg/mL) induced a slight, but significant, cytokine release (panel A) equal to 1.3±0.4 pg/mL ($p < 0.001$) and 0.6±0.2 pg/mL ($p < 0.01$), respectively. A slight, but significant, IFN-α release (1.3±0.7 pg/mL; $p < 0.001$) was observed also after 72 h of continuous exposure to the same FLG concentration. On the contrary, this cytokine was not detected neither after cells exposure to GO nor in the control (panel B).

TNF-α release by HaCaT cells was significantly increased by FLG (panel C) or GO (panel D) after "4h+20h" and "4h+68h" recovery exposure. In particular, FLG induced a significant release of TNF-α only at the highest concentration (1.0 μg/mL): 5.3±1.2 pg/mL ($p < 0.001$) and 5.6±1.4 pg/mL ($p < 0.001$) after "4h+20h" and "4h+68h" recovery exposure, respectively, corresponding to about 5-fold increase compared to untreated control. Cells exposure to 0.01, 0.1 and 1.0 μg/mL GO induced a slight but significant release of TNF-α after "4h+20h" recovery condition, equal to 1.3±0.1 pg/mL ($p < 0.01$), 1.3±0.1 pg/mL ($p < 0.001$) and 1.5±0.1 pg/mL ($p < 0.001$), respectively, which correspond to about 2-fold increase compared to untreated controls. Also "4h+68h" recovery exposure, GO (0.01, 0.1 and 1.0 μg/mL) induced a

slight but significant release of TNF-α, equal to 1.6±0.1 pg/mL ($p < 0.001$), 1.5±0.1 pg/mL ($p < 0.001$) and 1.9±0.1 pg/mL ($p < 0.001$), respectively. These values correspond to about 2-fold increase compared to untreated control.

Regarding GM-CSF, both FLG and GO significantly increased the release of the cytokine from HaCaT cells "4h+20h" and "4h+68h" recovery exposure. In particular, "4h+20h" recovery cells exposure to FLG (0.01, 0.1 and 1.0 μg/mL) induced the release of 19.3±0.7 pg/mL ($p < 0.01$), 19.6±0.4 pg/mL ($p < 0.01$) and 21.6±0.1 pg/mL ($p < 0.001$) GM-CSF, corresponding to about 2-fold increase compared to untreated control, respectively (panel E). Similarly, "4h+68h" recovery exposure to 0.01, 0.1 and 1.0 μg/mL FLG induced a significant release of GM-CSF equal to 24.0±0.8 pg/mL ($p < 0.001$), 27.3±1.2 pg/mL ($p < 0.001$) and 27.0±1.2 pg/mL ($p < 0.001$), respectively, corresponding to about 2-fold increase compared to untreated control (panel E). GO (0.01, 0.1 and 1.0 μg/mL) induced a significant release of GM-CSF only after "4h+68h" recovery exposure, equal to 19.8±2.7 pg/mL ($p < 0.001$), 24.1±1.2 pg/mL ($p < 0.001$) and 27.9±1.9 pg/mL ($p < 0.001$), respectively, corresponding to about 2-fold increase compared to untreated control (panel F).

A significant release of GM-CSF was observed also after continuous exposure to FLG or GO. FLG induced a significant release of GM-CSF after 24 and 72 h exposure only at the highest concentration (1.0 μg/mL), equal to 20.7±1.5 pg/mL ($p < 0.001$) and 19.8±4.4 pg/mL ($p < 0.01$), respectively, which correspond to 2-fold increase compared to untreated control (panel E). Cells exposure to GO for 24 h provoked a significant release of GM-CSF only at the highest concentration (1.0 μg/mL), equal to 20.0±2.0 pg/mL ($p < 0.001$), corresponding to 2-fold increase compared to untreated control. After 72 h, GO determined a significant GM-CSF release at 0.1 and 1.0 μg/mL, equal to 18.5±1.6 pg/mL ($p < 0.01$) and 21.7±1.6 pg/mL ($p <$

0.001), respectively, which correspond to 2-fold increase compared to untreated control (panel F).

On the contrary, MIP-1β was not detected in the culture medium of cells exposed to FLG (panel G) or GO (panel H).

The obtained results demonstrate, for the first time, a significant release of inflammatory mediators by skin keratinocytes exposed to GFNs. Our observations are supported by previous studies on other cell models reporting the ability of other GFNs to induce the release of inflammatory mediators (i.e. IL-1α, IL-6, IL-10, TNFα, GM-CSF and MIP-1β), such as a commercial few layer graphene in both primary murine macrophages and immortalized macrophages (Zhou et al., 2012), graphene oxide (obtained by the modified Hummers method) in RAW264.7 cells (Chen et al., 2012), human peritoneal macrophages (PMØ) and murine macrophages (J774A.1 cells) (Yue et al., 2012). However, in all these studies, endotoxin removal from the samples was not reported and its potential impact on the results remains unclear. Indeed, some of these studies report that GFNs-induced cytokine secretion was dependent on the signaling pathway of toll-like receptors (TLR), including TLR-4, which is known to be the PRR for LPS (Zhou et al., 2012; Chen et al., 2012). In addition, these effects were recorded in cells specialized in the production and release of cytokines, such as macrophages. Based on these observations, a direct comparison of these effects to those recorded with this study is not possible. In our model, at sub-cytotoxic GFN concentrations (0.1 and 1.0 μg/mL), the highest cytokines release was recorded after 4 h cells exposure to FLG or GO followed by 20 or 68 h of recovery. For these reasons, these conditions were chosen for the subsequent set of experiments.

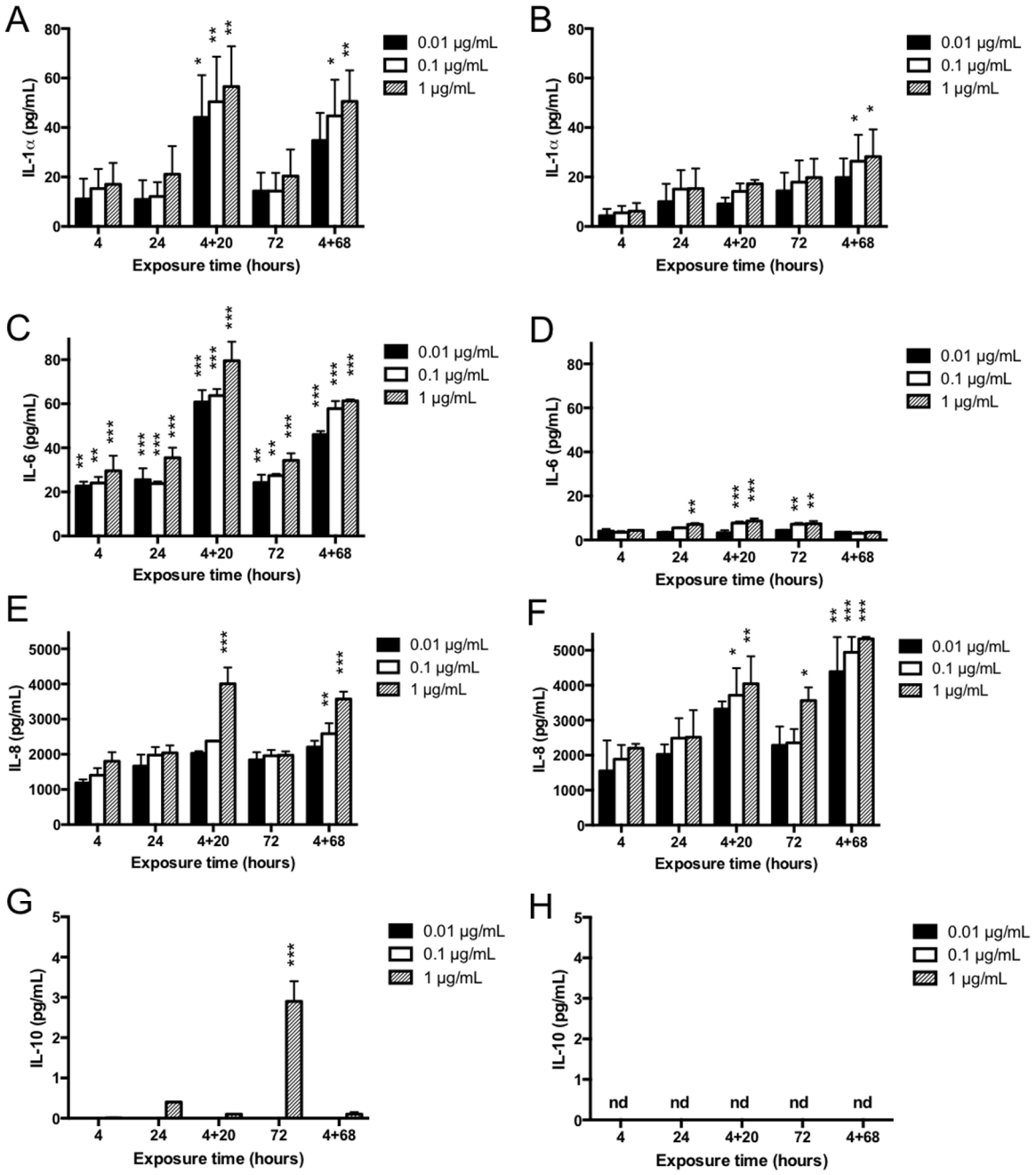

Figure 26. Effect of FLG (panel A, C, E, G) and GO (panel B, D, F, H) on IL-1α, IL-6, IL-8 and IL-10 release from HaCaT cells after continuous (4, 24 and 72 h) or recovery exposures to these materials (4 h exposure followed by 20 h or 68 h culture in fresh medium: "4h+20h" or "4h+68h"). Data are presented as pg/mL of cytokine released in cell media and are the mean ± SE of four independent experiments. Statistical differences: *, $p<0.05$; **, $p<0.01$; ***, $p<0.001$ (two-way ANOVA followed by Bonferroni's post test).

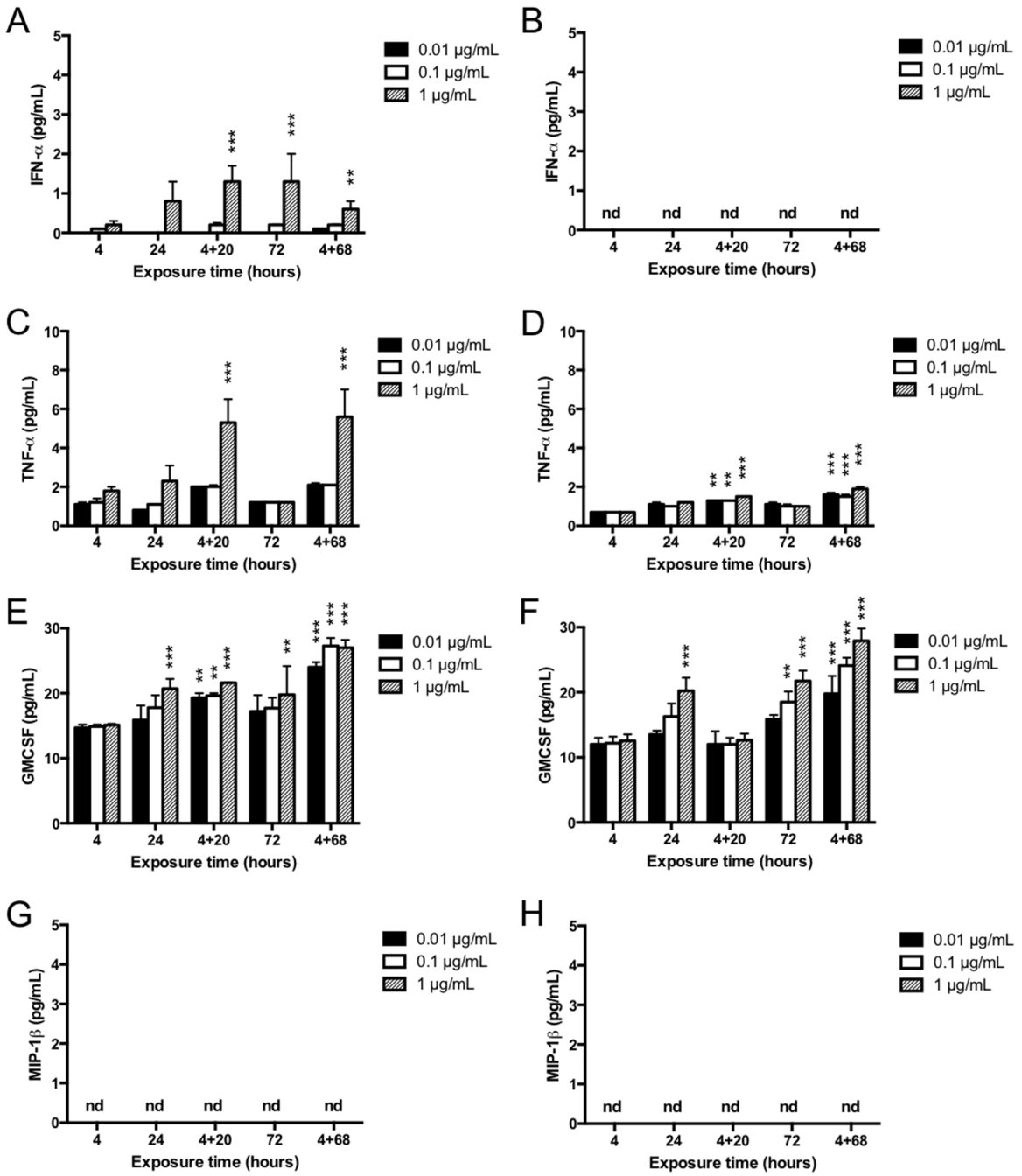

Figure 27. Effect of FLG (panel A, C, E, G) and GO (panel B, D, F, H) on IFN-α, TNF-α, GM-CSF and MIP-1β release from HaCaT cells after continuous (4, 24 and 72 h) or recovery exposures to these materials (4 h exposure followed by 20 h or 68 h culture in fresh medium:, "4h+20h" or "4h+68h"). Data are presented as pg/mL of cytokine released in cell media and are the mean ± SE of four independent experiments. Statistical differences: *, $p<0.05$; **, $p<0.01$; ***, $p<0.001$ (two-way ANOVA followed by Bonferroni's post test).

4.4.4 Effect of conditioned media from HaCaT cells exposed to GFNs on THP-1 monocytes differentiation

To assess if human skin HaCaT keratinocytes could be actively involved in the induction of an inflammatory response after cutaneous exposure to GFNs, the effects of conditioned media from GFNs-treated HaCaT cells on human monocytes (THP-1 cells) was investigated. The effects were evaluated by means of THP-1 cells differentiation and cytokine release from THP-1 cells. These experiments were carried out in collaboration with the Institute of Environmental Medicine (IMM) at the Karolinska Institutet (Stockholm, Sweden).

As reported in the previous section, for this purpose, the recovery exposure conditions to assess cytokine release from THP-1 cells were "4h+20h" and "4h+68h" and FLG or GO concentrations were 0.1 and 1.0 μg/mL, selected on the basis of the highest release of inflammatory cytokines from HaCaT cells. Considering cell differentiation, THP-1 cells were exposed for 48 and 120 h to conditioned media from HaCaT cells exposed to FLG or GO and the recorded effects were compared to control HaCaT cells-conditioned media. As shown in Figures 28 and 29, a panel of surface differentiation markers (CD14, CD54, CD86, HLA-DR and CD11b) were evaluated by flow cytometry. In general, none of the conditioned media from HaCaT cells exposed to FLG or GO significantly influenced the expression of the selected differentiation markers, as compared to controls. Only a slight but significant increase in the expression of HLA-DR was observed after 120 h exposure to the "4h+68h" conditioned medium from HaCaT cells exposed to the highest concentration of FLG (1.0 μg/mL). This effect could be due to a paracrine effect of inflammatory cytokines released by HaCaT cells rather than to an effective antigen presentation (Figure 28, panel D). On the contrary, as expected, positive controls (Figure 30) induced significant changes in the expression of differentiation markers after THP-1 cell differentiation into macrophages (10^{-7} M PMA for 72

h), immature dendritic cells (iDC; 100 ng/mL IL-4 and GM-CSF for 120 h) or mature dendritic cells (mDCs; 200 ng/mL IL-4, 100 ng/mL GM-CSF, 10 ng/mLTNF-α and 200 ng/mL ionomycin for 48 h).

It has been reported that other carbon-based nanomaterials induced DCs *in vitro* maturation, such as functionalized carbon nanotubes in THP-1 cells (Pescatori et al., 2013), carbon black nanoparticles in mouse bone marrow-derived dendritic cells (Koike et al., 2008) and fullerene derivatives in myeloid DC (Yang et al., 2010). However, while in these studies immune cells were directly exposed to the nanomaterials, in the present study immune cells were exposed to conditioned media from skin keratinocytes exposed to FLG or GO. In this condition, the tested GFNs appear to be safer at the immune system level compared to other carbon nanomaterials. Regarding GFNs, studies have been focused on dendritic cells and macrophages rather than on monocytes. Interestingly, Tkach and co-workers (Tkack et al., 2012) showed that, while endotoxin-free GO (modified Hummers' method) also potentiate the maturation of DCs by increasing the expression of major histocompatibility complex (MHC) and co-stimulatory molecules (i.e. CD86), it impairs the stimulatory potential of DCs by suppressing their ability of antigen presentation, resulting in an immunosuppressive regulatory effect. On the contrary, a recent study showed that multi-layer graphene (mechanical ablation method) did not induce any modulation of CD86 expression in murine RAW 264.7 macrophages (Muzi et al., 2016). However, no studies assessing the active involvement of skin keratinocytes in the modulation of inflammatory response to cutaneous contact with GFNs have been carried out, so far. These results, for the first time, demonstrate that skin keratinocytes exposure to FLG or GO does not induce any significant differentiation of monocytes, despite it induces a significant release of cytokines.

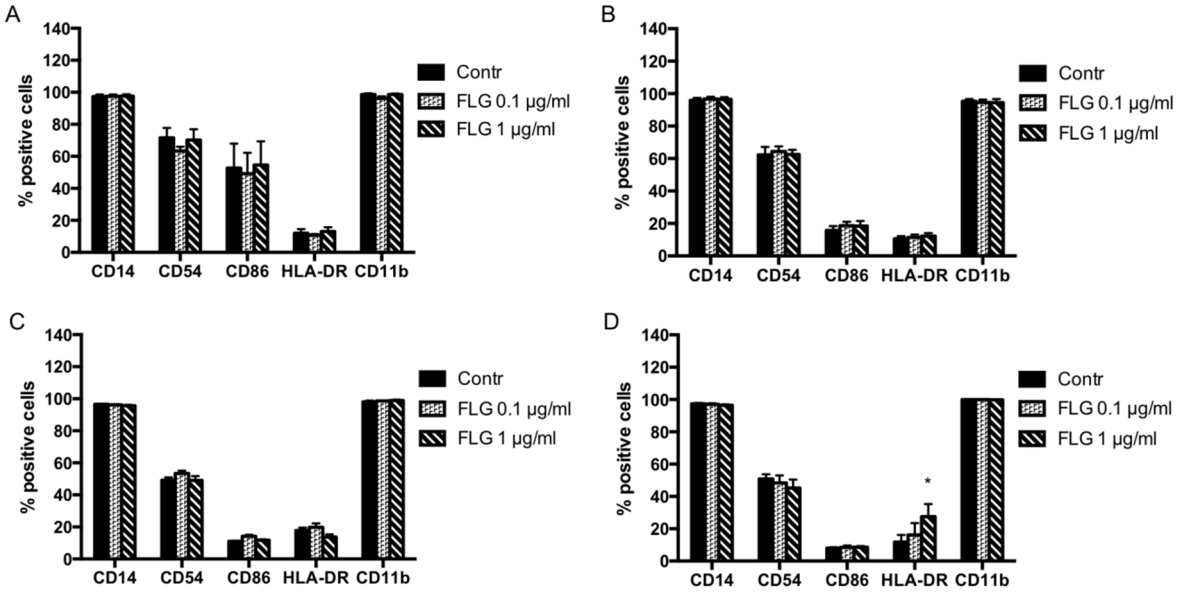

Figure 28. Effect of conditioned media from HaCaT cells exposed to FLG on monocytes differentiation. THP-1 cells were exposed for 48 h to the conditioned media from HaCaT cells exposed to FLG ("4h+20h", panel A, and "4h+68h", panel B) or for 120 h to the conditioned media from HaCaT cells exposed to FLG ("4h+20h", panel C, and "4h+68h", panel D). The levels of the differentiation markers CD14, CD54, CD86, HLA-DR and CD11b were evaluated by flow cytofluorometry. The results are expressed as % of positive cells to the markers considered and are the average of 3 experiments performed in duplicate. Statistical differences vs. HaCaT-conditioned media controls: *, $p < 0.05$ (one-way ANOVA and Bonferroni post-test).

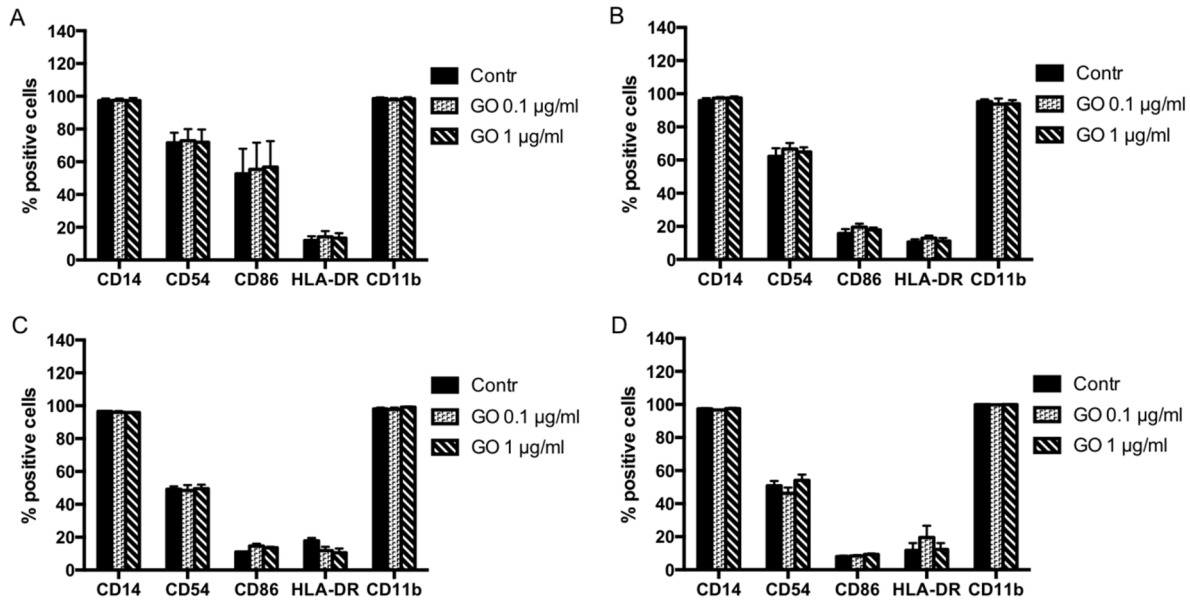

Figure 29. Effect of conditioned media from HaCaT cells exposed to GO on monocytes differentiation. THP-1 cells were exposed for 48 h to the conditioned media from HaCaT cells exposed to GO ("4h+20h", panel A, and "4h+68h", panel B) or for 120 h to the conditioned media from HaCaT cells exposed to GO ("4h+20h", panel C, and "4h+68h", panel D). The levels of the differentiation markers CD14, CD54, CD86, HLA-DR and CD11b were evaluated by flow cytofluorometry. The results are expressed as % of positive cells to the markers considered and are the average of 3 experiments performed in duplicate.

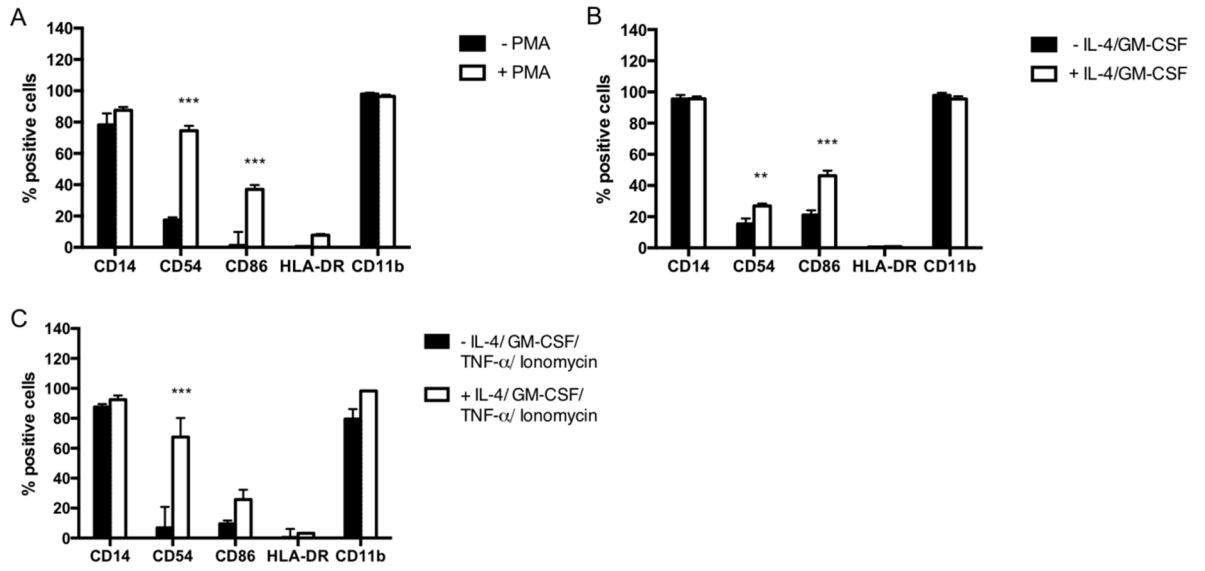

Figure 30. Expression of differentiation markers in monocytes differentiated to (A) macrophages (10^{-7} M PMA, for 72 h), (B) iDCs (100 ng/mL IL-4 and GM-CSF, for 120 h) and (C) mDCs (200 ng/mL IL-4, 100 ng/mL GM-CSF, 10 ng/mL TNF-α and 200 ng/mL ionomycin, for 48 h). The results are expressed as % of positive cells to the markers considered and are the average of 3 experiments performed in duplicate (black bars: undifferentiated monocytes; white bars: differentiated cells). Statistical differences vs. undifferentiated monocytes: **, $p < 0.01$; ***, $p < 0.001$ (one-way ANOVA and Bonferroni post-test).

4.4.5 Effects of conditioned media from HaCaT cells exposed to GFNs on inflammatory mediators release by THP-1 monocytes

The effect of conditioned media from HaCaT cells exposed to FLG or GO on inflammatory mediators release by THP-1 cells was evaluated by Luminex® technology. To this aim, THP-1 cells were exposed for 24 h to conditioned media from HaCaT cells exposed to FLG or GO after recovery conditions ("4h+20h", "4h+68h" and controls). Subsequently, THP-1 cells were washed and maintained in culture for additional 24 h in fresh THP-1 media to avoid any misinterpretation of the data due to cytokines presence in HaCaT cells-conditioned media (refer to section 4.4.3).

Then, culture media were collected and the following 27 inflammatory mediators released in cell media by THP-1 cells were quantified by Luminex® system according to the manufacturer's instructions: IL-1Ra, IL-1β, IL-2, IL-4, IL-5, IL-6, IL-7, IL-8, IL-9, IL-10, IL-12, IL-13, IL-15, IL-17, Eotaxin, fibroblast growth factor-basic (FGF basic), granulocyte-colony stimulating factor (G-CSF), GM-CSF, IFN-γ, IP-10, MCP-1, platelet derived growth factor BB (PDGF-BB), RANTES, TNF-α, vascular endothelial growth factor (VEGF) and MIP-1α -1β. LPS (0.1 μg/ml) was included as a positive control.

The obtained results are reported in Figure 31. The release of IL-1Ra, IL-1β, IL-2, IL-4, IL-5, IL-6, IL-7, IL-8, IL-9, IL-10, IL-12, IL-13, IL-15, IL-17, Eotaxin, FGF basic, G-CSF, GM-CSF, IFN-γ, IP-10, MCP-1, PDGF-BB, RANTES, TNF-α, VEGF, MIP-1α and MIP-1β by THP-1 cells exposed to conditioned media from HaCaT cells treated with FLG or GO were significantly lower than those recorded exposing the cells to LPS, used as positive control ($p<0.001$) (Panel A). The hierarchical cluster analysis, performed using R-program (version 3.3.2) according to Bhattacharya et al. (Bhattacharya, 2017), allowed to draw association dendrograms between the released proteins, suggesting two groups/clusters of cytokines,

chemokines and growth factors secretion after THP-1 cells exposure to conditioned media from HaCaT cells treated to FLG or GO (Panel B). The first cluster, ranging from IFN-γ to VEGF, includes inflammatory mediators involved mainly in the Janus kinase/signal transducers and activators of transcription (Jak-STAT) pathway (a cascade transducing a multitude of signals for regulating apoptosis, cell cycle and differentiation) or exerting growth factor activity. The second cluster, ranging from GM-CSF to MIP-1α, included mainly the inflammatory mediators involved in cell proliferation, chemotaxis and response to wounding. However, the level of cytokines, chemokines and growth factors secretion was significantly lower in THP-1 cells exposed to conditioned media from HaCaT cells treated with FLG or GO than that from negative control (THP-1 cells exposed to conditioned media from untreated HaCat cells) and thereby their secretion levels were not statistically significant.

Despite the ability of GFNs, such as GQDs (Qin et al., 2015) and GO (Wang et al., 2015), to trigger inflammatory mediators release from THP-1 cells (i.e. TNF-α, IL-1β and IL-8) has been previously reported, these results suggest that skin HaCaT keratinocytes exposed to FLG or GO do not significantly increase inflammatory mediators release from THP-1 monocytes.

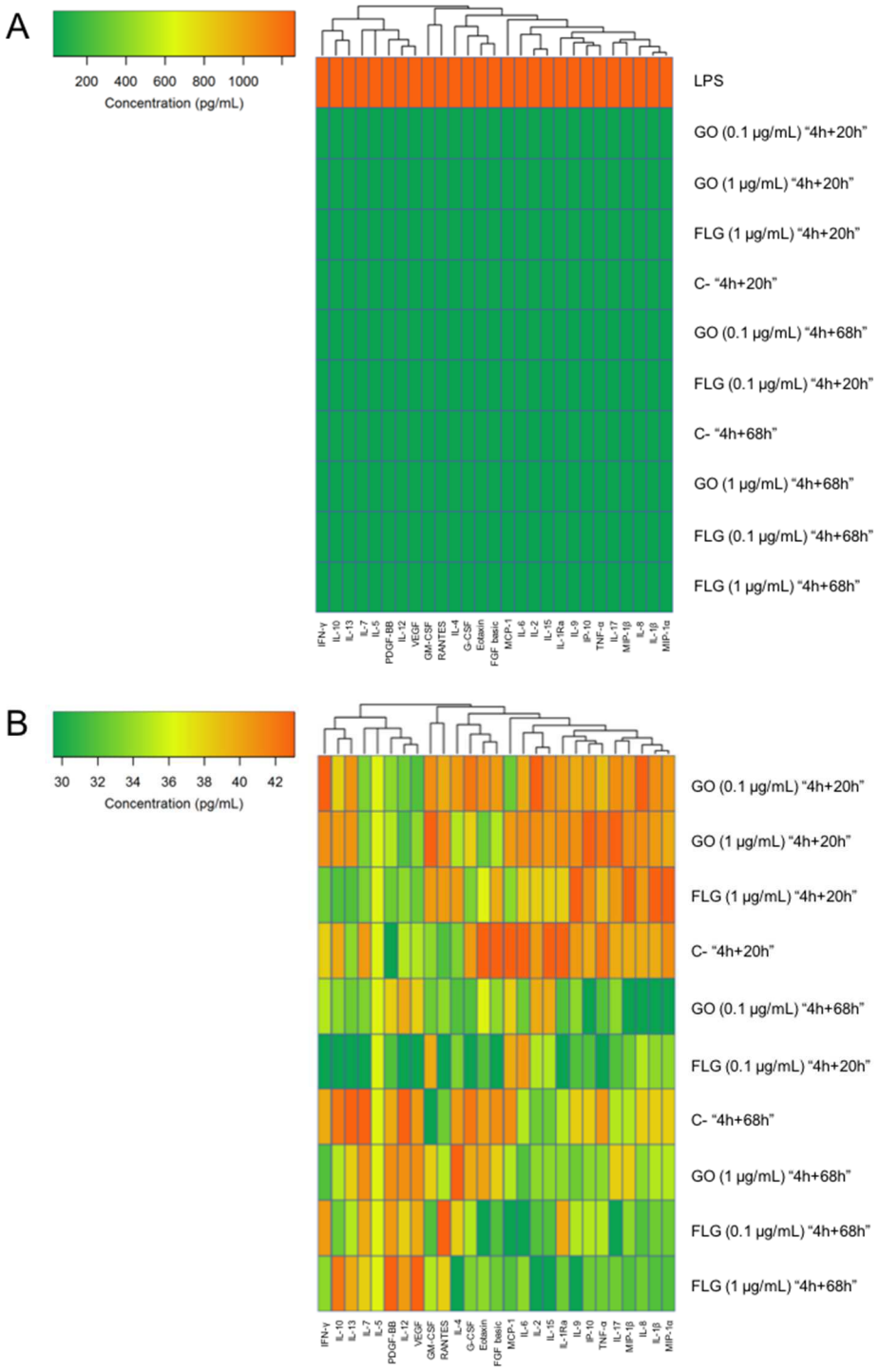

Figure 31. Heat map of the cytokines, chemokines and growth factors released by THP-1 monocytes exposed to conditioned media from HaCaT cells quantified by Luminex® multiplex

(27 plex) array. The levels of secreted proteins by THP-1 cells exposed to conditioned media from HaCaT cells treated with FLG or GO were significantly lower than those secreted by cells exposed to LPS (Panel A). Hierarchical cluster analysis suggested two groups/clusters of the cytokines, chemokines and growth factors levels secreted by THP-1 cells exposed to conditioned media from HaCaT cells exposed to FLG or GO (Panel B). Data are presented as pg/mL of each analyte released in cell media and are the mean ± SE of six independent experiments.

4.4.6 Assessment of the *in vitro* sensitization potential of FLG and GO (h-CLAT)

Skin sensitization is a key event of immunotoxicity following cutaneous exposure to a sensitizer, able to induce a cutaneous immune response resulting in immunological priming (sensitization). Since the evaluation of skin sensitization properties is an extremely important aspect for the safety assessment of new chemicals, GFNs were evaluated for their ability to induce sensitization by an *in vitro* sensitizing test based on the human cell line activation test (h-CLAT). To this aim, the specific OECD guideline for the testing of chemicals concerning the *in vitro* skin sensitization (OECD 442E) was followed. The h-CLAT method is proposed to address the activation of monocytes to dendritic cells (DC), a crucial event of the skin sensitization, quantifying changes in the expression of specific cell surface markers associated with the process of activation of THP-1 monocytes to DC after exposure to sensitizers. Thus, changes in CD54 and CD86 surface markers expression in THP-1 cells after 24 h exposure to FLG or GO were measured by flow cytometry to discriminate between sensitizers and non-sensitizers. The alterations of CD54 and CD86 expression after a 24 h treatment was calculated as a relative fluorescence intensities (RFI) % value.

The guideline reports a protocol divided into different steps. After an initial control on the reactivity of THP-1 cells (reactivity check), the dose finding assay is used to define the concentration range to be used for the evaluation of CD54 and CD86 expression levels. In particular, THP-1 cells were exposed to FLG or GO (7.81 - 1000 μg/mL) for 24 h and PI uptake was evaluated by flow cytometry to extrapolate the test chemical concentration resulting in 75% cell viability (CV75) compared to the solvent/vehicle control. However, it was not possible to determine the CV75 for FLG or GO due to the low cytotoxicity observed in the dose finding assay. In fact, as shown in Figure 32, even at the highest concentration (1000 μg/mL) the percentage of PI uptake, representatives of death cells, induced by FLG (20.4%) and GO

(12.4%) in THP-1 cells was lower than 25%. Therefore, for the CD54/CD86 expression measurement, 12 μg/mL was selected as a starting GFNs concentration to determine 8 concentrations of test materials (3.4 - 12 μg/mL) by a 1:1.2 dilution factor. This concentration was chosen basing on the OECD guidelines, suggesting that, if the CV75 cannot be determined, the highest stably dispersed concentration of test chemical should be used as starting concentration.

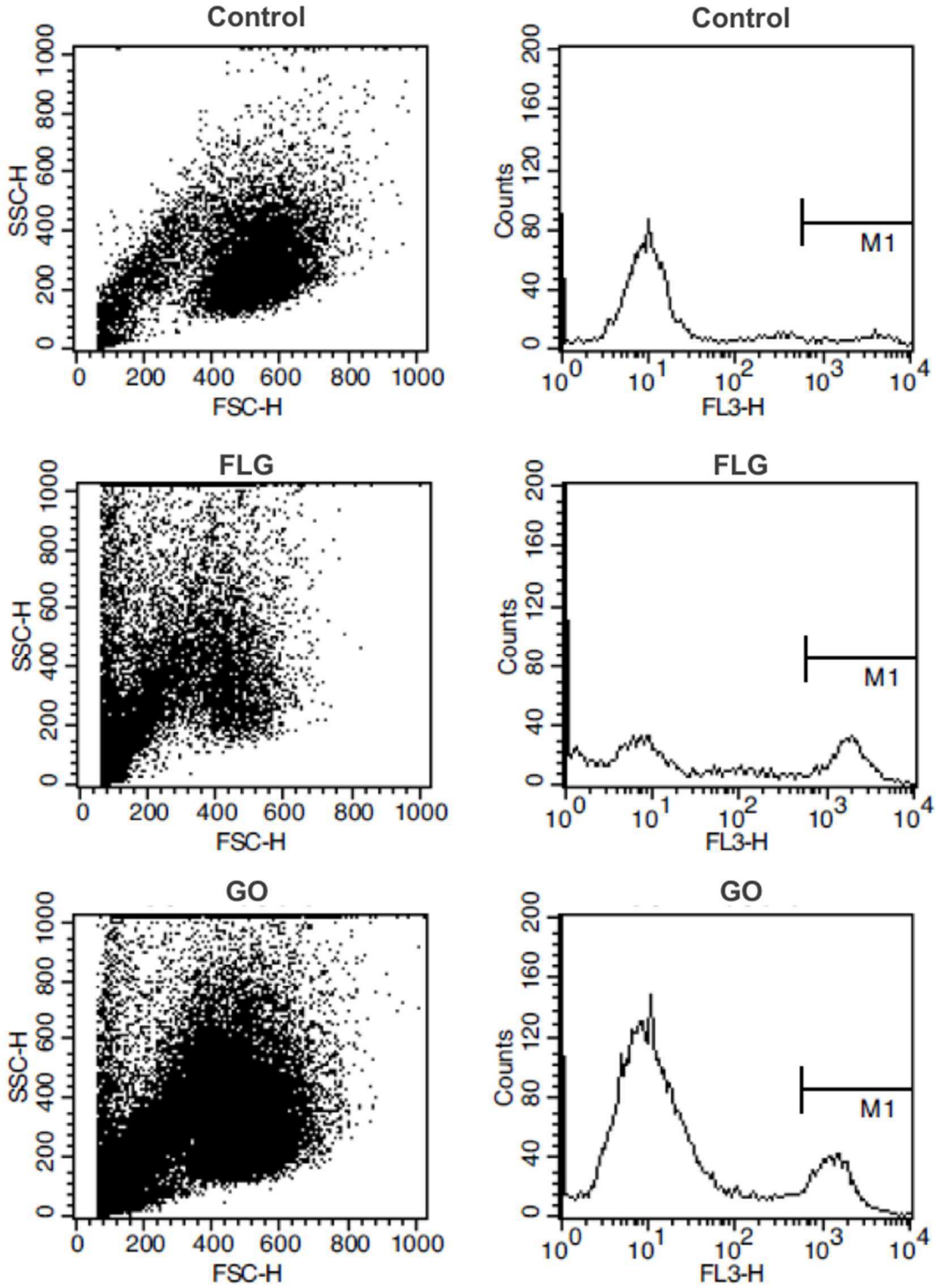

Figure 32. Forward vs Side scatter dot-plots (left panel) and histograms (right panel) representing the changes in PI uptake (death cells), acquired on the FL3 channel, after THP-1 cells exposure to the highest concentration of FLG or GO (1000 μg/mL), analyzed by flow cytometry. Negative control represents THP-1 cells cultured in solvent/vehicle control (0.2%

DMSO in medium). Markers M1 was set to delineate PI peak. Ten thousand cells were counted and analyzed per sample. The figure is representative of two independent experiments performed in duplicate.

Once defined the proper concentration range, THP-1 cells were exposed to FLG or GO (3.4 - 12 μg/mL) for 24 h. Dinitrochlorobenzene (DNCB, 4 μg/mL) and lactic acid (LA, 1500 μg/mL) were included as positive and negative control, respectively. Figures 33 e 34 represent histograms showing changes in surface markers (FL1) expression and PI uptake (FL3) in THP-1 cells exposed to the highest concentration of FLG or GO (12 μg/mL), analyzed by flow cytometry. Dot plots are representative of the morphology of the cells. As compared to the negative control (0.2 % DMSO), the relative fluorescence intensity (RFI%) values for CD54 recorded after cells exposure to FLG or GO were 120% and 137%, respectively, while RFI% for CD86 were 102% and 101%, respectively. Similar results were obtained for all the other GFNs selected concentrations (data not shown). These values are lower than the relevant RFI% thresholds (RFI% ≥150 and ≥ 200, for CD54 and CD86, respectively, with corresponding cell viabilities of ≥50%). Thus, in accordance with OECD 442E guidelines, FLG and GO resulted as negative sensitizers, at least regarding the third of the four phases leading to skin sensitization (i.e. activation of monocytes). However, as suggested by the OECD guidelines, further studies addressing other key events of the skin sensitization are required to integrate the obtained results and draw conclusions on the absence of skin sensitization potential of these nanomaterials. On the contrary, as expected, CD54 and CD86 expression induced by the positive control DNCB (260 and 329%, respectively) was above the respective thresholds, while CD54 and CD86 expression induced by the negative control LA (109 and 113%, respectively) was under the respective thresholds.

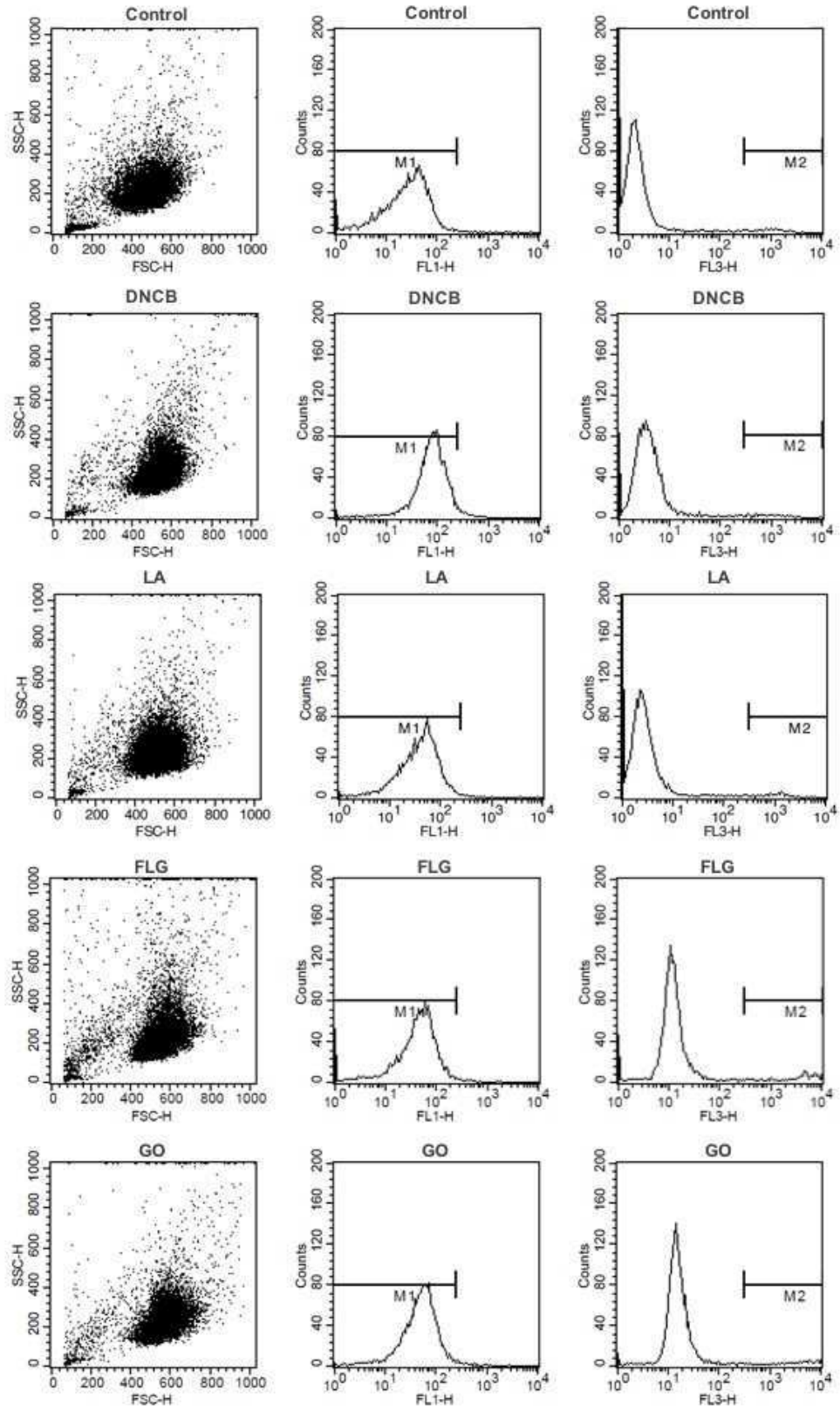

Figure 33. Forward vs Side scatter dot-plots (left panel) and histograms representing changes in CD54 expression (acquired on the FL1 channel, middle panel) and PI uptake (acquired on

the FL3 channel, right panel) after THP-1 cells exposure to FLG or GO, analyzed by flow cytometry. THP-1 cells were exposed to FLG or GO (12 μg/mL) for 24 h. DNCB (4 μg/mL) and LA (1500 μg/mL) were used as positive and negative control, respectively. The control represents THP-1 cultured in solvent/vehicle control (0.2% DMSO in medium). Markers M1 and M2 were set to delineate FITC and PI peaks, respectively. Results are shown from one representative experiment out of two. Ten thousand cells were counted and analyzed per sample.

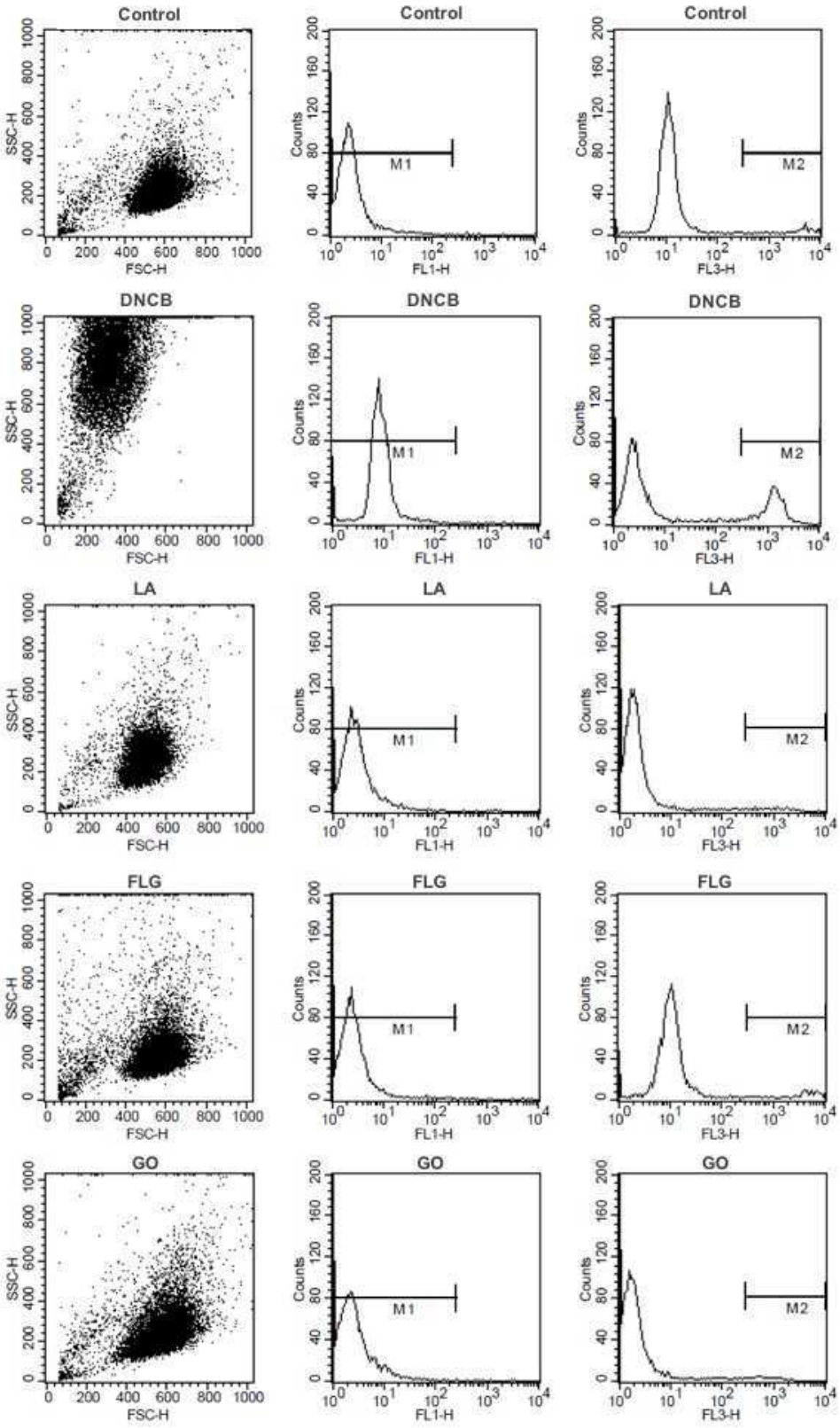

Figure 34. Forward vs Side scatter dot-plots (left panel) and histograms representing changes in CD86 expression (acquired on the FL1 channel, middle panel) and PI uptake (acquired on

the FL3 channel, right panel) after THP-1 cells exposure to FLG and GO, analyzed by flow cytometry. THP-1 cells were exposed to FLG or GO (12 μg/mL) for 24 h. DNCB (4 μg/mL) and LA (1500 μg/mL) were used as positive and negative control, respectively. The control represents THP-1 cultured in solvent/vehicle control (0.2% DMSO in medium). Markers M1 and M2 were set to delineate FITC and PI peaks, respectively. Results are shown from one representative experiment out of two. Ten thousand cells were counted and analyzed per sample.

5. Conclusions

Graphene Family Nanomaterials (GFNs) are promising tools for several applications in nanotechnology and biomedical fields, due to their extraordinary physicochemical properties. However, before their mass production, their safety for human health should be addressed. Cutaneous toxicity of GFNs is largely unexplored, although skin contact is one of the major exposure routes to GFNs. Hence, GFNs effects were evaluated on human HaCaT keratinocytes, a non-tumor cell line widely used to evaluate toxic effects at the skin level.

On this cell model, a comparative study of different GFNs effects was initially carried out. Even though 24 h HaCaT cells exposure to few layer graphene (FLG) or graphene oxides (GOs) did not induce any significant effect, increasing the exposure up to 72 h induced a significant mitochondrial and plasma membrane damage, leading to cytotoxicity, only at high concentrations (> 30 μg/mL and > 1.0 μg/mL for FLG and GOs, respectively), with variable potencies depending on GFNs oxidation state. In the effort to investigate the cellular damages induced by GFNs, the obtained results contribute to figure out a putative mechanism of toxicity of these materials at the cutaneous level. In particular, the mitochondrial damage, associated with a significant plasma membrane damage due to GFNs physical interaction with the plasma membrane, seems to be dependent on a sustained mitochondrial depolarization. Mitochondrial depolarization is not due to mitochondrial transition pore opening, but rather mediated by a concentration- and time-dependent ROS production induced by GFNs. The latter seems to be dependent on the activation of flavoprotein-based oxidative enzymes, such as NADH dehydrogenase and xanthine oxidase.

However, notwithstanding the definition of this mechanism of toxicity, more predictive models let us to conclude that GFNs may induce only minor inflammatory effects at the skin level. Indeed, subcytotoxic concentrations of FLG or GO induced a significant but in some case slight release of pro-inflammatory mediators from HaCaT cells, mainly after a short exposure time (4

h), followed by long recovery times in GFNs-free media (20 or 68 h). However, the conditioned media collected from HaCaT cells after FLG or GO exposure under these conditions, did not induce either a significant differentiation of THP-1 monocytes towards macrophages or dendritic cells nor a release of inflammatory mediators by these cells. These observations suggest that these materials may induce only a moderate inflammatory reaction at the skin level. These results were confirmed by the investigation of the sensitizing potential of FLG and GO on THP-1 monocytes (according to the specific OECD guideline n° 442E), suggesting that these nanomaterials are not skin sensitizers.

On the whole, these results suggest that FLG and GO may induce only minor toxic effects at the skin level, even though they should be confirmed by more predictive and complete *in vitro* and *in vivo* studies. Future aims of the study include the evaluation of: GFNs *in vitro* irritant properties using a reconstructed human epidermis (RhE) model, which closely mimics the biochemical and physiological properties of the upper parts of the human skin (i.e. the epidermis), following the OECD guideline 439 (OECD 439). The *in vitro* findings will be confirmed by *in vivo* models evaluating the sensitizing properties of GFNs, by the local lymph node activation assay (LLNA) measuring lymphocytes proliferation after cutaneous applications of GFNs on mice ears (OECD 442B), as well as the irritant potential of these nanomaterials as ear oedema and inflammatory cells infiltration (myeloperoxidase activity in the ear tissue as index of granulocytes infiltration).

6. References

Abbasi, E., Akbarzadeh, A., Kouhi, M., and Milani, M. (2016). Graphene: Synthesis, bio-applications, and properties. Artificial cells, nanomedicine, and biotechnology 44, 150-156.

Akhavan, O., Ghaderi, E., and Akhavan, A. (2012). Size-dependent genotoxicity of graphene nanoplatelets in human stem cells. Biomaterials 33, 8017-8025.

Ansel, J., Perry, P., Brown, J., Damm, D., Phan, T., Hart, C., Luger, T., and Hefeneider, S. (1990). Cytokine modulation of keratinocyte cytokines. J Invest Dermatol 94, 101S-107S.

Auwerx, J. (1991). The human leukemia cell line, THP-1: a multifacetted model for the study of monocyte-macrophage differentiation. Experientia 47, 22-31.

Avouris, P. (2010). Graphene: electronic and photonic properties and devices. Nano Lett 10, 4285-4294.

Bangert, C., Brunner, P.M., and Stingl, G. (2011). Immune functions of the skin. Clin Dermatol 29, 360-376.

Bao, H., Pan, Y., Ping, Y., Sahoo, N.G., Wu, T., Li, L., Li, J., and Gan, L.H. (2011). Chitosan-functionalized graphene oxide as a nanocarrier for drug and gene delivery. Small 7, 1569-1578.

Bao, Q., and Loh, K.P. (2012). Graphene photonics, plasmonics, and broadband optoelectronic devices. ACS Nano 6, 3677-3694.

Baraton, L., He, Z., Lee, C.S., Maurice, J.L., Cojocaru, C.S., Gourgues-Lorenzon, A.F., Lee, Y.H., and Pribat, D. (2011). Synthesis of few-layered graphene by ion implantation of carbon in nickel thin films. Nanotechnology 22, 085601.

Barker, J.N., Mitra, R.S., Griffiths, C.E., Dixit, V.M., and Nickoloff, B.J. (1991). Keratinocytes as initiators of inflammation. Lancet 337, 211-214.

Berges, C., Naujokat, C., Tinapp, S., Wieczorek, H., Hoh, A., Sadeghi, M., Opelz, G., and Volker, D. (2005). A cell line model for the differentiation of human dendritic cells. Biophy Res Commun 333, 896-907.

Bhattacharya, K., Kilic, G., Costa, P.M., and Fadeel, B. (2017). Cytotoxicity screening and cytokine profiling of nineteen nanomaterials enables hazard ranking and grouping based on inflammogenic potential. Nanotoxicology 11, 809-826.

Bianco, A. (2013). Graphene: safe or toxic? The two faces of the medal. Angew Chem Int Ed Engl 52, 4986-4997.

Bianco, A., Cheng, H.-M., Enoki, T., Gogotsi, Y., Hurt, R.H., Koratkar, N., Kyotani, T., Monthioux, M., Park, C.R., Tascon, J.M.D., et al. (2013). All in the graphene family – A recommended nomenclature for two-dimensional carbon materials. Carbon 65, 1-6.

Bishop, R.E. (2005). Fundamentals of endotoxin structure and function. Contrib Microbiol 12, 1-27.

Boehm, H.P. (2010). Graphene--how a laboratory curiosity suddenly became extremely interesting. Angew Chem Int Ed Engl 49, 9332-9335.

Boehm, H.P., Clauss, A., Fischer, G.O., and Hofmann, U. (1962). Das Adsorptionsverhalten sehr dünner Kohlenstoff-Folien. Zeitschrift für anorganische und allgemeine Chemie 316, 119-127.

Boehm, H.P., Setton, R., and Stumpp, E. (1986). Nomenclature and terminology of graphite intercalation compounds. Carbon 24, 241-245.

Boukhvalov, D.W., and Katsnelson, M.I. (2009). Chemical functionalization of graphene. J Phys-Condens Mat 21.

Briganti, S., and Picardo, M. (2003). Antioxidant activity, lipid peroxidation and skin diseases. What's new. Journal of the European Academy of Dermatology and Venereology: JEADV 17, 663-669.

Brodie, B.C. (1859). XIII. On the atomic weight of graphite. Philosophical Transactions of the Royal Society of London 149, 249-259.

Bussy, C., Jasim, D., Lozano, N., Terry, D., and Kostarelos, K. (2015). The current graphene safety landscape--a literature mining exercise. Nanoscale 7, 6432-6435.

Casati, S., Aeby, P., Basketter, D.A., Cavani, A., Gennari, A., Gerberick, G.F., Griem, P., Hartung, T., Kimber, I., Lepoittevin, J.P., et al. (2005). Dendritic cells as a tool for the predictive identification of skin sensitisation hazard. Altern Lab Anim 33, 47-62.

Chakraborty, S., and Massey, V. (2002). Reaction of reduced flavins and flavoproteins with diphenyliodonium chloride. J Biol Chem 277, 41507-41516.

Chang, H.X., and Wu, H.K. (2013). Graphene-based nanocomposites: preparation, functionalization, and energy and environmental applications. Energ Environ Sci 6, 3483-3507.

Chang, Y., Yang, S.T., Liu, J.H., Dong, E., Wang, Y., Cao, A., Liu, Y., and Wang, H. (2011). In vitro toxicity evaluation of graphene oxide on A549 cells. Toxicol Lett 200, 201-210.

Chen, G.Y., Yang, H.J., Lu, C.H., Chao, Y.C., Hwang, S.M., Chen, C.L., Lo, K.W., Sung, L.Y., Luo, W.Y., Tuan, H.Y., et al. (2012). Simultaneous induction of autophagy and toll-like receptor signaling pathways by graphene oxide. Biomaterials 33, 6559-6569.

Ciesielski, A., and Samorì, P. (2014). Graphene via sonication assisted liquid-phase exfoliation. Chem Soc Rev 43, 381-398.

Ciesielski, A., and Samorì, P. (2016). Supramolecular Approaches to Graphene: From Self-Assembly to Molecule-Assisted Liquid-Phase Exfoliation. Adv Mater 28, 6030-6051.

Coleman, J.N. (2013). Liquid exfoliation of defect-free graphene. Acc Chem Res 46, 14-22.

Coquette, A., Berna, N., Poumay, Y., and Pittelkow, M.R. (2000). The keratinocyte in cutaneous irritation and sensitization. In Biochemical modulation of skin reactions Transdermals, topicals, cosmetics, K.J. F Agis, J Wille, ed. (Boca Raton: CRC Press), pp. 125-143.

Coquette, A., Berna, N., Vandenbosch, A., Rosdy, M., De Wever, B., and Poumay, Y. (2003). Analysis of interleukin-1alpha (IL-1alpha) and interleukin-8 (IL-8) expression and

release in in vitro reconstructed human epidermis for the prediction of in vivo skin irritation and/or sensitization. Toxicol In Vitro 17, 311-321.

Cros, J., Cagnard, N., Woollard, K., Patey, N., Zhang, S.Y., Senechal, B., Puel, A., Biswas, S.K., Moshous, D., Picard, C., et al. (2010). Human CD14dim monocytes patrol and sense nucleic acids and viruses via TLR7 and TLR8 receptors. Immunity 33, 375-386.

Das, S., Singh, S., Singh, V., Joung, D., Dowding, J.M., Reid, D., Anderson, J., Zhai, L., Khondaker, S.I., Self, W.T., et al. (2013). Oxygenated Functional Group Density on Graphene Oxide: Its Effect on Cell Toxicity. Particle & Particle Systems Characterization 30, 148-157.

Debye, P., and Scherrer, P. (1916). Interferenzen an regellos orientierten Teilchen im Röntgenlicht. II. Nachrichten von der Gesellschaft der Wissenschaften zu Göttingen, Mathematisch-Physikalische Klasse 16, 16-26.

de Heer, W.A., Berger, C., Wu, X., First, P.N., Conrad, E.H., Li, X., Li, T., Sprinkle, M., Hass, J., Sadowski, M.L., et al. (2007). Epitaxial graphene. Solid State Communications 143, 92-100.

Dobrovolskaia, M.A., Germolec, D.R., and Weaver, J.L. (2009). Evaluation of nanoparticle immunotoxicity. Nat Nanotechnol 4, 411-414.

Duch, M.C., Budinger, G.R., Liang, Y.T., Soberanes, S., Urich, D., Chiarella, S.E., Campochiaro, L.A., Gonzalez, A., Chandel, N.S., Hersam, M.C., et al. (2011). Minimizing oxidation and stable nanoscale dispersion improves the biocompatibility of graphene in the lung. Nano Lett 11, 5201-5207.

Eedy, D.J. (1996). Carbon-fibre-induced airborne irritant contact dermatitis. Contact Dermatitis 35, 362-363.

Ema, M., Matsuda, A., Kobayashi, N., Naya, M., and Nakanishi, J. (2011). Evaluation of dermal and eye irritation and skin sensitization due to carbon nanotubes. Regulatory toxicology and pharmacology: RTP 61, 276-281.

Engel, M., Steiner, M., Lombardo, A., Ferrari, A.C., Löhneysen, H.V., Avouris, P., and Krupke, R. (2012). Light-matter interaction in a microcavity-controlled graphene transistor. Nat Commun 3, 906.

Monteiro-Riviere, N.A.R., Jim E. (2014). Dermatotoxicity of Nanomaterials. In Handbook of Safety Assessment of Nanomaterials (Pan Stanford), pp. 439-459.

Feliciani, C., Gupta, A.K., and Sauder, D.N. (1996). Keratinocytes and cytokine/growth factors. Crit Rev Oral Biol Med 7, 300-318.

Ferrari, A.C., and Basko, D.M. (2013). Raman spectroscopy as a versatile tool for studying the properties of graphene. Nat Nanotechnol 8, 235-246.

Freitag, M. (2008). Graphene: nanoelectronics goes flat out. Nat Nanotechnol 3, 455-457.
Gao, X.F., Jang, J., and Nagase, S. (2010). Hydrazine and Thermal Reduction of Graphene Oxide: Reaction Mechanisms, Product Structures, and Reaction Design. J Phys Chem C 114, 832-842.

Geim, A.K. (2012). Graphene prehistory. Physica Scripta 2012, 014003.

Geim, A.K., and Novoselov, K.S. (2007). The rise of graphene. Nature materials 6, 183-191.

Gibbs, S. (2009). In vitro irritation models and immune reactions. Skin Pharmacol Physiol 22, 103-113.

Gurunathan, S., Han, J.W., Eppakayala, V., and Kim, J.H. (2013). Green synthesis of graphene and its cytotoxic effects in human breast cancer cells. Int J Nanomedicine 8, 1015-1027.

Gutowska, I., Baranowska-Bosiacka, I., Baskiewicz, M. Milo, B., Siennicka, A., Marchlewicz, M., Wiszniewska, B., Machalinski, B., and Stachowska, E. (2010). Fluoride as a pro-inflammatory factor and inhibitor of ATP bioavailability in differentiated human THP1 monocytic cells. Toxycol Lett 196, 74-79.

Haake, A., Scott, G.A., and Holbrook, K.A. (2001). Structure and function of the skin: Overview of the epidermis and dermis.

Hänel, K.H., Cornelissen, C., Lüscher, B., and Baron, J.M. (2013). Cytokines and the skin barrier. Int J Mol Sci 14, 6720-6745.

Hernandez, Y., Nicolosi, V., Lotya, M., Blighe, F.M., Sun, Z., De, S., McGovern, I.T., Holland, B., Byrne, M., Gun'Ko, Y.K., et al. (2008). High-yield production of graphene by liquid-phase exfoliation of graphite. Nat Nanotechnol 3, 563-568.

Hu, W., Peng, C., Lv, M., Li, X., Zhang, Y., Chen, N., Fan, C., and Huang, Q. (2011). Protein corona-mediated mitigation of cytotoxicity of graphene oxide. ACS Nano 5, 3693-3700.

Jachak, A.C., Creighton, M., Qiu, Y., Kane, A.B., and Hurt, R.H. (2012). Biological interactions and safety of graphene materials. MRS Bull 37, 1307-1313.

James, D.K., and Tour, J.M. (2013). Graphene: Powder, Flakes, Ribbons, and Sheets. Accounts of chemical research 46, 2307-2318.

Jaworski, S., Sawosz, E., Kutwin, M., Wierzbicki, M., Hinzmann, M., Grodzik, M., Winnicka, A., Lipinska, L., Wlodyga, K., and Chwalibog, A. (2015). In vitro and in vivo effects of graphene oxide and reduced graphene oxide on glioblastoma. International journal of nanomedicine 10, 1585-1596.

Jayasena, B., Reddy, C.D., and Subbiah, S. (2013). Separation, folding and shearing of graphene layers during wedge-based mechanical exfoliation. Nanotechnology 24, 205301.

Jeong, H.K., Jin, M.H., So, K.P., Lim, S.C., and Lee, Y.H. (2009). Tailoring the characteristics of graphite oxides by different oxidation times. Journal of Physics D: Applied Physics 42, 065418.

Kalden, J.R. (1987). What is inflammation? European Heart Journal 8, 1-5.

Kasparov, A.A., Popova, T.B., Lebedeva, N.V., Gladkova, E.V., and Gurvich, E.B. (1989). Evaluation of the carcinogenic hazard in the manufacture of graphite articles. Vopr Onkol 35, 445-450.

Kim, J., Lee, J., Son, D., Choi, M.K., and Kim, D.H. (2016a). Deformable devices with integrated functional nanomaterials for wearable electronics. Nano Converg 3, 4.

Kim, J.K., Shin, J.H., Lee, J.S., Hwang, J.H., Lee, J.H., Baek, J.E., Kim, T.G., Kim, B.W., Kim, J.S., Lee, G.H., et al. (2016b). 28-Day inhalation toxicity of graphene nanoplatelets in Sprague-Dawley rats. Nanotoxicology 10, 891-901.

Koike, E., Takano, H., Inoue, K., Yanagisawa, R., Yanagisawa, R., and Kobayashi, T., (2008). Carbon black nanoparticles promote the maturation and function of mouse bone marrow-derived dendritic cells. Chemosphere 73, 371.

Kuila, T., Bose, S., Mishra, A.K., Khanra, P., Kim, N.H., and Lee, J.H. (2012). Chemical functionalization of graphene and its applications. Prog Mater Sci 57, 1061-1105.

Kumar, P., Das, B., Chitara, B., Subrahmanyam, K.S., Gopalakrishnan, K., Krupanidhi, S.B., and Rao, C.N.R. (2012). Novel Radiation-Induced Properties of Graphene and Related Materials. Macromol Chem Phys 213, 1146-1163.

Kupper, T.S., and Groves, R.W. (1995). The interleukin-1 axis and cutaneous inflammation. J Invest Dermatol 105, 62S-66S.

Lammel, T., Boisseaux, P., Fernandez-Cruz, M.L., and Navas, J.M. (2013). Internalization and cytotoxicity of graphene oxide and carboxyl graphene nanoplatelets in the human hepatocellular carcinoma cell line Hep G2. Particle and fibre toxicology 10, 27.

León, V., González-Domínguez, J.M., Fierro, J.L., Prato, M., and Vázquez, E. (2016). Production and stability of mechanochemically exfoliated graphene in water and culture media. Nanoscale 8, 14548-14555.

Leon, V., Quintana, M., Herrero, M.A., Fierro, J.L., de la Hoz, A., Prato, M., and Vazquez, E. (2011). Few-layer graphenes from ball-milling of graphite with melamine. Chem Commun (Camb) 47, 10936-10938.

León, V., Quintana, M., Herrero, M.A., Fierro, J.L., de la Hoz, A., Prato, M., and Vázquez, E. (2011). Few-layer graphenes from ball-milling of graphite with melamine. Chem Commun (Camb) 47, 10936-10938.

León, V., Rodriguez, A.M., Prieto, P., Prato, M., and Vázquez, E. (2014). Exfoliation of graphite with triazine derivatives under ball-milling conditions: preparation of few-layer graphene via selective noncovalent interactions. ACS Nano 8, 563-571.

Li, N., Zhang, X., Song, Q., Su, R., Zhang, Q., Kong, T., Liu, L., Jin, G., Tang, M., and Cheng, G. (2011). The promotion of neurite sprouting and outgrowth of mouse hippocampal cells in culture by graphene substrates. Biomaterials 32, 9374-9382.

Li, Y., Liu, Y., Fu, Y., Wei, T., Le Guyader, L., Gao, G., Liu, R.S., Chang, Y.Z., and Chen, C. (2012). The triggering of apoptosis in macrophages by pristine graphene through the MAPK and TGF-beta signaling pathways. Biomaterials 33, 402-411.

Li, Y.F., Yuan, H.Y., von dem Bussche, A., Creighton, M., Hurt, R.H., Kane, A.B., and Gao, H.J. (2013). Graphene microsheets enter cells through spontaneous membrane penetration at edge asperities and corner sites. P Natl Acad Sci USA 110, 12295-12300.

Liao, K.H., Lin, Y.S., Macosko, C.W., and Haynes, C.L. (2011). Cytotoxicity of graphene oxide and graphene in human erythrocytes and skin fibroblasts. ACS Appl Mater Interfaces 3, 2607-2615.

Liu, J., Poh, C.K., Zhan, D., Lai, L., Lim, S.H., Wang, L., Liu, X., Gopal Sahoo, N., Li, C., Shen, Z., et al. (2013). Improved synthesis of graphene flakes from the multiple electrochemical exfoliation of graphite rod. Nano Energy 2, 377-386.

Lotya, M., King, P.J., Khan, U., De, S., and Coleman, J.N. (2010). High-concentration, surfactant-stabilized graphene dispersions. ACS Nano 4, 3155-3162.

Luo, B., Liu, S., and Zhi, L. (2012). Chemical approaches toward graphene-based nanomaterials and their applications in energy-related areas. Small 8, 630-646.

Luo, Y.H., Chang, L.W., and Lin, P. (2015). Metal-Based Nanoparticles and the Immune System: Activation, Inflammation, and Potential Applications. Biomed Res Int 2015, 143720.

Lv, M., Zhang, Y., Liang, L., Wei, M., Hu, W., Li, X., and Huang, Q. (2012). Effect of graphene oxide on undifferentiated and retinoic acid-differentiated SH-SY5Y cells line. Nanoscale 4, 3861-3866.

Ma, J., Liu, R., Wang, X., Liu, Q., Chen, Y., Valle, R.P., Zuo, Y.Y., Xia, T., and Liu, S. (2015). Crucial Role of Lateral Size for Graphene Oxide in Activating Macrophages and Stimulating Pro-inflammatory Responses in Cells and Animals. ACS Nano 9, 10498-10515.

Mahanta, S., and Paul, S. (2015). Bovine α-lactalbumin functionalized graphene oxide nano-sheet exhibits enhanced biocompatibility: A rational strategy for graphene-based targeted cancer therapy. Colloids Surf B Biointerfaces 134, 178-187.

Mao, S., Pu, H.H., and Chen, J.H. (2012). Graphene oxide and its reduction: modeling and experimental progress. Rsc Adv 2, 2643-2662.

Marcano, D.C., Kosynkin, D.V., Berlin, J.M., Sinitskii, A., Sun, Z., Slesarev, A., Alemany, L.B., Lu, W., and Tour, J.M. (2010). Improved synthesis of graphene oxide. ACS Nano 4, 4806-4814.

McClure, J.W. (1956). Diamagnetism of Graphite. Physical Review 104, 666-671.

Medzhitov, R. (2008). Origin and physiological roles of inflammation. Nature 454, 428-435.

Meyer, J.C., Geim, A.K., Katsnelson, M.I., Novoselov, K.S., Booth, T.J., and Roth, S. (2007). The structure of suspended graphene sheets. Nature 446, 60-63.

Mills, C.D. (2012). M1 and M2 Macrophages: Oracles of Health and Disease. Crit Rev Immunol 32, 463-488.

Mittal, S., Kumar, V., Dhiman, N., Chauhan, L.K., Pasricha, R., and Pandey, A.K. (2016). Physico-chemical properties based differential toxicity of graphene oxide/reduced graphene oxide in human lung cells mediated through oxidative stress. Sci Rep 6, 39548.

Monteiro-Riviere, N.A., ed. (1991). Comparative anatomy, physiology, and biochemistry of mammalian skin (Washington, DC: CRC Press).

Monteiro-Riviere, N.A. (2010). Toxicology of the Skin. In Toxicology of the Skin (CRC Press), pp. 121-134.

Monteiro-Riviere, N.A., and Inman, A.O. (2006). Challenges for assessing carbon nanomaterial toxicity to the skin. Carbon 44, 1070-1078.

Mukherjee, S.P., Bottini, M., and Fadeel, B. (2017). Graphene and the Immune System: A Romance of Many Dimensions. Front Immunol 8, 673.

Mukherjee, S.P., Lozano, N., Kucki, M., Del Rio-Castillo, A.E., Newman, L., Vázquez, E., Kostarelos, K., Wick, P., and Fadeel, B. (2016). Detection of Endotoxin Contamination of Graphene Based Materials Using the TNF-α Expression Test and Guidelines for Endotoxin-Free Graphene Oxide Production. PLoS One 11, e0166816.

Murray, P.J., Allen, J.E., Biswas, S.K., Fisher, E.A., Gilroy, D.W., Goerdt, S., Gordon, S., Hamilton, J.A., Ivashkiv, L.B., Lawrence, T., et al. (2014). Macrophage activation and polarization: nomenclature and experimental guidelines. Immunity 41, 14-20.

Muzi, L., Mouchet, F., Cadarsi, S., Janowska, I., Russier, J., Ménard-Moyon, C., Risuleo, G., Soula, B., Galibert, A-M., Flahaut, E., et al. (2016). Examining the impact of multi-layer graphene using cellular and amphibian models. 2D Materials 3, 025009.

Norman, K.G., Canter, J.A., Shi, M., Milne, G.L., Morrow, J.D., and Sligh, J.E. (2010). Cyclosporine A suppresses keratinocyte cell death through MPTP inhibition in a model for skin cancer in organ transplant recipients. Mitochondrion 10, 94-101.

Novoselov, K.S. (2011). Graphene: materials in the Flatland (Nobel lecture). Angewandte Chemie 50, 6986-7002.

Novoselov, K.S., Geim, A.K., Morozov, S.V., Jiang, D., Zhang, Y., Dubonos, S.V., Grigorieva, I.V., and Firsov, A.A. (2004). Electric field effect in atomically thin carbon films. Science 306, 666-669.

O'Donnell, V.B., Smith, G.C., and Jones, O.T. (1994). Involvement of phenyl radicals in iodonium inhibition of flavoenzymes. Mol Pharmacol 46, 778-785.

OECT Test No. 439: In Vitro Skin Irritation: Reconstructed Human Epidermis Test Method (OECD Publishing).

OECD Test No. 442B: Skin Sensitization (OECD Publishing).

OECD Test No. 442E: In Vitro Skin Sensitisation (OECD Publishing).

Ott, M., Gogvadze, V., Orrenius, S., and Zhivotovsky, B. (2007). Mitochondria, oxidative stress and cell death. Apoptosis 12, 913-922.

Ou, L., Song, B., Liang, H., Liu, J., Feng, X., Deng, B., Sun, T., and Shao, L. (2016). Toxicity of graphene-family nanoparticles: a general review of the origins and mechanisms. Part Fibre Toxicol 13, 57.

Palframan, R.T., Jung, S., Cheng, G., Weninger, W., Luo, Y., Dorf, M., Littman, D.R., Rollins, B.J., Zweerink, H., Rot, A., et al. (2001). Inflammatory chemokine transport and presentation in HEV: a remote control mechanism for monocyte recruitment to lymph nodes in inflamed tissues. J Exp Med 194, 1361-1373.

Park, S., and Ruoff, R.S. (2009). Chemical methods for the production of graphenes. Nat Nanotechnol 4, 217-224.

Parvez, K., Li, R., Puniredd, S.R., Hernandez, Y., Hinkel, F., Wang, S., Feng, X., and Müllen, K. (2013). Electrochemically exfoliated graphene as solution-processable, highly conductive electrodes for organic electronics. ACS Nano 7, 3598-3606.

Pasparakis, M., Haase, I., and Nestle, F.O. (2014). Mechanisms regulating skin immunity and inflammation. Nat Rev Immunol 14, 289-301.

Passlick, B., Flieger, D., and Ziegler-Heitbrock, H.W. (1989). Identification and characterization of a novel monocyte subpopulation in human peripheral blood. Blood 74, 2527-2534.

Peng-Gang, R., Ding-Xiang, Y., Xu, J., Tao, C., and Zhong-Ming, L. (2011). Temperature dependence of graphene oxide reduced by hydrazine hydrate. Nanotechnology 22, 055705.

Pescatori, M., Bedognetti D., Venturelli, E., Menard-Moyon C., Bernardini, C., Bernardini C Fau - Muresu, E., Piana, A., Maida, G., Manetti, R., Sgarrella, F., Bianco, A., et al. (2013). Functionalized carbon nanotubes as immunomodulator systems. Biomaterials 34, 4395-403.

Peters, J.H., Ruppert, J., Gieseler, R.K., Najar, H.M., and Xu, H. (1991). Differentiation of human monocytes into CD14 negative accessory cells: do dendritic cells derive from the monocytic lineage? Pathobiology 59, 122-126.

Qin, Y., Zhou, Z.W., Pan, S.T., He, Z.X., Zhang, X., Qiu, J.X., Duan, W., Yang, T., and Zhou, S.F. (2015). Graphene quantum dots induce apoptosis, autophagy, and inflammatory response via p38 mitogen-activated protein kinase and nuclear factor-kappaB mediated signaling pathways in activated THP-1 macrophages. Toxicology 327, 62-76.

Quintana, M., Vazquez, E., and Prato, M. (2013). Organic functionalization of graphene in dispersions. Acc Chem Res 46, 138-148.

Randolph, G.J., Inaba, K., Robbiani, D.F., Steinman, R.M., and Muller, W.A. (1999). Differentiation of phagocytic monocytes into lymph node dendritic cells in vivo. Immunity 11, 753-761.

Rietschel, E.T., Kirikae, T., Schade, F.U., Mamat, U., Schmidt, G., Loppnow, H., Ulmer, A.J., Zähringer, U., Seydel, U., and Di Padova, F. (1994). Bacterial endotoxin: molecular relationships of structure to activity and function. FASEB J 8, 217-225.

Robbins (2013). Infiammazione e riparazione tissutale. In Fondamenti di Patologia e di Fisiopatologia, EDRA, ed., pp. 29-52.

Roche, S. (2011). Nanoelectronics: graphene gets a better gap. Nat Nanotechnol 6, 8-9.

Romani, N., Gruner, S., Brang, D., Kämpgen, E., Lenz, A., Trockenbacher, B., Konwalinka, G., Fritsch, P.O., Steinman, R.M., and Schuler, G. (1994). Proliferating dendritic cell progenitors in human blood. J Exp Med 180, 83-93.

Ruess, G., and Vogt, F. (1948). Höchstlamellarer Kohlenstoff aus Graphitoxyhydroxyd. Monatshefte für Chemie und verwandte Teile anderer Wissenschaften 78, 222-242.

Ruiz, O.N., Fernando, K.A., Wang, B., Brown, N.A., Luo, P.G., McNamara, N.D., Vangsness, M., Sun, Y.P., and Bunker, C.E. (2011). Graphene oxide: a nonspecific enhancer of cellular growth. ACS Nano 5, 8100-8107.

Ryoo, S.R., Kim, Y.K., Kim, M.H., and Min, D.H. (2010). Behaviors of NIH-3T3 fibroblasts on graphene/carbon nanotubes: proliferation, focal adhesion, and gene transfection studies. ACS nano 4, 6587-6598.

Sallusto, F., and Lanzavecchia, A. (1994). Efficient presentation of soluble antigen by cultured human dendritic cells is maintained by granulocyte/macrophage colony-stimulating factor plus interleukin 4 and downregulated by tumor necrosis factor alpha. J Exp Med 179, 1109-1118.

Salmon, J.K., Armstrong, C.A., and Ansel, J.C. (1994). The skin as an immune organ. West J Med 160, 146-152.

Sasidharan, A., Panchakarla, L.S., Sadanandan, A.R., Ashokan, A., Chandran, P., Girish, C.M., Menon, D., Nair, S.V., Rao, C.N., and Koyakutty, M. (2012). Hemocompatibility and macrophage response of pristine and functionalized graphene. Small 8, 1251-1263.

Sasidharan, A., Swaroop, S., Chandran, P., Nair, S., and Koyakutty, M. (2016). Cellular and molecular mechanistic insight into the DNA-damaging potential of few-layer graphene in human primary endothelial cells. Nanomedicine 12, 1347-1355.

Schinwald, A., Murphy F Fau - Askounis, A., Askounis A Fau - Koutsos, V., Koutsos V Fau - Sefiane, K., Sefiane K Fau - Donaldson, K., Donaldson K Fau - Campbell, C.J., and Campbell, C.J. (2013). Minimal oxidation and inflammogenicity of pristine graphene with residence in the lung. Nanotoxicology 8, 824-832.

Seabra, A.B., Paula, A.J., de Lima, R., Alves, O.L., and Duran, N. (2014). Nanotoxicity of graphene and graphene oxide. Chem Res Toxicol 27, 159-168.

Shen, H., Zhang, L., Liu, M., and Zhang, Z. (2012). Biomedical applications of graphene. Theranostics 2, 283-294.

Shin, S.R., Li, Y.C., Jang, H.L., Khoshakhlagh, P., Akbari, M., Nasajpour, A., Zhang, Y.S., Tamayol, A., and Khademhosseini, A. (2016). Graphene-based materials for tissue engineering. Adv Drug Deliv Rev 105, 255-274.

Shvedova, A.A., Castranova, V., Kisin, E.R., Schwegler-Berry, D., Murray, A.R., Gandelsman, V.Z., Maynard, A., and Baron, P. (2003). Exposure to carbon nanotube material: assessment of nanotube cytotoxicity using human keratinocyte cells. J Toxicol Environ Health A 66, 1909-1926.

Singh, S.K., Singh, M.K., Nayak, M.K., Kumari, S., Shrivastava, S., Grácio, J.J., and Dash, D. (2011). Thrombus inducing property of atomically thin graphene oxide sheets. ACS Nano 5, 4987-4996.

Singh, Z. (2016). Applications and toxicity of graphene family nanomaterials and their composites. Nanotechnol Sci Appl 9, 15-28.

Slonczewski, J.C., and Weiss, P.R. (1958). Band Structure of Graphite. Physical Review 109, 272-279.

Steinman, R.M., and Cohn, Z.A. (1973). Identification of a novel cell type in peripheral lymphoid organs of mice. I. Morphology, quantitation, tissue distribution. J Exp Med 137, 1142-1162.

Stone, V., and Donaldson, K. (2006). Nanotoxicology: signs of stress. Nat Nanotechnol 1, 23-24.

Sutter, P.W., Flege, J.I., and Sutter, E.A. (2008). Epitaxial graphene on ruthenium. Nat Mater 7, 406-411.

Tkach, A.V., Yanamala, N., Stanley, S., Shurin, M.R., Shurin, G.V., Kisin, E.R., Murray, A.R., Pareso, S., Khaliullin, T., Kotchey, G.P., Castranova, V., et al. (2013). Graphene oxide, but not fullerenes, targets immunoproteasomes and suppresses antigen presentation by dendritic cells. Small 9, 1686-90.

Tu, Y., Lv, M., Xiu, P., Huynh, T., Zhang, M., Castelli, M., Liu, Z., Huang, Q., Fan, C., Fang, H., et al. (2013). Destructive extraction of phospholipids from Escherichia coli membranes by graphene nanosheets. Nat Nanotechnol 8, 594-601.

Van Noorden, R. (2012). Production: Beyond sticky tape. Nature 483, S32-33.

Varol, C., Landsman, L., Fogg, D.K., Greenshtein, L., Gildor, B., Margalit, R., Kalchenko, V., Geissmann, F., and Jung, S. (2007). Monocytes give rise to mucosal, but not splenic, conventional dendritic cells. J Exp Med 204, 171-180.

Wallace, P.R. (1947). The Band Theory of Graphite. Physical Review 71, 622-634.

Wang, A., Pu, K., Dong, B., Liu, Y., Zhang, L., Zhang, Z., Duan, W., and Zhu, Y. (2013). Role of surface charge and oxidative stress in cytotoxicity and genotoxicity of graphene oxide towards human lung fibroblast cells. J Appl Toxicol 33, 1156-1164.

Wang, K., Ruan, J., Song, H., Zhang, J., Wo, Y., Guo, S., and Cui, D. (2011). Biocompatibility of Graphene Oxide. Nanoscale Res Lett 6, 8.

Wang, X., Duch, M.C., Mansukhani, N., Ji, Z., Liao, Y.-P., Wang, M., Zhang, H., Sun, B., Chang, C.H., Li, R., et al. (2015). Use of a Pro-Fibrogenic Mechanism-Based Predictive Toxicological Approach for Tiered Testing and Decision Analysis of Carbonaceous Nanomaterials. ACS Nano 9, 3032-3043.

Welss, T., Basketter, D.A., and Schröder, K.R. (2004). In vitro skin irritation: facts and future. State of the art review of mechanisms and models. Toxicol In Vitro 18, 231-243.

Westervelt, R.M. (2008). Applied physics. Graphene nanoelectronics. Science 320, 324-325.

Wick, P., Louw-Gaume, A.E., Kucki, M., Krug, H.F., Kostarelos, K., Fadeel, B., Dawson, K.A., Salvati, A., Vazquez, E., Ballerini, L., et al. (2014). Classification framework for graphene-based materials. Angew Chem Int Ed Engl 53, 7714-7718.

Wong, K.L., Tai, J.J., Wong, W.C., Han, H., Sem, X., Yeap, W.H., Kourilsky, P., and Wong, S.C. (2011). Gene expression profiling reveals the defining features of the classical, intermediate, and nonclassical human monocyte subsets. Blood 118, e16-31.

Wu, J., Yang, R., Zhang, L., Fan, Z., and Liu, S. (2015). Cytotoxicity effect of graphene oxide on human MDA-MB-231 cells. Toxicol Mech Methods 25, 312-319.

Yang, D., Zhao, Y., Guo, H., Li, Y., Tewary, P., Xing, G., Hou, W., Oppenheim, J.J., and Zhang, N. (2010). [Gd@C(82)(OH)(22)](n) nanoparticles induce dendritic cell maturation and activate Th1 immune responses. ACS Nano 4, 1178.

Yang, K., Feng, L.Z., Hong, H., Cai, W.B., and Liu, Z. (2013a). Preparation and functionalization of graphene nanocomposites for biomedical applications. Nat Protoc 8, 2392-2403.

Yang, K., Gong, H., Shi, X., Wan, J., Zhang, Y., and Liu, Z. (2013b). In vivo biodistribution and toxicology of functionalized nano-graphene oxide in mice after oral and intraperitoneal administration. Biomaterials 34, 2787-2795.

Yang, K., Wan, J., Zhang, S., Zhang, Y., Lee, S.T., and Liu, Z. (2011). In vivo pharmacokinetics, long-term biodistribution, and toxicology of PEGylated graphene in mice. ACS Nano 5, 516-522.

Yoshida, Y., Sakaguchi, H., Ito, Y., Okuda, M., and Suzuki, H. (2003). Evaluation of the skin sensitization potential of chemicals using expression of co-stimulatory molecules, CD54 and CD86, on the naive THP-1 cell line. Toxicol In Vitro 17, 221-228.

Yue, H., Wei, Z., Yue, Z., Wang, B., Luo, N., Gao, Y., Ma, D., Ma, G., and Su, Z. (2012). The role of the lateral dimension of graphene oxide in the regulation of cellular responses. Biomaterials 33, 4013-21.

Zhang, L., Xia, J., Zhao, Q., Liu, L., and Zhang, Z. (2010a). Functional graphene oxide as a nanocarrier for controlled loading and targeted delivery of mixed anticancer drugs. Small 6, 537-544.

Zhang, L.W., Zeng, L., Barron, A.R., and Monteiro-Riviere, N.A. (2007). Biological interactions of functionalized single-wall carbon nanotubes in human epidermal keratinocytes. Int J Toxicol 26, 103-113.

Zhang, X., Hu, W., Li, J., Tao, L., and Wei, Y. (2012). A comparative study of cellular uptake and cytotoxicity of multi-walled carbon nanotubes, graphene oxide, and nanodiamond. Toxicology Research 1, 62-68.

Zhang, X., Yin, J., Peng, C., Hu, W., Zhu, Z., Li, W., Fan, C., and Huang, Q. (2011). Distribution and biocompatibility studies of graphene oxide in mice after intravenous administration, Vol 49.

Zhang, Y., Ali, S.F., Dervishi, E., Xu, Y., Li, Z., Casciano, D., and Biris, A.S. (2010b). Cytotoxicity effects of graphene and single-wall carbon nanotubes in neural phaeochromocytoma-derived PC12 cells. ACS Nano 4, 3181-3186.

Zhou, H., Zhao, K., Li, W., Yang, N., Liu, Y., Chen, C., and Wei, T. (2012). The interactions between pristine graphene and macrophages and the production of cytokines/chemokines via TLR- and NF-κB-related signaling pathways. Biomaterials 33, 6933-6942.

Ziegler-Heitbrock, L. (2015). Blood Monocytes and Their Subsets: Established Features and Open Questions. Front Immunol 6, 423.

Ziegler-Heitbrock, L., Ancuta, P., Crowe, S., Dalod, M., Grau, V., Hart, D.N., Leenen, P.J., Liu, Y.J., MacPherson, G., Randolph, G.J., et al. (2010). Nomenclature of monocytes and dendritic cells in blood. Blood 116, e74-80.

Zou, X., Zhang, L., Wang, Z., and Luo, Y. (2016). Mechanisms of the Antimicrobial Activities of Graphene Materials. J Am Chem Soc 138, 2064-2077.

7. Appendices

Appendix A

GBM	Elemental Analysis ± SD (wt%)					Atomic ratio (at. %)[a]			TGA weight lost (%)[b]	Lateral Dimension ± SD (nm)[c]
	C	H	N	O	S	N/C	O/C	S/C		
FLG	94.03 ± 0.64	0.32 ± 0.03	0.31 ± 0.03	5.34 ± 0.64	—	0.011	0.074	—	7	552 ± 245
GO1	43.20 ± 0.07	3.67 ± 0.07	0.07 ± 0.01	42.70 ± 0.02	10.37 ± 0.03	—	0.53	0.047	50	622 ± 581
GO2	47.71 ± 0.03	3.04 ± 0.02	0.15	48.84 ± 0.02	0.27 ± 0.03	—	0.51	—	52	845 ± 427
GO3	41.88 ± 1.06	3.04 ± 0.14	0.04	52.23 ± 0.46	2.82 ± 0.52	—	0.51	0.030	45	979 ± 498

Table 1. Summarized materials properties of GBMs. [a]Ratios determined from the XPS survey spectra. [b]Values determined at 700 °C. [c]Values determined by HRTEM on 150 sheets.

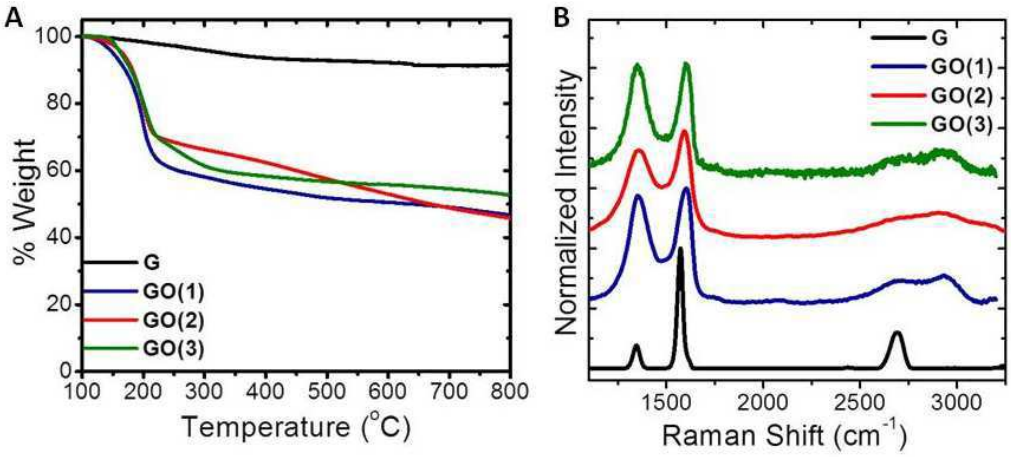

Figure 1. TGA plot of GFNs (A). Representative Raman spectra of GFNs where spectra for GO1, GO2 and GO3 were performed with a baseline correction (B).

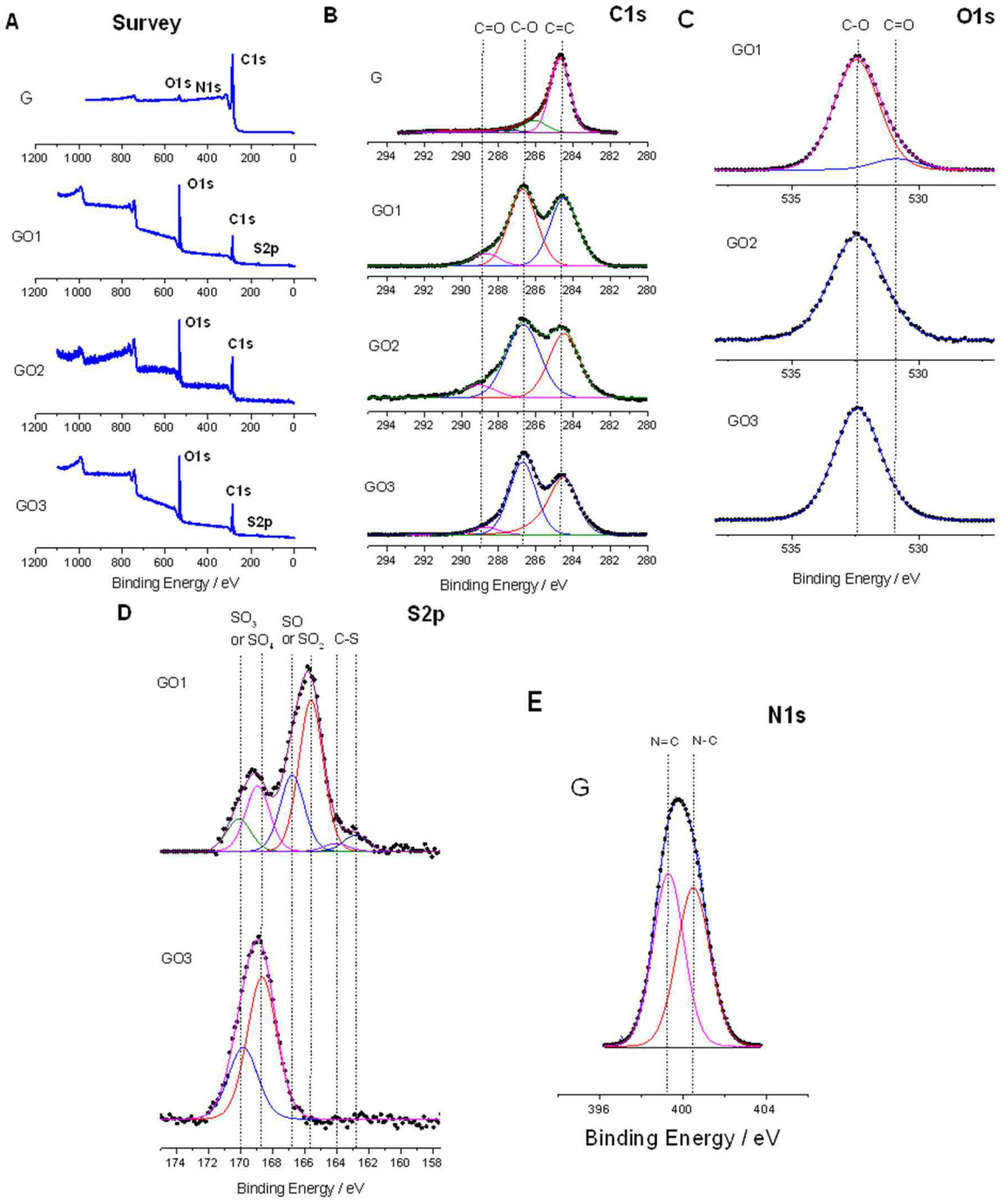

Figure 2. XPS survey spectra (A) and C1s high resolution spectra (B) for G, GO1, GO2 and GO3. O1s high resolution spectra for GO1, GO2 and GO3 (C). S2p high resolution spectra for GO1 and GO3 (D). N1s high resolution spectra for G (E).